Erasmus University Rotterdam

Erasmus School of Economics

Master Thesis Quantitative Finance

Macro-Finance Shadow-Rate Modelling:

Estimating the term structure with macroeconomic factors in a zero lower bound environment

Author:
Nadine Nieuwstad

Student ID:
385009

Supervisor:
Prof.dr. Michel van der Wel

Second assessor:
Dr. Xiao Xiao

Date: May 18, 2019

Abstract

Although shadow-rate term structure models can replicate the yield curve's characteristics in a zero-lower bound environment, there could be additional information which the yield curve that is constrained by the lower bound cannot incorporate. I thus develop a macro-finance shadow-rate model with three macro factors: economic activity, inflation, and the policy rate. I estimate the model on monthly U.S. interest rates under various restrictions using a Maximum Likelihood-based extended Kalman filter. The key findings are as follows. First, the results are sensitive to initialisation values and parameter restrictions, particularly with respect to the factors' persistence and yield dynamics. Second, incorporating macroeconomic information can improve in-sample fit and help to mitigate underestimation of persistence, while replicating relevant term structure dynamics and macro-finance linkages. Third, relative to the yields-only shadow-rate model and the macro-finance affine model, this model is better at replicating two key stylised facts near the lower bound: the nonnegativity of yield rates and the compression of yield volatilities for short and intermediate maturities. The evidence suggests that the macro-finance shadow-rate model is preferred over affine and yields-only models in a zero-lower bound environment.

Keywords: shadow rate, zero lower bound, macro-finance, state space, maximum likelihood, extended Kalman filter, arbitrage-free Nelson-Siegel model

Contents

1 Introduction

Understanding the yield curve's dynamic evolution is key in financial processes, such as the pricing of financial assets and derivatives, monetary policy decision-making, financial risk management, and portfolio allocation (Christensen and Rudebusch, 2015). As the workhorse representation in term structure modelling, Gaussian affine term structure models (GATSMs) fail to capture the yields' dynamics at the zero lower bound (ZLB), leading to misspecified models. The ZLB-constrained yield curve also cannot fully incorporate all relevant information and reflect information in other key state variables (Bauer and Rudebusch, 2016). Thus, can I develop a model that adheres to a lower bound and incorporates information which yield rates cannot?

The key contribution of this thesis is the development of a macro-finance shadow-rate model. It extends Christensen and Rudebusch (2016)'s yields-only shadow-rate model by adding three macro factors to the state equation. The factors are derived by principal component analysis (PCA) and represent economic activity, inflation, and the policy rate. I follow the steps of Krippner (2013) and Christensen and Rudebusch (2016) to derive the yield-adjustment term and volatility effect for the ZLB-constrained zero-coupon bond yield equation. Subsequently, I provide the steps of a Maximum Likelihood-based extended Kalman filter (EKF) in a macro-finance context. The EKF differs from the standard Kalman filter by using a linearised measurement equation, through a first-order Taylor expansion, in the update step. I derive six model variations based on parameter restrictions from existing literature. Using three initialisations, I estimate the six-factor model, having three yield and three macro factors, on a data set of U.S. interest rates with eight maturities (0.25, 0.5, 1, 2, 3, 5, 7, and 10 years) and macroeconomic data between January 1985 and December 2018. I compare the results with macro-finance affine models and yields-only shadow-rate models to assess whether the estimation method yields reasonable parameter estimates and filtered states and whether incorporating macroeconomic variables adds relevant information to the yield curve. Using impulse response functions, I analyse the factor interactions, relating them to macro-finance theory. Based on yearly rolling-window re-estimations, I evaluate whether the models replicate the term structure's stylised facts.

Due to nonzero probabilities of negative rates, GATSMs ignore the availability of the physical currency (Krippner, 2012). Arbitrage profit could be realised by borrowing, thus receiving the absolute interest rate, to buy and hold physical currency with zero return. Alternatively, with nonzero probabilities of negative interest rates, bond options with zero probability of out-of-the-money expiry could exist. If term structure data are constrained by the ZLB, yet the model is unconstrained, this model misspecification could affect model applications, such as monitoring the estimated level and shape of the term structure to measure the monetary policy stance. The effect could be compounded for macro-finance relationships between the model and macroeconomic data, as the latter are not constrained to be nonnegative.

Even so, GATSMs remain widely used. They are applied to decompose the break-even inflation rate, i.e. the difference between the nominal and real yields of the same maturity, into expected inflation and an inflation risk premium (Centre for Economic Policy Research, 2015). They are used in probability-based stress tests to generate distributional interest rate forecasts and attach probabilities to specific portfolio outcomes. They also allow for the analysis of monetary policy effects, such as quantitative easing.

Unlike GATSMs, shadow-rate term structure models adhere to the nonnegativity of interest rates. In shadow-rate models, the shadow short rate freely ranges from negative to positive values, while the short rate is defined as the maximum between the shadow short rate and zero, thus enforcing nonnegativity. There are two main shadow-rate frameworks: Black (1995)'s and Krippner (2012)'s. Black (1995) introduces the concept that physical currency provides an option against negative interest rates. While his framework has arbitrary flexibility in principle, application can be too computationally burdensome or infeasible, such as in a three-factor model. Krippner (2012) thus develops a tractable framework with an explicit function of maturity that represents the optionality associated with the present and future availability of physical currency, resulting in analytical formulas for the instantaneous shadow forward rates. Despite that this framework is not theoretically self-consistent (i.e. fully arbitrage-free), unlike Black (1995)'s framework, Krippner (2013) shows that results from the two-factor are very similar to those from a comparable Black model. Christensen and Rudebusch (2015) confirm this by showing that the option-based approximation errors, i.e. the difference between employing Black (1995)'s and Krippner (2012)'s framework, are sufficiently small.

Most authors opt for the extended Kalman filter (EKF) for estimating shadow-rate models. Christensen and Rudebusch (2015) compare the extended and unscented Kalman filter for their sample of Japanese yields, concluding very little difference. They thus prefer the EKF, which is less computationally intensive. Through simulation exercises, Christensen (2015) finds that the EKF is almost as efficient in estimating shadow-rate models as the standard Kalman filter is in estimating Gaussian affine models. Yet, filtering deteriorates in quality when yields are severely compressed against the ZLB. Thus, while the EKF can be implemented on U.S. yield data, its application on Japanese yield data should be questioned.

Comparing shadow-rate arbitrage-free Nelson-Siegel (AFNS) models with their standard Gaussian versions on Japanese term structure data, Christensen and Rudebusch (2015) find that shadow-rate models can provide better in-sample fit and capture the yields' dynamics at the ZLB. Christensen and Rudebusch (2016) find similar evidence for U.S. yield data. In terms of real-time forecast performance, they conclude that the shadow-rate model is competitive in the recent ZLB period and on par with the standard model before this period. Analysing UK data, Carriero et al. (2018) also show that the shadow-rate model is better able to replicate the stylised facts of the term structure near the ZLB.

In a low-interest rate environment, the shadow-rate literature is becoming more important as it addresses the potential shortcomings of GATSMs. However, research has mainly been focused on yields-only shadow-rate models, while the effect of the ZLB could also be important for macro-finance relationships. Incorporating macroeconomic variables can be valuable when making inferences about monetary policy expectations near the ZLB, such as the time until liftoff and the subsequent pace of tightening, as shown by Bauer and Rudebusch (2016). However, their method possibly yields inaccurate estimates, as they estimate the affine model in the pre-ZLB period and apply the same parameter estimates to the shadow-rate model for the ZLB period. As evidence against this approach, Christensen and Rudebusch (2016) find sizable differences between the estimated parameters of a standard affine model and a shadow-rate model.

A macro-finance shadow-rate model could also outperform in forecasting exercises. Krippner

and Lewis (2018) find that including yield curve information improves forecasts of inflation and the federal funds rate, compared to a macro-only model. Meanwhile, it only improves forecasts of capacity utilisation for longer horizons. In the reverse direction, i.e. including macroeconomic information when forecasting the ZLB-constrained yield curve, the evidence is less convincing, although there are still gains for longer horizons.

Building upon these findings, my research yields three additional insights. First, I elaborate on the estimation method, addressing several implementation issues and how to overcome these. I develop three initialisations: one uninformed, another using the macro-finance affine model estimates, and another based on a two-step OLS-VAR estimation. Comparing the resulting in-sample fit and parameter estimates, I conclude that convergence to the global optimum is sensitive to the initialisation values. Thus, I apply constrained optimisation with multiple starting points. Alternatively, this issue can be mitigated by employing the Expectation Maximisation-based extended Kalman filter, for which I provide preliminary steps. Comparing results for the correlated factors model (Christensen et al., 2011; Diebold et al., 2006), the independent variances model, the independent macro-finance factors model (Ang and Piazzesi, 2003), the independent factors model (Christensen et al., 2011), Christensen and Rudebusch (2016)'s macro-extended model, and Krippner and Lewis (2018)'s model, I find that there is no one-size-fits-all set of parameter restrictions. Various restrictions should be tested on a given data set, as they affect whether the model replicates the factors' persistence and yield dynamics well. In-sample fit should also guide model preferences. Addressing these issues results in more realistic parameter estimates and filtered states, benefiting model application.

Second, I provide evidence that macroeconomic variables add information to the ZLB-constrained yield curve. I find that shadow-rate macro-finance models yield higher in-sample fit than their affine versions and at least equal fit with their yields-only versions. My sample favours two models: one in which yield factors are independent of macro factors, another in which all factors are interdependent through their mean-reversion processes, yet have independent innovation processes. Excluding the macroeconomic variables that are the least correlated with yields, the data set shows a clear preference for a model with macro-finance interactions. Thus, the extent of adding information will depend on the variables. Allowing for macro-finance interactions affects how yield factors co-move with interest rates of different maturities. This reflects the yield factors' linkage with monetary policy, which is strongest for the model with macro-finance interactions, compared to a model with independent yield and macro factors and a yields-only model. Furthermore, using impulse response functions and confidence bounds derived by Monte Carlo simulation, I analyse the effects of a shock to one factor on another. I find that the macro-finance model's impulse responses replicate important macro-finance linkages. This is relevant in applications of term structure models related to monetary policy and macroeconomic measures. Moreover, previous research suggests imposing a unit-root restriction on the level factor to mitigate underestimation of persistence. My results show that this measure could be insufficient. Instead, models with full macro-finance interactions suffer less from this issue.

Third, I extend the formulas for the expected short rate and predicted conditional yield volatilities to the macro-finance shadow-rate model. Using re-estimations on a rolling window basis, I show that the macro-finance shadow-rate model consistently reproduces nonnegative

expected short rates in a ZLB environment and outperforms its yields-only version under the same restrictions in terms of forecast accuracy. It is also better able to the replicate the compression of yield volatilities at short maturities and, to a lesser extent, at intermediate maturities. Altogether, my findings support the application of the macro-finance shadow-rate model in lieu of GATSMs and yields-only shadow-rate models in a ZLB environment.

This paper is structured as follows. Chapter 2 elaborates on the model and its variations, while Chapter 3 describes the estimation method employed. Chapter 4 discusses the data set, its key characteristics, and constructing the factors from the variables. Chapter 5 presents the results, their interpretation, and robustness of the findings. Chapter 6 reports the conclusions, discussion points, and potential ideas for future research.

2 Models

Section 2.1 presents Christensen and Rudebusch (2016)'s yields-only shadow-rate model. Section 2.2 elaborates on its extension to a macro-finance setting by adding macro factors and resulting changes to the state and measurement equations. Section 2.3 describes the affine version of the macro-finance model, so that I can compare their results. Furthermore, Section 2.4 present models variations based on parameter restrictions from previous literature.

2.1 Yields-Only Shadow-Rate Model

This section closely follows Christensen and Rudebusch (2016)'s exposition of the yields-only shadow-rate model. The 'base' model is the arbitrage-free Nelson-Siegel model (AFNS) of Christensen et al. (2011), in which three latent factors, namely the level, slope, and curvature factors (L_t, S_t, C_t), describe the yield curve. This term structure model is appealing due to the factor loadings' functional form and the interpretation of the latent factors. The instantaneous risk-free rate and the representation of nominal zero-coupon yields are affine functions of the state variables. Given the affine structure, the conventional Kalman filter is used for estimation.

Christensen and Rudebusch (2016), who build upon Krippner (2013)'s work, present a yields-only shadow-rate model (hereafter: 'ZLB model'). In the ZLB model, the latent shadow rate s_t has the same dynamics as the instantaneous risk-free rate in the AFNS model, such that it is the sum of the level and slope factors, L_t and S_t respectively, as in

$$s_t = L_t + S_t. \tag{1}$$

The instantaneous rate r_t in the ZLB model is the maximum of the shadow rate and zero,

$$r_t = max\{0, s_t\}. \tag{2}$$

In the pre-ZLB period, the shadow and ZLB representation are equivalent, since

$$r_t = s_t. \tag{3}$$

Thus, the absence of the ZLB constraint implies that the shadow term structure estimated from the ZLB model coincides with the AFNS estimates.

Given a loading parameter λ, the shadow discount bond yield $y_t(\tau)$ for maturity τ, in terms of years, is a function of L_t, S_t, and the curvature factor C_t, such that

$$y_t(\tau) = L_t + \left(\frac{1-e^{-\lambda\tau}}{\lambda\tau}\right) S_t + \left(\frac{1-e^{-\lambda\tau}}{\lambda\tau} - e^{-\lambda\tau}\right) C_t - \frac{A(\tau)}{\tau}. \tag{4}$$

The instantaneous shadow forward rate $f_t(\tau)$ is

$$f_t(\tau) = -\frac{\delta}{\delta\tau} \ln P_t(\tau) = L_t + e^{-\lambda\tau} S_t + \lambda\tau e^{-\lambda\tau} C_t + A^f(\tau), \tag{5}$$

where $A(\tau)/\tau$ and $A^f(\tau)$ are yield-adjustment terms given by

$$\begin{aligned} A^f(\tau) &= -\frac{\delta A(\tau)}{\delta\tau} \\ &= -\frac{1}{2}\sigma_{11}^2\tau^2 - \frac{1}{2}(\sigma_{21}^2+\sigma_{22}^2)\left(\frac{1-e^{-\lambda\tau}}{\lambda}\right)^2 \\ &\quad - \frac{1}{2}(\sigma_{31}^2+\sigma_{32}^2+\sigma_{33}^2)\left[\frac{1}{\lambda^2} - \frac{2}{\lambda^2}e^{-\lambda\tau} - \frac{2}{\lambda}\tau e^{-\lambda\tau} + \frac{1}{\lambda^2}e^{-2\lambda\tau} + \frac{2}{\lambda}\tau e^{-2\lambda\tau} + \tau^2 e^{-2\lambda\tau}\right] \\ &\quad - \sigma_{11}\sigma_{21}\tau\left(\frac{1-e^{-\lambda\tau}}{\lambda}\right) - \sigma_{11}\sigma_{31}\left[\frac{1}{\lambda}\tau - \frac{1}{\lambda}\tau e^{-\lambda\tau} - \tau^2 e^{-\lambda\tau}\right] \\ &\quad - (\sigma_{21}\sigma_{31}+\sigma_{22}\sigma_{32})\left[\frac{1}{\lambda^2} - \frac{2}{\lambda^2}e^{-\lambda\tau} - \frac{1}{\lambda}\tau e^{-\lambda\tau} + \frac{1}{\lambda^2}e^{-2\lambda\tau} + \frac{1}{\lambda}\tau e^{-2\lambda\tau}\right]. \end{aligned} \tag{6}$$

The yield rate and forward rate factor loadings, $B(\tau)$ and $B^f(\tau)$ respectively, which represent the shadow yield curve, are

$$B(\tau) = \begin{pmatrix} 1 & \frac{1-e^{-\lambda\tau}}{\lambda\tau} & \frac{1-e^{-\lambda\tau}}{\lambda\tau} - e^{-\lambda\tau} \end{pmatrix}, \tag{7}$$

$$B^f(\tau) = \begin{pmatrix} 1 & e^{-\lambda\tau} & \lambda\tau e^{-\lambda\tau} \end{pmatrix}. \tag{8}$$

The instantaneous ZLB forward rate has two terms. The first depends on the instantaneous shadow forward rate, as given by Eq. (5). The second component is a function of the conditional variance of a European call. The ZLB forward rate $\underline{f}_t(\tau)$ is given by

$$\underline{f}_t(\tau) = f_t(\tau)\Phi\left(\frac{f_t(\tau)}{\omega(\tau)}\right) + \omega(\tau)\frac{1}{\sqrt{2\pi}}\exp\left(-\frac{1}{2}\left[\frac{f_t(\tau)}{\omega(\tau)}\right]^2\right), \tag{9}$$

where

$$\begin{aligned}\omega(\tau) = {} & \sigma_{11}^2\tau + (\sigma_{21}^2 + \sigma_{22}^2)\frac{1-e^{-2\lambda\tau}}{2\lambda} \\ & + (\sigma_{31}^2 + \sigma_{32}^2 + \sigma_{33}^2)\left[\frac{1-e^{-2\lambda\tau}}{4\lambda} - \frac{1}{2}\tau e^{-2\lambda\tau} - \frac{1}{2}\lambda\tau^2 e^{-2\lambda\tau}\right] \\ & + 2\sigma_{11}\sigma_{21}\left(\frac{1-e^{-\lambda\tau}}{\lambda}\right) + 2\sigma_{11}\sigma_{31}\left[-\tau e^{-\lambda\tau} + \frac{1-e^{-\lambda\tau}}{\lambda}\right] \\ & + (\sigma_{21}\sigma_{31} + \sigma_{22}\sigma_{32})\left[-\tau e^{-2\lambda\tau} + \frac{1-e^{-2\lambda\tau}}{2\lambda}\right].\end{aligned} \tag{10}$$

The state variables and scalar exponential functions of τ define $f_t(\tau)$, while $A^f(\tau)$ and $\omega(\tau)$ are defined by state variable innovation variance and covariance terms and scalar exponential functions of τ. It is thus feasible to evaluate the standard cumulative normal function $\Phi[f_t(\tau)/\omega(\tau)]$ and scalar exponential function $\exp(-\frac{1}{2}[f_t(\tau)/\omega(\tau)]^2)$. As a result, Eq. (9) is a closed-form analytical expression (Krippner, 2013). The ZLB zero-coupon bond yield rates are

$$\begin{aligned}\underline{y}_t(\tau) &= \frac{1}{\tau}\int_t^{t+\tau} \underline{f}_t(\tau)ds \\ &= \frac{1}{\tau}\int_t^{t+\tau}\left[f_t(s)\Phi\left(\frac{f_t(s)}{\omega(s)}\right) + \omega(s)\frac{1}{\sqrt{2\pi}}\exp\left(-\frac{1}{2}\left[\frac{f_t(s)}{\omega(s)}\right]^2\right)\right]ds.\end{aligned} \tag{11}$$

The computation of Eq. (11) requires numerical integration, which I elaborate in Section 3.1.

The state dynamics are described in continuous time, following Christensen and Rudebusch (2016). In state space terms, the measurement equation is Eq. (11) and the state equation is

$$\begin{pmatrix} dL_t \\ dS_t \\ dC_t \end{pmatrix} = \begin{pmatrix} \kappa_{11}^P & \kappa_{12}^P & \kappa_{13}^P \\ \kappa_{21}^P & \kappa_{22}^P & \kappa_{23}^P \\ \kappa_{31}^P & \kappa_{32}^P & \kappa_{33}^P \end{pmatrix}\left[\begin{pmatrix} \theta_1^P \\ \theta_2^P \\ \theta_3^P \end{pmatrix} - \begin{pmatrix} L_t \\ S_t \\ C_t \end{pmatrix}\right]dt + \begin{pmatrix} \sigma_{11} & 0 & 0 \\ \sigma_{21} & \sigma_{22} & 0 \\ \sigma_{31} & \sigma_{32} & \sigma_{33} \end{pmatrix}\begin{pmatrix} dW_t^{L,P} \\ dW_t^{S,P} \\ dW_t^{C,P} \end{pmatrix}, \tag{12}$$

where κ^P is the real-world mean-reversion matrix and θ^P is the real-world long-term mean. The model is completed using the essentially affine risk premium specification. In an unrestricted case, κ^P and θ^P can vary freely relative to their counterparts under the Q-measure. Common restrictions include a diagonal Σ and a nonstationary Nelson-Siegel level factor.

2.2 Macro-Finance Shadow-Rate Model

I extend the ZLB model to a macro-finance shadow-rate model (hereafter: 'ZLB-MF model') by adding the macroeconomic factors to the state equation as additional state variables, following Diebold et al. (2006). I compare the ZLB-MF model with the ZLB model, as described in Section 2.1, to infer whether adding macroeconomic information helps to explain the yield curve in a ZLB environment. The macro factors z_t, π_t, and r_t respectively represent real economic activity, inflation, and the effective policy rate, each at time t. The first two factors are extracted from a group of variables using principal component analysis (PCA). The new state equation is

$$dX_t = K^P\left[\theta^P - X_t\right]dt + \Sigma\, dW_t^P, \tag{13}$$

where $X_t = (L_t, S_t, C_t, z_t, \pi_t, r_t)$, θ^P is a 6-dimensional vector, κ^P is a 6-by-6 matrix, and Σ is a lower triangular 6-by-6 matrix.

The measurement equation, as in Eq. (11), remains unchanged as the macro factors affect the yields via the Nelson-Siegel factors in the state equation, Eq. (13), following Diebold et al. (2006). Thus, the yield rate and forward rate loadings for the macro factors, i.e. the elements corresponding to z_t, π_t, and r_t in factor loading matrices $B(\tau)$ and $B^f(\tau)$, equal zero, as in

$$y_t(\tau) = \begin{pmatrix} 1 & \frac{1-e^{-\lambda\tau}}{\lambda\tau} & \frac{1-e^{-\lambda\tau}}{\lambda\tau} - e^{-\lambda\tau} & 0 & 0 & 0 \end{pmatrix} X_t - \frac{A(\tau)}{\tau}, \tag{14}$$

$$f_t(\tau) = \begin{pmatrix} 1 & e^{-\lambda\tau} & \lambda\tau e^{-\lambda\tau} & 0 & 0 & 0 \end{pmatrix} X_t + A^f(\tau). \tag{15}$$

The yield-adjustment terms $A(\tau)/\tau$ in $y_t(\tau)$ and $A^f(\tau)$ in $f_t(\tau)$, and the volatility effect $\omega(\tau)$ are unchanged. The intuition behind this is that $A(\tau)/\tau$ and $\omega(\tau)$ are respectively functions of multiplications of Σ and $B(\tau)$ and of Σ and $B^f(\tau)$. Multiplying the macro factors' innovation variance and covariance terms with the macro factor loadings yields zero. Since only terms containing the yield factors' innovation variance and covariance terms remain, Eq. (6) and (10) also hold in a macro-finance model. Appendix A provides the complete derivation.

An alternative method would be to include the macro variables in the measurement equation directly, in which case the macro factor loadings would be unequal to zero. Since the macro factors' innovation variance and covariance terms would be multiplied by a nonzero value, Eq. (6) and (10) would contain additional terms. This approach would enable predicting future values of macro variables, which exceeds the scope of my research. It would thus unnecessarily increase the number of parameters to be estimated in an already high-dimensional problem.

2.3 Macro-Finance Affine Model

I compare the results of the ZLB-MF model, which is described in Section 2.2, to the results of its affine version: an arbitrage-free Nelson-Siegel model with macro factors (hereafter: 'AFNS-MF'). This allows me to infer whether the shadow-rate structure helps to explain the yield curve compared to a model that is not constrained by the ZLB, when both models incorporate macroeconomic information. Given the absence of the ZLB constraint, the AFNS-MF model is equivalent to the shadow representation given in Section 2.2. The instantaneous rate of the AFNS-MF model is given by Eq. (1). The zero-coupon bond yield and forward rate equations are given by Eq. (4) and (5), respectively. The observation equation of the AFNS-MF state space system is thus Eq. (4), while the state equation is Eq. (13).

2.4 Model Variations

I use several model variations from the literature: the correlated factors (CF) model (Christensen et al., 2011; Diebold et al., 2006), the independent variances (IV) model, the independent macro-finance factors (IMF) model (Ang and Piazzesi, 2003), the independent factors (IF) model (Christensen et al., 2011), a macro extension of Christensen and Rudebusch (2016)'s (B-CR) model, and Krippner and Lewis (2018) (KL) model. Leaving the lower bound as a free parameter periodically produces effectively zero volatility of short-term yields and poorer yield

forecast performance at longer forecast horizons, except for the ten-year maturity (Christensen and Rudebusch, 2016). Thus, I fix this parameter at zero for all models, following the literature. Moreover, consistent with literature, the yield observations' innovation terms are independent.

Christensen and Rudebusch (2016) argue that small-sample estimation bias cause the estimated model to be less persistent than the true process, such that the estimates of the real-world mean-reversion matrix are upward biased and expected longer-term averages are too stable. Thus, in the B-CR and KL models, the level factor has a unit-root process, which translates to the restriction $\kappa^P_{1,1} = 10^{-7}$, while $\theta^P_1 = 0$ is arbitrarily set. Appendix B elaborates on how this restriction influences the initialisation of the EKF.

The CF model is the least restricted model. The IF model is a restricted version of the IMF and IV models. The B-CR and KL models are also restricted versions of the IV model. In the KL model, the policy rate does not affect other variables other than itself based on the assumption that the information it contains is already summarised by the yield factors, while the curvature state variable does not affect the macroeconomic variables, in line with Diebold et al. (2006)'s findings. In the B-CR model, $\kappa^P_{1,2} = \kappa^P_{1,3} = \kappa^P_{3,1} = \kappa^P_{3,2} = 0$. The IF model has a diagonal κ^P matrix. In the IMF model, the upper-right and lower-left corner of κ^P and Σ of the IMF model are blocks of zero, such that yield factors are independent of macro factors. The remaining blocks of Σ are lower triangular, which are sufficiently identified (Ang and Piazzesi, 2003). In the IV, IF, B-CR, and KL models, Σ is restricted to be diagonal. In the CF model, Σ remains lower triangular.

The same variations apply for the ZLB-MF and AFNS-MF models. However, in a yields-only setting, the IMF and CF variations coincide, as well as the KL and IV variations. Hence, there are four ZLB model variations, namely CF, IV, IF, and B-CR.

3 Methodology

The following Chapter elaborates on the methodology for estimating the models elaborated in Chapter 2. In Section 3.1, I extend Christensen and Rudebusch (2016)'s estimation methodology to a macro-finance setting. Section 3.2 provides the formulas for the conditional expected short rate and predicted yield volatilities, which I use to assess whether the model can replicate the yield curve's stylised facts.

3.1 Extended Kalman Filter

One-step estimation with the Kalman filter delivers Maximum Likelihood estimates and optimal filtered and smoothed estimates of factors (Diebold et al., 2006). This is preferred to Diebold and Li (2006)'s two-step estimation, in which the parameter estimation and signal extraction uncertainty in the first step are not acknowledged in the second step. Given its affine measurement equation, as in Eq. (4), an affine Gaussian model is estimated with a standard Kalman filter. However, in a shadow-rate model, Eq. (11) shows that the zero-coupon bond yields are not affine functions of the state variables, which I elaborate further in Appendix C, suggesting the extended Kalman filter (EKF). Christensen (2015) argues that the EKF is preferred if yields are not severely compressed against the ZLB, which holds true for U.S. yield data.

This section closely follows the description of the EKF by Christensen (2015). In the EKF, the nonaffine measurement equation is linearised through a first-order Taylor expansion around the best guess of the state vector X_t in the prediction step, namely $X_{t|t-1}$, such that

$$\begin{aligned} \underline{y}_t &= z(X_t;\theta) + u_t \\ &\approx z(X_{t|t-1};\theta) + \frac{\delta z(X_t;\theta)}{\delta X_t}|_{X_t=X_{t|t-1}}(X_t - X_{t|t-1}) + u_t, \end{aligned} \tag{16}$$

where θ represents the set of parameters and the error term u_t has a diagonal covariance matrix

$$H(\theta) = diag(\sigma_\varepsilon^2(\tau_1), ..., \sigma_\varepsilon^2(\tau_N)), \tag{17}$$

since the innovation terms of the yield observations are independent. By defining

$$A_t(\theta) = z(X_{t|t-1};\theta) - \frac{\delta z(X_t;\theta)}{\delta X_t}|_{X_t=X_{t|t-1}} X_{t|t-1}, \tag{18}$$

$$B_t(\theta) = \frac{\delta z(X_t;\theta)}{\delta X_t}|_{X_t=X_{t|t-1}} X_{t|t-1}, \tag{19}$$

where the derivatives are calculated numerically, the measurement equation given by Eq. (16) can be presented in an affine form as

$$\underline{y}_t = A_t(\theta) + \begin{pmatrix} B_t^l(\theta) & B_t^m(\theta) \end{pmatrix} \begin{pmatrix} X_t^l \\ X_t^m \end{pmatrix} + u_t. \tag{20}$$

The state equation is

$$X_t = \Phi^0 + \Phi^1 X_{t-1} + \varepsilon_t, \tag{21}$$

where

$$\Phi_t^0 = (I - \exp(-\kappa^P \Delta t))\theta^P, \tag{22}$$

$$\Phi_t^1 = \exp(-\kappa^P \Delta t). \tag{23}$$

The linearisation is part of the update step of the Kalman filter, such that

$$X_t = X_{t|t-1} + \Sigma_{t|t-1} B_t(\theta)' F_t^{-1} \nu_t, \tag{24}$$

$$\Sigma_t = \Sigma_{t|t-1} - \Sigma_{t|t-1} B_t(\theta)' F_t^{-1} B_t(\theta) \Sigma_{t|t-1}, \tag{25}$$

where $B_t(\theta)$ is calculated as in Eq. (19). The error term ν_t is calculated directly,

$$\nu_t = \underline{y}_t - y_t^{implied}, \tag{26}$$

where $y_t^{implied}$ is the model-implied yield rate. Computing $y_t^{implied}$ requires numerical integration, as integration by parts and brute force analytical integration are unsuccessful (Krippner, 2012). The integration is univariate, with respect to τ only, and elementary. I compute $\omega(i)$, $B^f(i)$, and $A^f(i)$ for each grid point i in $[0.01, \tau_{max}]$, with step sizes of 0.01. Substituting into Eq. (5) to calculate the shadow forward rate $f_t(\tau)$ and subsequently into Eq. (9) to calculate

the ZLB forward rate $\underline{f}_t(i)$, I compute the model-implied yield rates as

$$y_t^{implied}(\tau) = \frac{0.01}{\tau} \sum_{i=1}^{\tau \cdot 100} \underline{f}_t(i). \tag{27}$$

Meanwhile, the covariance of the error term, F_t, is calculated using $B_t(\theta)$ from Eq. (19) as

$$F_t = cov(\nu_t) = B_t(\theta)\Sigma_{t|t-1}B_t(\theta)' + H(\theta). \tag{28}$$

For a yields-only model, the log likelihood of yield observations,

$$LL(\theta) = \sum_{t=1}^{T} \left(-\frac{N}{2}\log(2\pi) - \frac{1}{2}\log|F_t| - \frac{1}{2}\nu_t' F_t^{-1}\nu_t \right), \tag{29}$$

is maximised, following Christensen (2015).

In a macro-finance setting, the state vector is $X_t = (X_t^l, X_t^m)$, where $X_t^l = (L_t, S_t, C_t)$ and $X_t^m = (z_t, \pi_t, r_t)$. Thus, in the update step, X_t^m is updated with the macro factors derived by PCA. Following Ang and Piazzesi (2003) and Hamilton and Wu (2012), I maximise the joint log likelihood of yield and macro observations. By prediction error decomposition, the joint log likelihood function is given by

$$\begin{aligned} LL(\theta) = \sum_{t=1}^{T} & -\log|det(J_t)| - \frac{k}{2}\log -\frac{N}{2}\log(2\pi) \\ & - \frac{1}{2}\log(det(\Sigma_t)) - \frac{1}{2}(X_t - \Phi^0 - \Phi^1 X_{t-1})'(\Sigma_t)^{-1}(X_t - \Phi^0 - \Phi^1 X_{t-1}) \\ & - \frac{1}{2}\log\sum_{i=1}^{N} H_{i,i} - \frac{1}{2}\sum_{i=1}^{N}\frac{(u_{t,i})^2}{H_{i,i}}, \end{aligned} \tag{30}$$

where k is the number of states and J_t is the Jacobian matrix.

I use the maximised (joint) log likelihood and root mean squared error (RMSE) values to compare model variations. The Likelihood Ratio test is applied if models are nested and the level factor is stationary. A comprehensive overview of the EKF steps is given in Appendix B.

3.2 Stylised Facts

Key stylised facts of yield curves which term structure models should be able to replicate are the compression of short-term and intermediate yield volatility and the nonnegativity of yield rates in a ZLB environment. Re-estimating the models on a rolling window basis, I compute one-step ahead short rate and conditional yield volatility predictions following Christensen and Rudebusch (2016)'s steps. In the prediction step of the EKF for the ZLB-MF model, the conditional expectation of the shadow rate $E_t^P[s_{t+\tau}]$ is

$$E_t^P[s_{t+\tau}] = \begin{pmatrix} 1 & 1 & 0 & 0 & 0 & 0 \end{pmatrix} E_t^P[X_{t+\tau}], \tag{31}$$

since the instantaneous shadow rate is the sum of the level (L_t) and slope (S_t) factor, as in Eq. (1). The conditional covariance matrix of the shadow rate $V_t^P[s_{t+\tau}]$ is computed as

$$V_t^P[s_{t+\tau}] = \begin{pmatrix} 1 & 1 & 0 & 0 & 0 & 0 \end{pmatrix} V_t^P[X_{t+\tau}] \begin{pmatrix} 1 & 1 & 0 & 0 & 0 & 0 \end{pmatrix}', \tag{32}$$

where the conditional covariance matrix of the state vector,

$$V_t^P[X_{t+\tau}] = \int_0^\tau \exp(-\kappa^P s)\Sigma\Sigma' \exp(-\kappa^P s)' ds, \tag{33}$$

is already computed in the EKF. The short rate projections $E_t^P[r_{t+\tau}]$ are given by

$$E_t^P[r_{t+\tau}] = E_t^P[s_{t+\tau}] N\left(\frac{E_t^P[s_{t+\tau}]}{\sqrt{V_t^P[s_{t+\tau}]}}]\right) + \frac{1}{\sqrt{2\pi}}\sqrt{V_t^P[s_{t+\tau}]} \exp\left(-\frac{1}{2}\frac{(E_t^P[s_{t+\tau}])^2}{\sqrt{V_t^P[s_{t+\tau}]}}]\right). \tag{34}$$

For the ZLB model, the same formulas hold, except that $(1, 1, 0, 0, 0, 0)$ is replaced by $(1, 1, 0)$, since X_t only contains yield factors. For the AFNS-MF model, the instantaneous and shadow rate are equivalent, hence

$$E_t^P[r_{t+\tau}] = \begin{pmatrix} 1 & 1 & 0 & 0 & 0 & 0 \end{pmatrix} E_t^P[X_{t+\tau}]. \tag{35}$$

The one-step ahead predicted conditional yield volatilities are the square foot of

$$V_t^P[y_{t+1}^N(\tau)] = \frac{1}{\tau^2} B(\tau)' V_t^P[X_{t+1}] B(\tau), \tag{36}$$

where τ is the yield maturity and $B(\tau)$ is the factor loadings matrix. For the ZLB-MF and ZLB models, this is merely an approximation, since yields are nonlinear functions of the state variables and $B(\tau)$ is approximated by its first derivatives, as in Eq. (19). A more accurate computation method requires Monte Carlo simulations (Christensen and Rudebusch, 2016).

I limit my analysis to yearly re-estimations of the CF, IV, and IMF models based on a rolling window with the first in-sample period from January 1985 to December 2004. With this period, I predict January 2005. The final prediction is for January 2019. I compare the predicted volatilities with realised volatilities using the same data at a daily frequency. For the three-month, six-month, one-year, and two-year yield volatilities, I calculate the daily changes in interest rates for respectively the 91-, 182-, 365-, and 730-day period ahead on a rolling basis.

4 Data

This Chapter covers the models' input. Section 4.1 describes the yield rates and macroeconomic variables. Section 4.2 discusses summary statistics and visual analyses of the data. Section 4.3 discusses the factors extracted from these variables using principal component analysis.

4.1 Variables

Following Christensen and Rudebusch (2016), I obtain yield data with eight maturities (0.25, 0.5, 1, 2, 3, 5, 7, and 10 years) starting from January 1985. My sample ends in December

	Yield Rates					Policy	Inflation			Economic Activity			
	3M	1Y	3Y	5Y	10Y	FFR	Core CPI	Core PCE	Core PPI-F	IP	CU-N	UNEMP	EMP
Mean	0.034	0.038	0.043	0.047	0.054	0.037	2.69	2.24	1.95	2.04	-0.01	-0.83	1.18
Std	0.027	0.027	0.027	0.026	0.023	0.028	1.07	0.93	1.06	3.77	3.99	16.36	1.31
Skew	0.149	0.137	0.178	0.242	0.282	0.207	0.79	1.00	0.23	-1.85	-1.30	2.30	-1.86
Kurt	1.774	1.779	1.946	2.106	2.294	1.811	2.80	2.92	3.01	8.64	7.63	9.02	7.37
Lag 1	0.996	0.996	0.994	0.993	0.992	0.998	0.99	0.99	0.96	0.97	0.97	0.97	0.96
Lag 2	0.991	0.989	0.986	0.985	0.984	0.993	0.98	0.98	0.93	0.93	0.93	0.95	0.94
Lag 3	0.984	0.982	0.978	0.977	0.978	0.986	0.98	0.97	0.89	0.89	0.87	0.92	0.90

Table 1: Summary statistics of selected yield rates [3-month, 1-year, 3-year, 5-year, and 10-year] and macro variables [federal funds rate (FFR), Core Consumer Price Index (Core CPI), Core Personal Consumption Expenditure (Core PCE), Core Production Price Index for Finished Goods (Core PPI-F), Industrial Production Index (IP), Capacity Utilisation - NAICS (CU-N), Unemployment Rate (UNEMP), and Employment Level (EMP)] before normalisation. 'Core' implies the exclusion of high-volatility goods, e.g. energy and food. Inflation and economic activity variables represent annual differences in percentage. Central moments include the mean, standard deviation, skewness, and kurtosis. Autocorrelation coefficients are provided for the first, second, and third lag. The sample covers the period from January 1985 until December 2018 and the sampling frequency is monthly.

2018. The three- and six-month Treasury bill yields are from the H.15 series of the Federal Reserve Board (FRB) and the remainder are from the database of Gürkaynak et al. (2007)[1], both available on the FRB's website. Based on the monthly frequency of most macroeconomic data, I use the first available yeld observation of each month, resulting in 408 observations.

I use common macroeconomic variables in the literature (Ang and Piazzesi, 2003; Bauer and Rudebusch, 2016; Diebold et al., 2006; Krippner and Lewis, 2018)[2], sourced from the FRED database of the Federal Reserve Bank of St. Louis[3]. The policy rate is measured by the monthly effective federal funds rate. The second factor captures real economic activity through capacity utilisation, industrial production, unemployment rate, and employment level. The third factor, inflation, is measured by the Consumer Price Index (CPI), Personal Consumption Expenditure (PCE), and Producer Price Index (PPI). I incorporate core[4] and headline inflation measures. The inflation and economic activity variables represent annual differences in percentage. All macroeconomic variables are normalised before the principal component analysis (PCA).

4.2 Summary Statistics

On average, the yield curves are upward sloping, standard deviations of yields decrease with maturity, and yields are highly autocorrelated. Table 1 reports the summary statistics of selected variables prior to normalisation. Yield and policy rates are in decimals, following Christensen and Rudebusch (2016). Skewness is only slightly positive, between 0.137 (1Y) and 0.282 (10Y), and kurtosis is rather small, between 1.774 (3M) and 2.294 (10Y). Both skewness and kurtosis are generally increasing with maturity. The stylised fact that longer-maturity yields are more persistent is not supported in this data set, yet the differences are minimal. The macro variables are also highly persistent. The variation in means and standard deviations, ranging from 0.028 (FFR) to 16.36 (UNEMP), strongly suggests normalising the variables. As expected, inflation variables are somewhat positively skewed (0.79, 1.00, 0.23). Economic activity variables are

[1] Available at https://www.federalreserve.gov/PUBS/FEDS/2006//200628/200628abs.html

[2] The variables 'spot market commodity prices' and 'index of Help Wanted Advertising in Newspapers' of Ang and Piazzesi (2003) seem to be discontinued.

[3] Available at https://fred.stlouisfed.org/

[4] 'Core' implies the exclusion of high-volatility goods, such as energy and food.

	3M	1Y	5Y	FFR	Core CPI	Core PCE	PPI All	Core PPI-F	IP	CU-N	UNEMP	EMP
3M	1											
1Y	0.994	1										
5Y	0.945	0.965	1									
FFR	0.996	0.990	0.936	1								
Core CPI	0.799	0.806	0.838	0.799	1							
Core PCE	0.734	0.743	0.784	0.742	0.931	1						
PPI All	0.093	0.082	0.026	0.101	-0.042	0.138	1					
Core PPI-F	0.306	0.298	0.266	0.322	0.544	0.579	0.117	1				
IP	0.270	0.282	0.239	0.267	0.021	0.096	0.405	-0.294	1			
CU-N	-0.044	-0.024	-0.012	-0.040	-0.108	0.095	0.458	-0.211	0.815	1		
UNEMP	-0.131	-0.136	-0.050	-0.136	0.035	-0.068	-0.275	0.158	-0.771	-0.701	1	
EMP	0.402	0.411	0.320	0.406	0.214	0.268	0.193	-0.069	0.677	0.514	-0.874	1

Table 2: Cross-correlation coefficients of yield variables [3-month, 1-year, 3-year, 5-year, and 10-year yield rates], the federal funds rate (FFR), inflation variables [Core Consumer Price Index (Core CPI), Core Personal Consumption Expenditure (Core PCE), Production Price Index for All Commodities (PPI All), and Core Production Price Index for Finished Goods (Core PPI-F)], and economic activity variables [Industrial Production Index (IP), Industrial Production - NAICS (IP-N), Capacity Utilisation - NAICS (CU-N), Unemployment Rate (UNEMP), and Employment Level (EMP)]. 'Core' implies the exclusion of goods with high-volatility prices, e.g. energy and food. Inflation and economic activity variables are calculated as annual differences in percentage. The sample covers the period from January 1985 until December 2018 and the sampling frequency is monthly.

generally negatively skewed (-1.85, -1.30, -1.86), although the opposite holds for unemployment rates (2.30). Unlike inflation variables (2.80, 2.92, 3.01), economic activity variables have excess kurtosis (8.64, 7.63, 9.02, 7.37), implying fat tails in the distribution.

As expected, yield rates for different maturities have high cross-correlations, although long-term rates have less deep troughs, and short-term interest rates move closely with the federal funds rate (FFR). Table 2 presents the cross-correlation coefficients of selected variables before normalisation, while Fig. 1 and Fig. 2 depict their co-movement. Yields are highly correlated with consumption-based inflation variables and moderately correlated with the employment level (EMP). CPI and PCE are rather stable, while PPI variables are more volatile. Headline PPI variables have low correlation with core inflation variables in general. In the economic activity group, EMP and capacity utilisation (CU-N) are only moderately correlated (0.514). The spikes in inflation and economic activity variables correspond to recessions in the early 1990s, early 2000s, and between 2007 and 2009. Concerning intergroup correlations, consumption-based inflation variables co-move with FFR (Fig. 2). EMP is moderately correlated with FFR (0.406), as is PPI All with other production-related measures, IP (0.405) and CU-N (0.458).

4.3 Principal Component Analysis

Consistent with the literature, I use three yield factors and the first principal component (PC) of each group of macro variables. Conducting PCA on the monthly yields, I find that the first three PC's explain 99.97% of the variation. For the inflation group, 62.2% of the variation is explained by the first PC, while the second explains 26.7%. The first PC loads positively on all variables, while the second loads negatively on Core CPI, Core PCE, and Core PPI-F, and has near-zero loadings on CPI and PCE. Regarding the economic activity group, 82.3% and 10.6% of the variation are explained by the first and second PC's, respectively. The first PC loads positively on all variables, except for UNEMP. The second PC has near-zero loadings on the IP variables, loads positively on CU variables and UNEMP, but negatively on EMP. Fig. 3

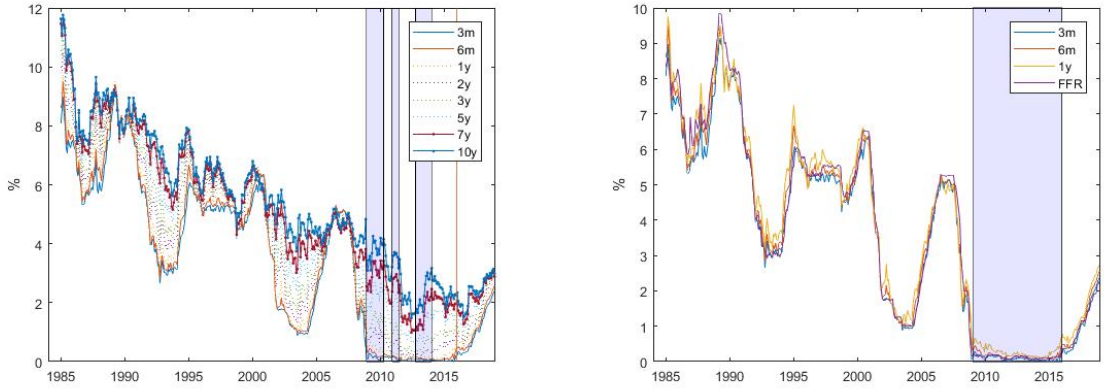

Figure 1: Monthly yield rates [3-month, 6-month, 1-year, 2-year, 3-year, 5-year, 7-year, 10-year], and the federal funds rate (FFR) before normalisation. The shaded areas in the left figure represent periods of Quantitative Easing. The shaded area in the right figure represents the period of the Zero Interest Rate Policy. The sample covers the period from Jan 1985 until Dec 2018.

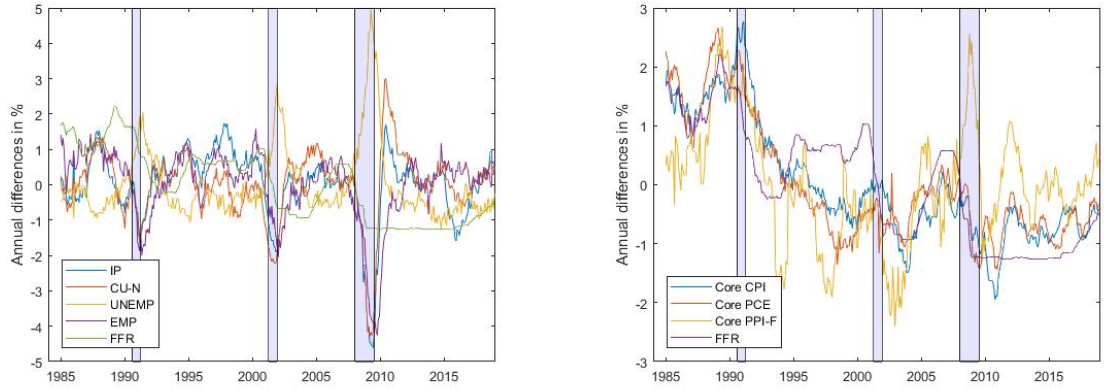

Figure 2: Left: monthly effective federal funds rates (FFR) and economic activity data [Industrial Production Index (IP), Capacity Utilisation - NAICS (CU-N), Unemployment Rate (UNEMP), and Employment Level (EMP)]. Right: FFR and inflation data [Core Consumer Price Index (Core CPI), Core Personal Consumption Expenditure (Core PCE), and Production Price Index for Finished Goods (PPI-F)] before normalisation. 'Core' implies the exclusion of goods with high-volatility prices, e.g. energy and food. Inflation and economic activity variables are calculated as annual differences in percentage. The shaded areas represent recessions in the early 1990s, early 2000s, and between 2007 and 2009. The sampling period is from Jan 1985 until Dec 2018.

presents the development of the economic activity and inflation variables, as well as their first PC's. The graphs show that the first PC's capture much of the variation.

5 Results

This Chapter presents the results of model estimation for the six variations presented in Chapter 2. Section 5.1 highlights some caveats of the estimation methodology. Section 5.2 compares the results of the model variations. Section 5.3 discusses the added value of incorporating macroeconomic information by comparing the in-sample fit of ZLB-MF and ZLB models (Section 5.3.1), by presenting an analysis on term structure dynamics (Section 5.3.2), and by elaborating on factor interactions based on impulse responses (Section 5.3.3). In Section 5.4, I assess whether the ZLB-MF models can replicate the stylised facts in a ZLB environment. Finally, Section 5.5 discusses the robustness of the results using a subset of variables and a subsample.

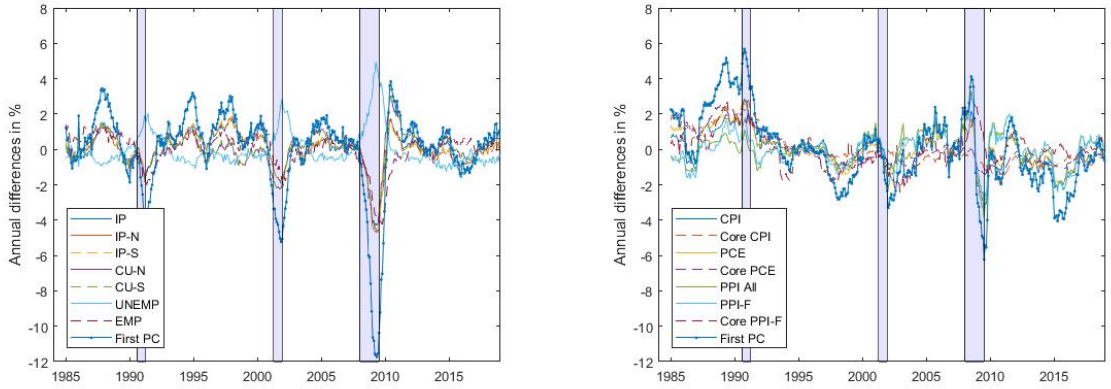

Figure 3: Left: economic activity time series [Industrial Production Index (IP), Industrial Production (IP-N, IP-S), Capacity Utilisation (CU-N, CU-S), Unemployment Rate (UNEMP), and Employment Level (EMP)] and their first principal component. Right: inflation time series [Consumer Price Index (CPI, Core CPI), Personal Consumption Expenditure (PCE, Core PCE), Production Price Index for All Commodities (PPI All), Production Price Index for Finished Goods (PPI-F, Core PPI-F)] and their first principal component. 'Core' implies the exclusion of goods with high-volatility prices, e.g. energy and food. Inflation and economic activity variables are calculated as annual differences in percentage. The shaded areas represent recessions in the early 1990s, early 2000s, and between 2007 and 2009. The sampling period is from Jan 1985 until Dec 2018 and the sampling frequency is monthly.

5.1 Initialisation

Although the Nelder-Mead simplex method is commonly used to optimise the ZLB model (Christensen and Rudebusch, 2015; Krippner, 2013), convergence to the global optimum is sensitive to the initialisation values. Table 3 reports the results for re-estimating the ZLB model, as described by Eq. (11) and (12) in Section 2.1, on Christensen and Rudebusch (2016)'s data set, consisting of weekly yield rates with the same eight maturities from January 4, 1985, until October 31, 2014. For Panel A, I initialise at the reported AFNS parameter estimates[5] and find that the algorithm converges to the global optimum, as the parameter estimates approximate those reported by Christensen and Rudebusch (2016)[6]. For Panel B, I initialise at the same values, except $\sigma^2_{i,i} = 0.01$ and $h_{j,j} = 0.01$. Most notably, the κ^P estimates differ up to the first decimal (e.g. $\kappa^P_{1,1} = 0.2737$ versus $\kappa^P_{1,1} = 0.5907$), and the maximum log likelihood differ considerably (71408.6 versus 67725.5). I derive similar conclusions when changing other parameter values. Given the sensitivity to initialisation values, I opt for a constrained optimisation algorithm with multiple trial starting points[7].

It is possible that parameter estimates do not diverge from the initialisation values. Table 4 provides the estimated ZLB parameters for my data set. For Panel A and B, I initialise at respectively the ZLB and AFNS parameter estimates reported by Christensen and Rudebusch (2016) (e.g. $\kappa^P_{2,1} = 0.1953$ and $\kappa^P_{2,1} = 0.3390$). The log likelihood values are nearly identical (17888.0 versus 17887.8), while the κ^P parameters differ up to the first decimal (e.g. $\kappa^P_{2,1} = 0.2229$ versus $\kappa^P_{2,1} = 0.3374$). Hence, the log likelihood function could be rather flat around the optimum. Panel C reports the parameter estimates for the same initialisation as Panel A, except $\sigma^2_{i,i} = 0.1$ and $h_{j,j} = 0.01$. The parameter estimates differ considerably, especially λ

[5]Estimates are reported in Table 1 in Christensen and Rudebusch (2016)'s article.
[6]Estimates are reported in Table 2 in Christensen and Rudebusch (2016)'s article.
[7]'GlobalSearch' in Matlab is based on 'fmincon', which utilises the interior-point algorithm, and generates trial points using the scatter search algorithm.

Panel A

κ^P	$\kappa^P_{.,1}$	$\kappa^P_{.,2}$	$\kappa^P_{.,3}$	θ^P		Σ
$\kappa^P_{1,.}$	10^{-7}	0	0	0	σ_{11}	0.0069
$\kappa^P_{2,.}$	0.2737	0.2942	-0.4404	0.0261	σ_{22}	0.0112
$\kappa^P_{3,.}$	0	0	0.4979	-0.0230	σ_{33}	0.0257

Panel B

κ^P	$\kappa^P_{.,1}$	$\kappa^P_{.,2}$	$\kappa^P_{.,3}$	θ^P		Σ
$\kappa^P_{1,.}$	10^{-7}	0	0	0	σ_{11}	0.0110
$\kappa^P_{2,.}$	0.5907	0.5228	-0.7348	0.0241	σ_{22}	0.0066
$\kappa^P_{3,.}$	0	0	0.8044	-0.0562	σ_{33}	0.0209

Table 3: Parameter estimates for the yields-only shadow-rate model for Christensen and Rudebusch (2016)'s data set of weekly yield rates from Jan 4, 1985 to Oct 31, 2014. For Panel A, I initialise at the AFNS estimates from Table 1 in Christensen and Rudebusch (2016)'s paper. For Panel B, I do the same, except $\sigma^2_{i,i} = 0.01$ and $h_{j,j} = 0.01$. For Panel A and B, λ is 0.4699 and 0.5032, respectively. Using the extended Kalman filter, the log likelihood is maximised at 71408.6 and 67725.5 for Panel A and B, respectively. Run time is 10470 seconds (2.9 hours) and 13659 seconds (3.8 hours) for Panel A and B, respectively.

(0.5465), $\sigma^2_{2,2}$ (0.1087), and $\sigma^2_{3,3}$ (0.1384). The latter two are close to the initialisation values instead. Since the log likelihood is lower (16670.7), the algorithm converges to a local optimum.

Given the aforementioned issues, I proceed with three initialisation points, one uninformed and two informed, to estimate the ZLB-MF model, as described in Section 2.2. For the uninformed initialisation, $\kappa^P = I, \theta^P = 0.1, \lambda = 0.5, \sigma^2_{i,i} = 0.1, \sigma_{i,j} = 0$, and $h_{j,j} = 0.01$, which are of reasonable magnitudes considering the parameter estimates of Christensen and Rudebusch (2016) as well as the variables' standard deviations and autocorrelations. $\kappa^P = I$ ensures that its eigenvalues and eigenvectors are real, such that the covariance matrix required in the prediction step of the EKF,

$$Q = \int_0^{\Delta t} \exp\left(-\kappa^P s\right)\Sigma\Sigma' \exp\left(-\kappa^P s\right)' ds, \tag{37}$$

can be calculated analytically, following Fisher and Gilles (1996). The first informed initialisation is derived by estimating the AFNS-MF model, as described in Section 2.3, using the uninformed initialisation and in turn estimating the ZLB-MF model using the AFNS-MF parameter estimates as initialisation values. If AFNS-MF parameter estimates are good approximations of ZLB-MF estimates, this could substantially decrease estimation time, as the linearity in the AFNS-MF model implies less computational burden. The second informed initialisation uses a two-step OLS-VAR estimation. In the first step, the factor loadings of the Dynamic Nelson-Siegel (DNS) model, $B(\lambda)$, are regressed cross-sectionally on yield observations, as in

$$y_t(\tau) = L_t + \left(\frac{1 - e^{-\lambda\tau}}{\lambda\tau}\right) S_t + \left(\frac{1 - e^{-\lambda\tau}}{\lambda\tau} - e^{-\lambda\tau}\right) C_t = B(\lambda) \cdot \hat{\beta}_t, \tag{38}$$

for each time t. The time series of $\hat{\beta}_t$ is used in the second step to estimate the VAR model

$$\hat{\beta}^{aug}_{t+1} = \Phi_{0,t} + \Phi_{1,t} \cdot \hat{\beta}^{aug}_t, \tag{39}$$

where $\hat{\beta}^{aug}_{t+1} = (\hat{\beta}_{1,t}, \hat{\beta}_{2,t}, \hat{\beta}_{3,t}, z_t, \pi_t, r_t)$. Re-writing Eq. (22) and (23), the initialisation values for the mean-reversion matrix κ^P and long-term mean vector θ^P are computed using estimates of

Panel A

κ^P	$\kappa^P_{.,1}$	$\kappa^P_{.,2}$	$\kappa^P_{.,3}$	θ^P		Σ
$\kappa^P_{1,.}$	10^{-7}	0	0	0	σ_{11}	0.0082
$\kappa^P_{2,.}$	0.2229	0.3046	-0.4197	0.0150	σ_{22}	0.0147
$\kappa^P_{3,.}$	0	0	0.5299	-0.0199	σ_{33}	0.0264

Panel B

κ^P	$\kappa^P_{.,1}$	$\kappa^P_{.,2}$	$\kappa^P_{.,3}$	θ^P		Σ
$\kappa^P_{1,.}$	10^{-7}	0	0	0	σ_{11}	0.0082
$\kappa^P_{2,.}$	0.3374	0.4219	-0.4808	0.0147	σ_{22}	0.0147
$\kappa^P_{3,.}$	0	0	0.6251	-0.0238	σ_{33}	0.0267

Panel C

κ^P	$\kappa^P_{.,1}$	$\kappa^P_{.,2}$	$\kappa^P_{.,3}$	θ^P		Σ
$\kappa^P_{1,.}$	10^{-7}	0	0	0	σ_{11}	0.0123
$\kappa^P_{2,.}$	0.1196	0.2725	-0.3545	-0.0050	σ_{22}	0.1087
$\kappa^P_{3,.}$	0	0	0.5653	0.0266	σ_{33}	0.1384

Table 4: Parameter estimates for the yields-only shadow-rate model. For Panel A and B, I initialise at the ZLB estimates from Table 2 and Table 1 respectively in Christensen and Rudebusch (2016)'s paper. Panel C uses the same initialisation as Panel A, except $\sigma^2_{i,i} = 0.1$ and $h_{j,j} = 0.01$. For Panel A, B, and C, λ is 0.4756, 0.4735, and 0.5465, respectively. Using the extended Kalman filter, the log likelihood is maximised at 17888.0, 17887.8, and 16670.7 for Panel A, B, and C, respectively. The sampling period is from Jan 1985 until Dec 2018. Run time is 2202 seconds (0.61 hours), 2774 seconds (0.77 hours), and 3688 seconds (1.0 hour) for Panel A, B, and C, respectively.

Φ_0 and Φ_1, such that

$$\kappa^P = -\frac{\log(\Phi_1)}{\Delta t}, \tag{40}$$

$$\theta^P = (I - \Phi_1)^{-1}\Phi_0. \tag{41}$$

The initialisation for Σ is the covariance of the error term of Eq. (39). I maintain $h_{j,j} = 0.01$. λ is estimated by repeating the procedure for different values between 0.01 and 1. The λ value yielding the lowest total squared error is selected. A disadvantage of the OLS-VAR initialisation is the inability to readily transform the restrictions on κ^P and θ^P, which are presented in Section 2.4, to the VAR model. Thus, the two-step method yields invalid initialisation values for the B-CR and KL models, given the non-stationary level factor.

The uninformed and AFNS-MF initialisations yield high in-sample fit of the ZLB-MF models. It is not surprising that the OLS-VAR initialisation yields the lowest fit, as the two-step estimates are computed assuming no restrictions. Table 5 reports the (joint) log likelihood and RMSE values for the AFNS-MF models using uninformed initialisation and for the ZLB-MF models using uninformed (UN), AFNS-MF, and OLS-VAR initialisation. In terms of joint log likelihood, the IF model's fit seems to be independent of the initialisation (37452.7, 35944.4, 36739.4). The IV (28543.0) and KL (27681.4) models have the highest fit using AFNS-MF initialisation. For all other models, the uninformed initialisation is superior. In terms of log likelihood and RMSE, the uninformed initialisation provides higher in-sample fit than the AFNS-MF initialisation for the IMF model. Under other restrictions, the differences are small.

Concerning Christensen and Rudebusch (2016)'s claim that shadow-rate term structure models yield higher in-sample fit than their affine versions, for macro-finance models, I find that this depends on the restrictions and initialisation values. As shadow-rate models are more complex than their affine versions, even more so when incorporating macro factors, the algorithm

	Joint Log Likelihood				Log Likelihood				RMSE			
	AFNS-MF	ZLB-MF			AFNS-MF	ZLB-MF			AFNS-MF	ZLB-MF		
		UN	AFNS-MF	OLS-VAR		UN	AFNS-MF	OLS-VAR		UN	AFNS-MF	OLS-VAR
CF	22305.3	24338.8	20861.65	3663.6	9918.6	12766.3	14121.1	6563.2	1.17	0.17	0.22	1.14
IV	27252.9	26045.0	28543.0	3702.9	14749.7	14904.9	14753.4	6594.9	0.18	0.18	0.19	1.14
IMF	32690.2	39363.7	32395.6	11493.2	12203.7	14084.3	12438.5	7828.0	0.30	0.21	0.47	1.26
IF	35977.9	37452.7	35944.4	36739.4	14460.3	14144.2	14540.7	5078.2	0.21	0.22	0.21	2.89
B-CR	23718.7	28184.3	26014.1	-	3412.2	6105.7	5738.4	-	1.91	1.48	1.58	-
KL	26487.9	25943.3	27681.4	-	7756.7	7654.4	8173.5	-	1.46	1.45	1.28	-

Table 5: Joint ($f(y, X_m)$) and individual ($f(y)$) log likelihood values, and root mean squared errors (RMSE) for the macro-finance affine (AFNS-MF) models using uninformed initialisation and for the macro-finance shadow-rate (ZLB-MF) models using uninformed (UN), AFNS-MF, and OLS-VAR initialisations. The uninformed initialisation means $\kappa^P = I, \theta^P = 0.1, \lambda = 0.5, \sigma^2_{i,i} = 0.1, \sigma_{i,j} = 0$, and $h_{j,j} = 0.01$. The AFNS-MF and OLS-VAR initialisation respectively use the AFNS-MF and OLS-VAR parameter estimates. In the IV, IF, B-CR, and KL models, Σ is diagonal. In the IMF model, the upper-right and lower-left corner of κ^P and Σ are blocks of zero. The IF model has a diagonal κ^P matrix. In the B-CR and KL models, the level factor is a unit-root process, meaning $\kappa^P_{1,1} = 10^{-7}$ and $\theta^P_1 = 0$. In the B-CR model, $\kappa^P_{1,2} = \kappa^P_{1,3} = \kappa^P_{3,1} = \kappa^P_{3,2} = 0$. In the KL model, $\kappa^P_{1,6} = \kappa^P_{2,6} = \kappa^P_{3,6} = \kappa^P_{4,6} = \kappa^P_{5,6} = 0$ and $\kappa^P_{4,3} = \kappa^P_{5,3} = \kappa^P_{6,3} = 0$. The B-CR, KL, and IF models are restricted versions of the IV model. All models are restricted versions of the CF model. The sampling period is from Jan 1985 until Dec 2018.

is more likely to converge to a local optimum. This finding supports using an algorithm with multiple starting points, which helps to mitigate this issue.

Assuming uninformed initialisation, ZLB-MF models generally have higher in-sample fit than AFNS-MF models. The evidence is especially strong in terms of joint log likelihood, although in-sample fit is higher for the AFNS-MF models under the IV and KL restrictions. In terms of log likelihood and RMSE, the ZLB-MF models have higher fit in the least restricted case and under the IMF, B-CR, and KL restrictions.

Using the iterated extended Kalman filter (IEKF) could further improve estimation performance, as Krippner (2015) finds that it produces more reliable and accurate maximum likelihood estimations from different starting points. Specifically, an IEKF-based optimisation algorithm could yield a materially higher likelihood value with different parameter estimates than one based on the EKF. An alternative method for mitigating the sensitivity to initialisation values to employ the Expectation Maximisation (EM) procedure for several iterations and using the estimates as initialisation values for the Maximum Likelihood (ML) procedure. The Expectation Maximisation-based extended Kalman filter (EM-EKF) is a novel method in the literature of shadow-rate models. Employing the EM-EKF for the models presented in Section 2.4 requires accounting for parameter restrictions and goes beyond the scope of my research. Thus, I provide preliminary steps to be continued in future research in Appendix D. I suggest to describe the model in terms of the parameters Φ_0 and Φ_1, which the EM algorithm updates. Imposing restrictions directly on Φ_0 and Φ_1, rather than on κ^P and θ^P, eliminates the need to transform variables between the final EM-step and the ML procedure, greatly facilitating this method.

This sensitivity issue highlights a potential underlying problem regarding model identification. For GATSMs, the maximum number of parameters that can be uniquely identified with econometric estimation is $1 + 2.5N + 1.5N^2$, where N is the number of state variables (Krippner, 2015). Estimating more parameters than this maximum hinders the optimisation algorithm converging to a unique set of estimates. This also seems to apply to the shadow-rate model. While Krippner (2015) discusses the identification of yields-only shadow-rate models, the problem remains for models with macro factors. In future research, insights from existing literature on identified GATSMs (Dai and Singleton, 2000; Hamilton and Wu, 2012; Joslin et al.,

2011) could be applied to address model identification in the context of shadow-rate models.

Concluding, given the sensitivity of the results to initialisation values, the parameter estimates and log likelihood values should not be considered exact and the results presented in this paper should be interpreted in broad terms. The general conclusion is that using a ZLB-MF model can increase in-sample fit relative to an AFNS-MF model, given the right initialisation and when employing an algorithm with multiple starting points.

5.2 Parameter Restrictions

In general, imposing restrictions on parameters improves the models' in-sample fit. Section 2.4 describes each set of parameter restrictions. In terms of the joint log likelihood of yield and macro observations, Table 5 shows that the fit is highest under the IMF and IF restrictions and that each set of restrictions yields a higher fit than the least restricted case (CF). A Likelihood Ratio test rejects the IF restrictions in favour of the IMF restrictions, with a test statistic of 3822 and critical value 28.9, given 18 parameter restrictions. In terms of the log likelihood of yield observations, the IV model performs on par with the IMF and IF models. A Likelihood Ratio test rejects the IF restrictions in favour of the IV restrictions, with a test statistic of 98.6 and critical value 43.8, given 30 parameter restrictions.

In addition to in-sample fit, I assess whether the restrictions yield reasonable parameters, which affect the filter's output. Table 6 reports the parameter estimates for the ZLB-MF models using uninformed initialisation. The estimates for the AFNS-MF and OLS-VAR initialisations are provided in Appendix E. The standard errors can be computed as the square root of the diagonal elements of the inverse Hessian matrix. However, the log likelihood function is likely to be rather flat around the optimum. Computing the standard errors results in infinite values and they are thus not meaningful to report[8]. Instead, I compute impulse response functions to evaluate the extent of the effects of one factor on itself and on other factors.

Based on the uninformed initialisation, the IV and IMF restrictions yield reasonable parameter estimates. Focusing on the mean-reversion parameters, the diagonal elements of κ^P typically have the highest values. Hence, the dynamics of a factor are mostly driven by its mean-reversion process rather than by changes in other factors. Often, the diagonal elements of κ^P are higher for macro factors, suggesting stronger mean reversion, i.e. lower persistence, than yield factors. $\kappa^P_{i,j} = 1$ means that the difference between the independent factor j's long-term average and j's current value has a one-to-one effect on the change in the dependent factor i. Often, the diagonal values of κ^P exceed one, indicating that the effect on the change in i is more than one-to-one. This reproduces a strong mean-reversion process. Since the estimated model could be less persistent than the true process due to finite-sample bias, imposing the unit-root process on the level factor could help to overcome this (Christensen and Rudebusch, 2016). However, in the B-CR and KL models, the diagonal values of κ^P, which exceed one, may not yield sufficient persistence. This is confirmed by Fig. 4, which shows the impulse responses of one unit shock to the yield factors on themselves for the six model variations. Appendix F presents all impulse response functions for completeness. The B-CR and KL models depict the least persistence of shock effects in yield factors, as does the IF model's curvature factor. The

[8] I compute the Hessian using the 'fminunc' function or manually by approximating the gradients.

	CF Model	IV Model	IMF Model	IF Model	B-CR Model	KL Model
Mean-reversion						
$\kappa^P_{1,1}$	0.2059	0.1326	0.9321	0.0146	10^{-7}*	10^{-7}*
$\kappa^P_{2,2}$	0.3758	0.7620	0.6174	0.1903	1.2493	1.2486
$\kappa^P_{3,3}$	1.4380	1.3084	0.2809	17.8470	1.2497	1.2497
$\kappa^P_{4,4}$	6.0032	1.5930	1.5420	22.3709	1.2494	1.2500
$\kappa^P_{5,5}$	2.8753	1.5950	1.2808	11.3891	1.2500	1.2491
$\kappa^P_{6,6}$	3.2945	1.5960	1.2712	7.7814	1.2494	1.2498
Long-term average						
θ_1	0.1247	0.1070	0.0860	0.1125	0*	0*
θ_2	-0.0367	-0.0199	-0.0032	-0.0214	0.1224	0.1120
θ_3	-0.0297	0.0034	0.0253	-0.0173	0.1261	0.1311
θ_4	-0.3248	0.3109	0.0593	0.1162	0.1252	0.1259
θ_5	0.1893	0.1000	0.1056	0.1162	0.1248	0.1250
θ_6	0.5075	0.6341	0.1196	0.1162	0.1249	0.1250
State innovation						
$\sigma^2_{1,1}$	0.0163	0.0099	0.0005	0.0052	0.0003	0.0002
$\sigma^2_{2,2}$	0.0121	0.0097	0.0005	0.0041	$1.3 \cdot 10^{-5}$	$5.8 \cdot 10^{-5}$
$\sigma^2_{3,3}$	0.0177	0.0072	0.0010	$1.0 \cdot 10^{-5}$	$3.2 \cdot 10^{-5}$	0.0002
$\sigma^2_{4,4}$	$1.8 \cdot 10^{-5}$	0.0048	$-1.5 \cdot 10^{-8}$	$1.0 \cdot 10^{-5}$	$1.5 \cdot 10^{-5}$	0.0003
$\sigma^2_{5,5}$	0.0043	0.0042	$-1.65 \cdot 10^{-6}$	$1.0 \cdot 10^{-5}$	$7.6 \cdot 10^{-5}$	$7.4 \cdot 10^{-5}$
$\sigma^2_{6,6}$	0.0293	0.0040	$-5.7 \cdot 10^{-11}$	$1.0 \cdot 10^{-5}$	$6.0 \cdot 10^{-5}$	0.0016
Loading parameter						
λ	0.6434	0.4964	0.4633	0.7378	0.4999	0.4997

Table 6: Parameter estimates for the macro-finance shadow-rate models using uninformed initialisation ($\kappa^P = I, \theta^P = 0.1, \lambda = 0.5, \sigma^2_{i,i} = 0.1, \sigma_{i,j} = 0, h_{j,j} = 0.01$). * denotes a restriction. In the IV, IF, B-CR, and KL models, Σ is diagonal. In the IMF model, the upper-right and lower-left corner of κ^P and Σ are blocks of zero. The IF model has a diagonal κ^P matrix. In the B-CR and KL models, the level factor is a unit-root process, meaning $\kappa^P_{1,1} = 10^{-7}$ and $\theta^P_1 = 0$. In the B-CR model, $\kappa^P_{1,2} = \kappa^P_{1,3} = \kappa^P_{3,1} = \kappa^P_{3,2} = 0$. In the KL model, $\kappa^P_{1,6} = \kappa^P_{2,6} = \kappa^P_{3,6} = \kappa^P_{4,6} = \kappa^P_{5,6} = 0$ and $\kappa^P_{4,3} = \kappa^P_{5,3} = \kappa^P_{6,3} = 0$. The sampling period is from Jan 1985 until Dec 2018.

highest mean-reversion parameters are estimated for the curvature and macro factors under the IF restrictions. Imposing independent factors pushes estimates upwards, reducing persistence, except for the level and slope. The IF model's curvature graph in Fig. 4 supports this.

Concerning the long-term averages (θ^P), I find that imposing restrictions can change their signs. This is most clear for the economic activity factor, which is only negative in the least restricted case (CF). Under the unit-root restriction, all long-term averages converge to the same value, approximately 0.125, and the sign of θ^P_2 changes. The estimates for variance ($\sigma^2_{i,i}$) and covariance terms ($\sigma_{i,j}$) are of similar magnitude as those reported by Christensen and Rudebusch (2016). Estimates for $\sigma^2_{i,i}$ decrease when κ^P restrictions are imposed, as in the IMF, IF, B-CR, and KL models. A smaller state innovation implies that a larger part of the state dynamics is explained by its mean-reversion, thus κ^P plays a greater role. The estimates for the measurement noise parameters $h_{j,j}$ are generally quite small, as expected given the standard deviations of the yield rates. Estimates of λ are high under the IF restrictions (0.7378) and in the least restricted case (0.6434). A low value would indicate that the slope factor operates almost as a level factor for the fit to the cross section of yields (Christensen and Rudebusch, 2015). In all other models, estimates of λ are approximately 0.5, consistent with the literature.

Generally, the uninformed initialisation results in more reasonable estimates than the AFNS-

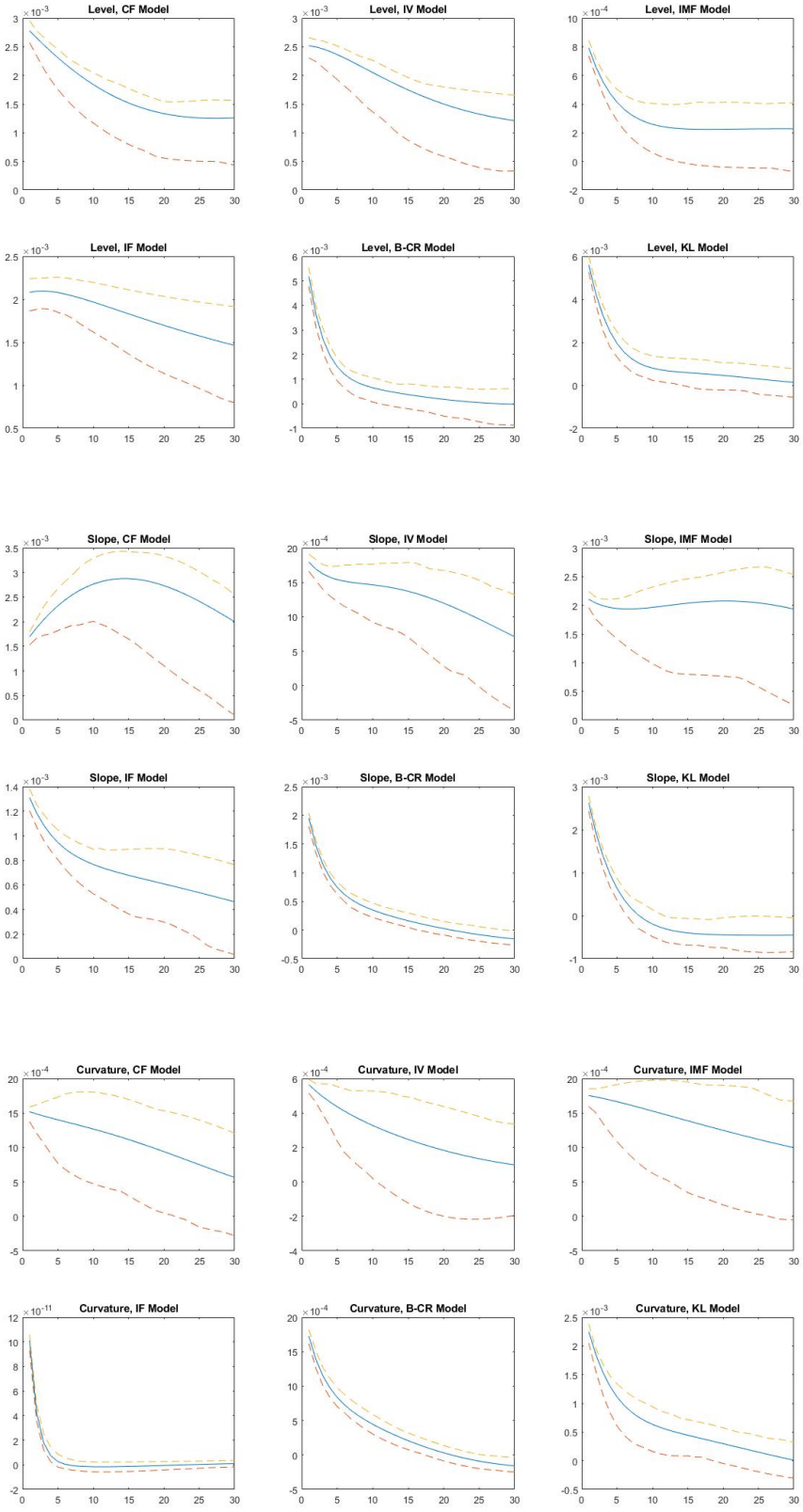

Figure 4: Impulse response functions of the yield factors of the six macro-finance shadow-rate models: correlated factors (CF), independent variances (IV), independent macro-finance factors (IMF), independent factors (IF), Christensen and Rudebusch (2016)'s macro-extended model (B-CR), and Krippner and Lewis (2018)'s model (KL). The first and second rows present the level factor, the third and fourth present the slope factor, the fifth and sixth present the curvature factor. The vertical axis measures the effect of one unit of shock to the factor after k periods, where $k = 1, ..., 30$ months on the horizontal axis. 95% confidence bounds are estimated using Monte Carlo simulation. The sampling period is from Jan 1985 until Dec 2018.

	UN				AFNS-MF				OLS-VAR			
	CF	IV	IMF	IF	CF	IV	IMF	IF	CF	IV	IMF	IF
$\kappa^P_{1,1}$	0.2059	0.1326	0.9321	0.0146	1.1923	-0.7193	1.4264	0.0096	2.1948	2.1948	2.1473	39.4891
$\kappa^P_{2,2}$	0.3758	0.7620	0.6174	0.1903	1.1696	2.2374	0.9342	0.0042	1.7275	1.7274	1.7541	27.1372
$\kappa^P_{3,3}$	1.4380	1.3084	0.2809	17.8470	1.1664	6.2163	0.9341	0.0898	1.2701	1.2701	1.2280	69.7389
$\kappa^P_{4,4}$	6.0032	1.5930	1.5420	22.3709	1.2994	5.4441	1.8717	9.9981	0.1759	0.1759	0.2083	68.7564
$\kappa^P_{5,5}$	2.8753	1.5950	1.2808	11.3891	1.3271	8.0474	2.6629	9.6925	0.6180	0.6179	0.6319	68.6925
$\kappa^P_{6,6}$	3.2945	1.5960	1.2712	7.7814	1.3075	6.1480	2.1339	9.6925	1.0867	1.0867	1.0916	68.9861

Table 7: κ^P estimates for the macro-finance shadow-rate models using uninformed (UN) initialisation ($\kappa^P = I, \theta^P = 0.1, \lambda = 0.5, \sigma^2_{i,i} = 0.1, \sigma_{i,j} = 0$, and $h_{j,j} = 0.01$), AFNS-MF initialisation, and OLS-VAR initialisation. In the IV and IF models, Σ is diagonal. In the IMF model, the upper-right and lower-left corner of κ^P and Σ are blocks of zero. The IF model has a diagonal κ^P matrix. The sampling period is from Jan 1985 until Dec 2018.

MF and OLS-VAR initialisations. To illustrate this and the parameter estimates' sensitivity to intialisation values, Table 7 shows the differences between the diagonal elements of κ^P for different initialisations. The AFNS-MF initialisation yields higher mean-reversion estimates, except for the CF model's macro factors and the IF model's yield factors, which are highly persistent. Overall, κ^P estimates under the IF restrictions are less extreme. The negative estimate of $\kappa^P_{1,1}$ under the IV restrictions is striking. It suggests that the level factor moves farther away from the mean, rather than reverting. The AFNS-MF initialisation also yields more non-diagonal κ^P elements exceeding one, specifically for the IV and IMF restrictions, and high estimates of θ^P values for the macro factors in the IV model. Estimates of λ are consistently between 0.4 and 0.5.

Relative to the uninformed initialisation, the OLS-VAR initialisation results in more extreme parameter estimates. This includes higher non-diagonal κ^P elements, especially concerning the effects on changes in macro factors. This is expected given the high initialisation values for κ^P. The same can be said about $\sigma^2_{i,i}$. Estimates of θ^P are mostly negative, and specifically under the IF restrictions, have extreme values. The estimate of λ is also extremely high for the IF model. Under the IF restrictions, the joint log likelihood values of the uninformed and AFNS-MF initialisation are quite similar, although the parameter estimates differ considerably. This analysis shows that although the IF restrictions result in high in-sample fit, the parameter estimates are not in line with expectations. Thus, assuming independent factors is likely incorrect.

Overall, the IF, B-CR, and KL restrictions seem to be the least preferred. This conclusion is supported by a graphical depiction of the evolution of yield factors over time, given in Fig. 5 for the ZLB-MF models and in Appendix G for the AFNS-MF and ZLB models. The graphs representing the B-CR and KL models (fifth and sixth row) and the curvature factor of the IF model (fourth row, right graph) differ considerably from the graphs produced by Christensen and Rudebusch (2016)'s algorithm[9]. Specifically, the graphs in Fig. 5 show less variation, which seems unreasonable given that the sample encompasses a pre-ZLB, ZLB, and post-ZLB period.

5.3 Macroeconomic Information

I evaluate whether incorporating macroeconomic information improves the shadow-rate term structure models in three ways. 5.3.1 compares the in-sample fit of ZLB-MF and ZLB models. Section 5.3.2 compares the term structure dynamics of the IV and IMF models to evaluate

[9] Available at https://cepr.org/event/1854/Codes_slides.

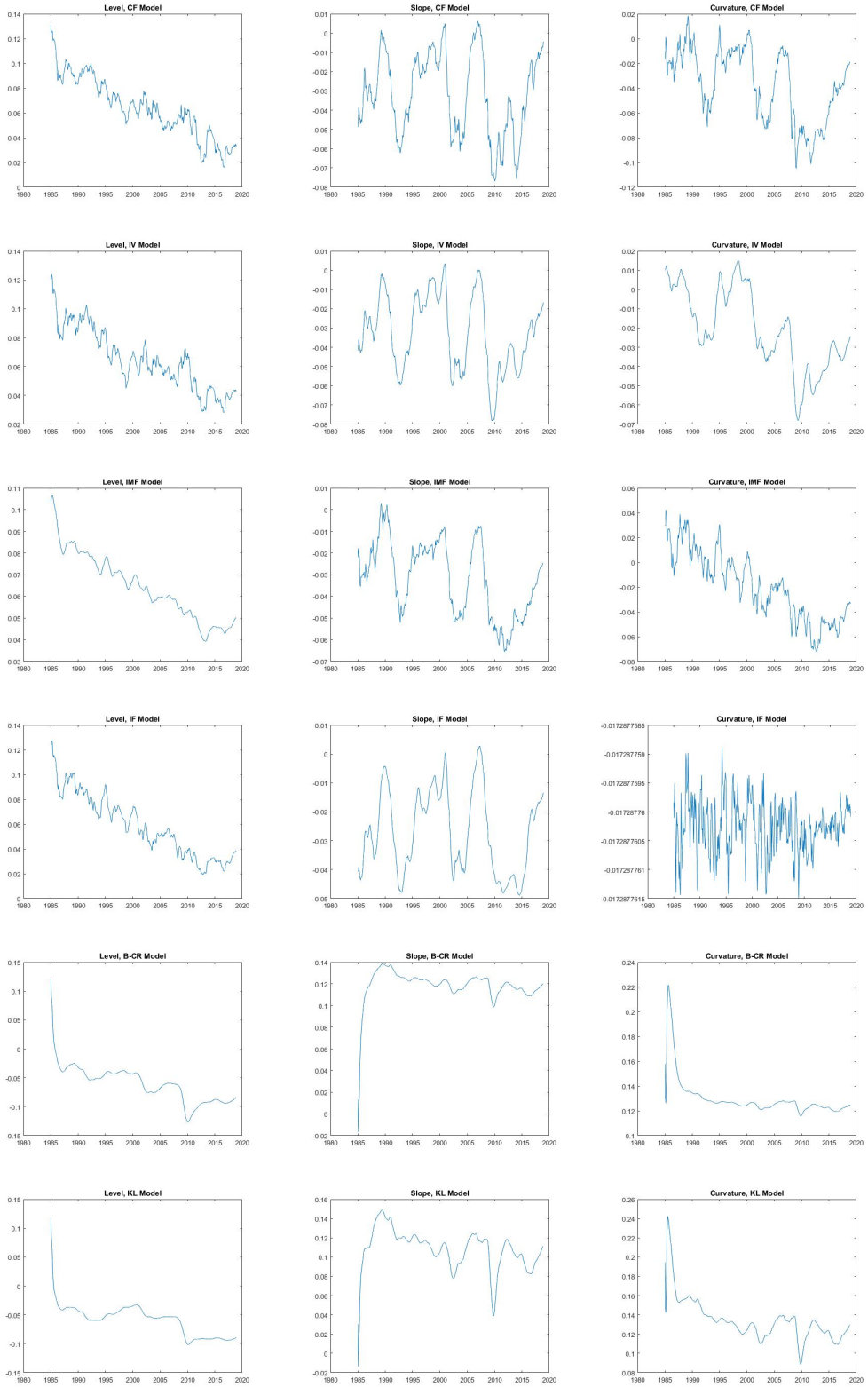

Figure 5: Evolution of the yield factors (level, slope, curvature) as filtered by the extended Kalman filter. The first until the sixth rows respectively depict six macro-finance shadow-rate models: correlated factors (CF), independent variance (IV), independent macro-finance factors (IMF), independent factor (IF), Christensen and Rudebusch (2016)'s macro-extended model (B-CR), and Krippner and Lewis (2018)'s model (KL). The sampling period is from Jan 1985 until Dec 2018.

	ZLB		ZLB-MF	
	Log Likelihood	RMSE	Log Likelihood	RMSE
CF	18218.8	0.28	18243.0	0.04
IV	17736.4	0.76	17853.7	0.04
IF	17894.0	0.25	-	-
B-CR	15605.8	0.72	-	-

Table 8: Maximised log likelihood of yield observations and implied root mean squared errors (RMSE) for the yields-only (ZLB) and macro-finance (ZLB-MF) shadow-rate models using uninformed initialisation ($\kappa^P = I, \theta^P = 0.1, \lambda = 0.5, \sigma^2_{i,i} = 0.1, \sigma_{i,j} = 0$, $h_{j,j} = 0.01$). In the IV, IF, and B-CR models, Σ is diagonal. The IF model has a diagonal κ^P matrix. In the B-CR model, the level factor is a unit-root process, , meaning $\kappa^P_{1,1} = 10^{-7}$ and $\theta^P_1 = 0$, while $\kappa^P_{1,2} = \kappa^P_{1,3} = \kappa^P_{3,1} = \kappa^P_{3,2} = 0$. The sampling period is from Jan 1985 until Dec 2018.

whether allowing macro-finance interactions (IV) affects how the term structure evolves over time relative to imposing no interactions (IMF). Section 5.3.3 presents an analysis of macro-finance linkages in the IV model using impulse response functions.

5.3.1 In-Sample Fit

Table 5 and the two left columns in Table 8 suggest that the ZLB-MF models have lower in-sample fit in terms of log likelihood than the ZLB models. The left columns in Table 8 report the maximised log likelihood of yield observations and RMSE values for the ZLB models, described in Section 2.1 and estimated using uninformed initialisation. The KL and IMF models, which are identical to respectively the IV and CF models in a yields-only context, are excluded. Possibly, macroeconomic information adds noise and worsens the model's fit. However, this conclusion would be premature, as the ZLB-MF models are optimised in terms of the *joint* log likelihood of yield and macro observations. To check whether the ZLB-MF models can outperform the ZLB models in terms of the log likelihood of yield observations, I re-fit several models to maximise this log likelihood, which are reported in Table 8, in addition to the RMSE values.

Maximising in terms of the log likelihood of yield observations results in very similar log likelihood values between the ZLB-MF and ZLB models. Moreover, adding macroeconomic information to the ZLB-MF model improves the in-sample fit in terms of RMSE. When comparing the parameter estimates of the ZLB-MF models in Table 6 and those of ZLB models in Table 9[10], the latter show higher persistence of the yield factors in the least restricted case and under the IF restrictions, while the opposite holds true for the IV restrictions. Summarising, the ZLB-MF models have at least equal in-sample fit as the ZLB models.

5.3.2 Term Structure Dynamics

Yield factors move differently with interest rates of various maturities. This is linked to how monetary policy actions affect the shape of the yield curve. The level factor is considered to affect interest rates of different maturities equally, while the slope and curvature factors mainly affect short-term and intermediate interest rates, respectively (Wu, 2003). Fig. 6 depicts the yield factors of the IV and IMF models, along with the effective policy rate and interest rates of a short (three-month), intermediate (two-year), and long (ten-year) maturity. It also highlights

[10]Similar to Tables 6 and 7, computing the standard errors using the Hessian results in infinite values. They are thus not meaningful to report in Table 9. I compute the Hessian using the 'fminunc' function or manually by approximating the gradients.

	CF Model	IV Model	IF Model	B-CR Model
Mean-reversion				
$\kappa^P_{1,1}$	0.1581	0.2639	0.0140	10^{-7}*
$\kappa^P_{2,2}$	0.2171	1.4442	0.0665	0.6964
$\kappa^P_{3,3}$	0.5932	1.65311	0.5186	1.9533
Long-term average				
θ_1	0.0491	0.3087	0.0785	0*
θ_2	0.1767	0.0774	-0.0667	-0.5597
θ_3	0.0449	0.0380	-0.2011	-0.1620
State innovation				
$\sigma^2_{1,1}$	0.0108	0.0091	0.0081	0.0042
$\sigma^2_{2,2}$	0.0093	0.0163	0.0140	0.1437
$\sigma^2_{3,3}$	0.0288	0.0292	0.0279	0.1023
Loading parameter				
λ	0.5009	0.5180	0.5101	0.5457

Table 9: Parameter estimates for the yields-only shadow-rate models using uninformed initialisation ($\kappa^P = I, \theta^P = 0.1, \lambda = 0.5, \sigma^2_{i,i} = 0.1, \sigma_{i,j} = 0, h_{j,j} = 0.01$). * denotes a restriction. In the IV, IF, and B-CR models, Σ is diagonal. The IF model has a diagonal κ^P matrix. In the B-CR model, the level factor is a unit-root process, meaning $\kappa^P_{1,1} = 10^{-7}$ and $\theta^P_1 = 0$, while $\kappa^P_{1,2} = \kappa^P_{1,3} = \kappa^P_{3,1} = \kappa^P_{3,2} = 0$. The sampling period is from Jan 1985 until Dec 2018.

periods of Quantitative Easing (QE) and the interest rate hike at the end of 2015, which signifies the end of the Fed's Zero Interest Rate Policy. In the IV model, the term structure evolves assuming interactions between yield and macro factors, unlike the IMF model.

Focusing on the ZLB-MF model, the level factor closely follows the ten-year interest rate under the IV restrictions (first row in Fig. 6), while the dynamics of the slope and curvature factors follow the three-month rate and to some extent the two-year rate during the pre-ZLB period. However, during the ZLB period, interest rates of short and intermediate maturities remain flat, whereas the factors continue to show up- and downward movements. Under the IMF restrictions (second row in Fig. 6), the level factor is less volatile than the ten-year rate. The slope factor's graph resembles that of the three-month rate and to some extent the two-year rate. The curvature factor somewhat follows the two-year rate, yet has more extreme spikes.

Monetary policy events affect the short end of the yield curve directly, since short-term interest rates move closely with the federal funds rate. When the Federal Reserve adjusts the policy rate based on macroeconomic considerations, such as inflation targets, long-term interest rates are affected, since expectations about future inflation, economic activity and the further development of the policy rate also change (Wu, 2003). This suggests that macroeconomic information helps to explain both the short and long end of the yield curve. This explains why the relation between the level factor, which affects interest rates of different maturities equally, and long-term interest rates is strong in the IV model, where yield and macro factors are assumed to interact. However, when yield and macro factors are assumed to be independent, i.e. in the IMF model, this relation largely disappears and the level factor's graph becomes much flatter, showing little to no impact from monetary policy events.

The slope factor is related to monetary policy tightening, i.e. decreasing money supply. Tightening pushes short-term interest rates upwards for a short time period, yet they revert soon due to anti-inflationary effects (Wu, 2003). As long-term interest rates are affected by

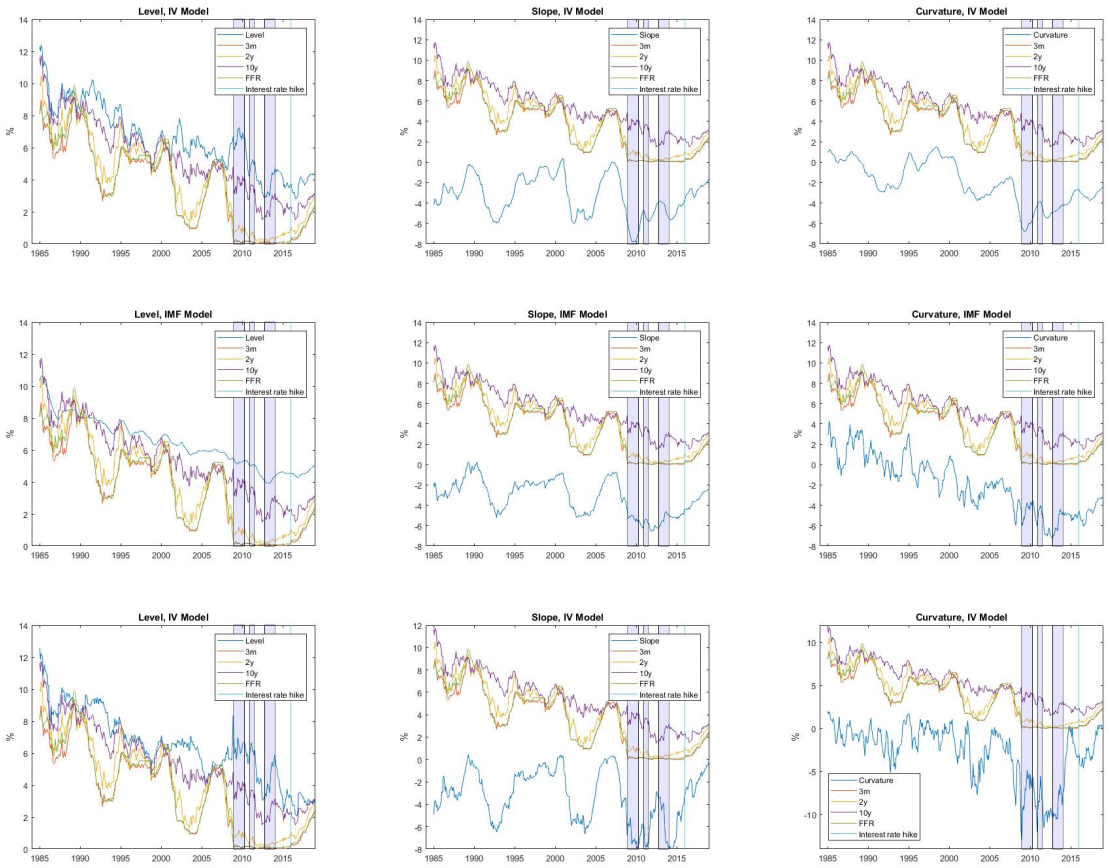

Figure 6: Time series of selected interest rates (three-month, two-year, ten-year), the effective policy rate (FFR), and the shadow-rate model's yield factors (level, slope, curvature) as filtered by the extended Kalman filter. The first, second, and third row respectively represent the macro-finance independent variances (IV) model, the macro-finance independent macro-finance factors (IMF) model, and the yields-only independent variances (IV) model. The shades areas represent the three phases of Quantitative Easing. The vertical line signifies the end of the Zero Interest Rate Policy. The sampling period is from Jan 1985 until Dec 2018.

expectations of the future short rate, they only increase marginally. Overall, short-term interest rates increase more than long-term rates, causing the yield curve to become less steep. Fig. 6 shows that the slope factor moves with short-term interest rates during the pre-ZLB period. During the ZLB period, short-term interest rates remain flat and near-zero. Through the purchase of long-maturity assets, QE pushes the prices of these securities upwards, resulting in lower long-term interest rates and, hence, the slope declines. The IV model's slope factor follows this development, as the graph shows within the shaded areas.

Analysing the ZLB model under the IV restrictions (third row in Fig. 6), the level factor and long-term interest rate show less co-movement relative to the ZLB-MF model under the same restrictions. The slope factor is more volatile, although it shows substantial drops during periods of QE. The curvature factor behaves quite erratically. In short, a shadow-rate model with macro-finance interactions, i.e. the ZLB-MF model under IV restrictions, can reproduce two important monetary policy effects on the term structure's dynamics: the link between the level factor and long-term rates and the decline of the slope factor during periods of QE.

5.3.3 Impulse Response Functions

Using impulse response functions, I analyse the interactions between factors, to examine macro-finance linkages reproduced by the ZLB-MF model. The confidence bounds are derived by Monte Carlo simulation of a VAR(1) model, where the autoregressive variables are the filtered states produced by the EKF[11]. Fig. 7 and 8 respectively show the effects of shocks to yield factors on macro factors and vice versa for the independent variances (IV) model. I compare them to findings in previous research on macro-finance linkages (Ang and Piazzesi, 2003; Dewachter and Lyrio, 2006; Diebold et al., 2006).

Focusing on the yields-to-macro interactions, a shock to the level factor causes an initial increase in the macro factors. The effect is persistent as it requires at least 30 months to disappear completely. For the inflation factor and policy rate, the effect remains stable or even accumulates over time and does not show obvious signs of reverting within the 30-month window. This relation between the level and macro factors is consistent with Diebold et al. (2006)'s findings. They argue that an increase in the level factor, which they interpret as the future perceived inflation, lowers ex ante real interest rate, computed as the difference between the policy rate and level factor. The Fed raises the nominal policy rate to accommodate a portion of the expected rise in inflation. This should slow economic activity and inflation, yet the graphical illustration of this effect is mainly convincing for economic activity. The effect on inflation seems to be more persistent.

A shock to the slope factor causes an immediate increase in the policy rate, which accumulates for roughly ten months. Subsequently, the effect starts to revert, yet the mean impulse response shows that it could be rather persistent and not disappear completely within the 30-month period. Diebold et al. (2006) provide two different theories for the initial increase. First, it could represent the Fed's reaction to yields by setting the policy rate. Second, in anticipation of actions by the Fed, the yield rates could be responding to macroeconomic information before these actions can take place, assuming a delay in monetary policy decision-making. The latter theory requires some level of predictability and transparency of monetary policy, for which the Fed has been taking measures since the 1990s (FRBSF, 2006). Considering all other effects of shocks to the yield factors on macro factors, the confidence bounds are too wide to make reliable inferences. Diebold et al. (2006) also do not find additional linkages.

Considering the macro-to-yields interactions, my findings partly diverge from those of Diebold et al. (2006). Regarding the response of the level factor to a positive inflation shock, although the mean shows a positive effect, it could be negligible given the lower bound of the confidence interval. Diebold et al. (2006) find an obvious, long-lasting effect, while Dewachter and Lyrio (2006) conclude that inflation primarily determines the short end of the yield curve. My results are in line with those of Dewachter and Lyrio (2006). Perhaps long-run inflation expectations are more firmly anchored in this sample, causing future inflation expectations to be less sensitive to inflation shocks. Meanwhile, the level factor shows an initial decrease following a shock to the economic activity factor and policy rate. The mean impulse responses indicate reversion after ten months or more, yet the confidence intervals are rather wide. The link between the level factor and policy rate can be explained in two ways (Diebold et al., 2006). Monetary

[11] I use the 'irf' function in the Econometrics Toolbox of Matlab.

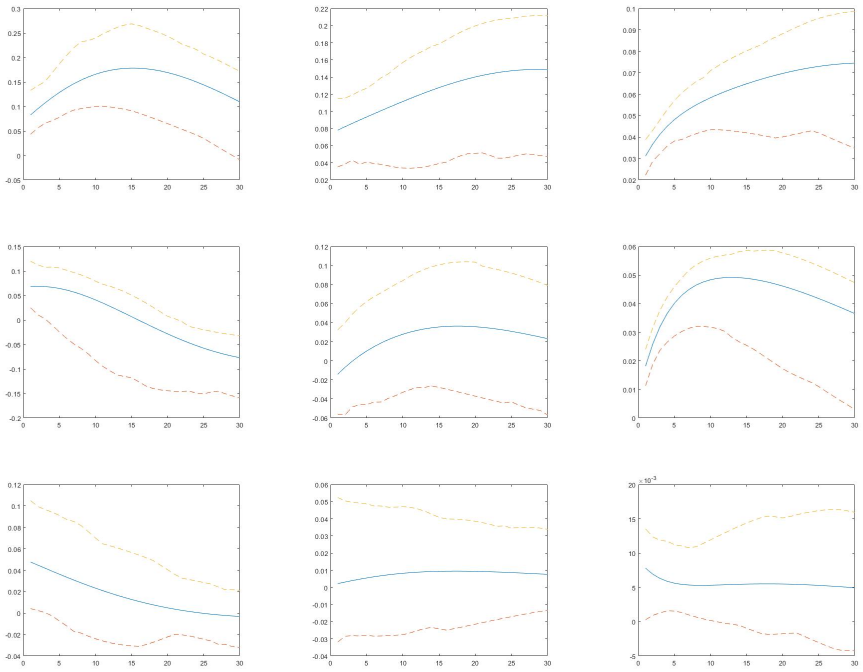

Figure 7: Impulse response functions of the independent variances (IV) macro-finance shadow-rate model estimated on the full sample (Jan 1985 until Dec 2018). From top to bottom, the row represents the effect of one unit of shock to the level, slope, and curvature factor. From left to right, the column represents the effect on economic activity, inflation, and policy rate. The vertical axis measures the effect of one unit of shock to the factor after k periods, where $k = 1, ..., 30$ months on the horizontal axis. 95% confidence bounds are estimated using Monte Carlo simulation.

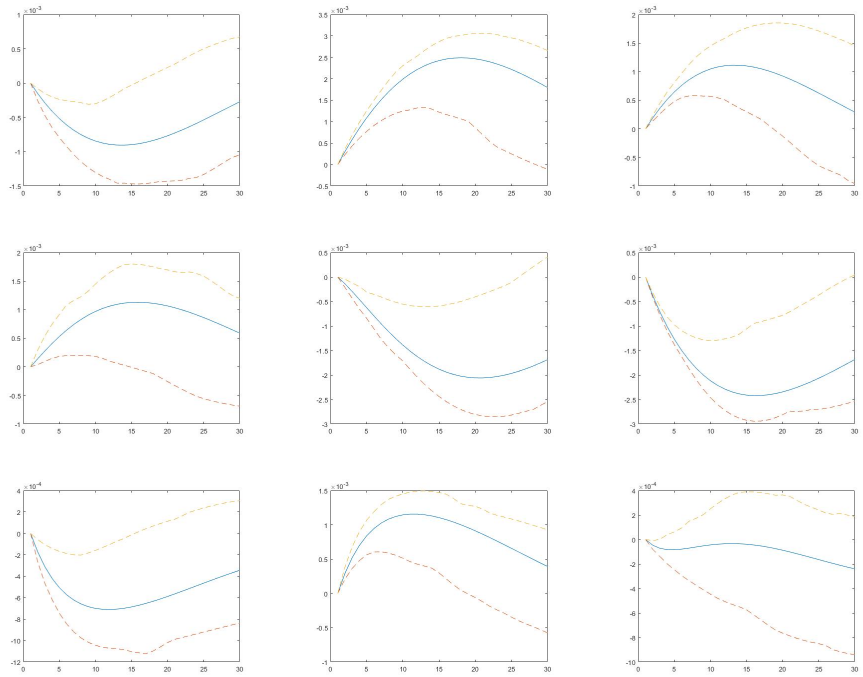

Figure 8: Impulse response functions of the independent variances (IV) macro-finance shadow-rate model estimated on the full sample (Jan 1985 until Dec 2018). From top to bottom, the row represents the effect of one unit of shock to economic activity, inflation, and policy rate. From left to right, the column represents the effect on the level, slope, and curvature factor. The vertical axis measures the effect of one unit of shock to the factor after k periods, where $k = 1, ..., 30$ months on the horizontal axis. 95% confidence bounds are estimated using Monte Carlo simulation.

policy tightening could signal a lower inflation target, thereby lowering inflation expectations. Alternatively, tightening could boost inflation expectations and thus the level factor by signalling the Fed's concerns about overheating and rising inflation. Given the negative relation in this sample, there is more support for the first theory. However, Dewachter and Lyrio (2006)'s output gap factor only affect short and intermediate maturities, which my results contradict. It seems that economic activity shocks also affect long-term interest rates.

Positive shocks to the economic activity factor and policy rate initially increase the slope factor. A positive shock to economic activity has a more persistent effect, while the effect of a policy rate shock could revert excessively, with a negative effect as the final result. Instead, an inflation shock results in a decrease of the slope factor, which is rather persistent. Diebold et al. (2006) relate the effects on the slope factor to monetary policy, as the policy rate is adjusted according to macroeconomic developments, the inflation target, and other macroeconomic objectives, such as output. Given positive economic activity and inflation shocks, the policy rate is adjusted upwards, thus raising the short end of the term structure and changing the yield curve's tilt. Ang and Piazzesi (2003) also find that inflation accounts for a large portion of the dynamics of the slope factor through rising short-term interest rates. However, the mean impulse response of an inflation shock on the slope factor moves in an opposite direction than theorised, although the upper bound is close to zero.

The curvature factor increases slightly following a positive shock to the economic activity factor and decreases following a positive inflation shock, whereby the latter effect shows more persistence. This finding also diverges from the literature. Diebold et al. (2006) find little response in the curvature factor following macro shocks, while Dewachter and Lyrio (2006) suggest that the curvature factor represents the monetary policy stance. It captures policy actions beyond endogenous responses to inflation deviations and the output gap, as the slope factor already captures such business cycle conditions.

The difference between my findings regarding macro-finance interactions compared to previous research could be partially attributed to the presence of the ZLB. As shown before in Fig. 6, during the ZLB period, short-term rates remain flat, while yield factors continue to evolve. Since short-term rates are constrained, the presence of the ZLB could diminish the link between the slope and macro factors. Meanwhile, as intermediate rates are unconstrained, being farther from the ZLB, there could be a stronger link between the curvature and macro factors. Krippner and Lewis (2018) argue that usual measures of the slope understate the degree of monetary accommodation in the ZLB period due to the constraint on shorter-maturity rates, thereby distorting associated macroeconomic outcomes relative to the unconstrained period.

Adding macroeconomic variables changes the behaviour of some of the ZLB model's impulse response functions. Fig. 9 depicts the yield factors' own-dynamics, in a macro-finance model, which I compare to a yields-only model, captured by Fig. 10. A macro-finance model produces effects of level and slope shocks on the curvature, and no effects of curvature shocks on the level and slope. Moreover, the level factor does not show obvious responses to shocks in other yield factors. Fig. 10 clearly shows that the yields-only model produces the opposite effects, as the curvature does not respond to level and slope shocks. Meanwhile, the level responds to both slope and curvature shocks. A curvature shock also affects the slope. In the macro-finance

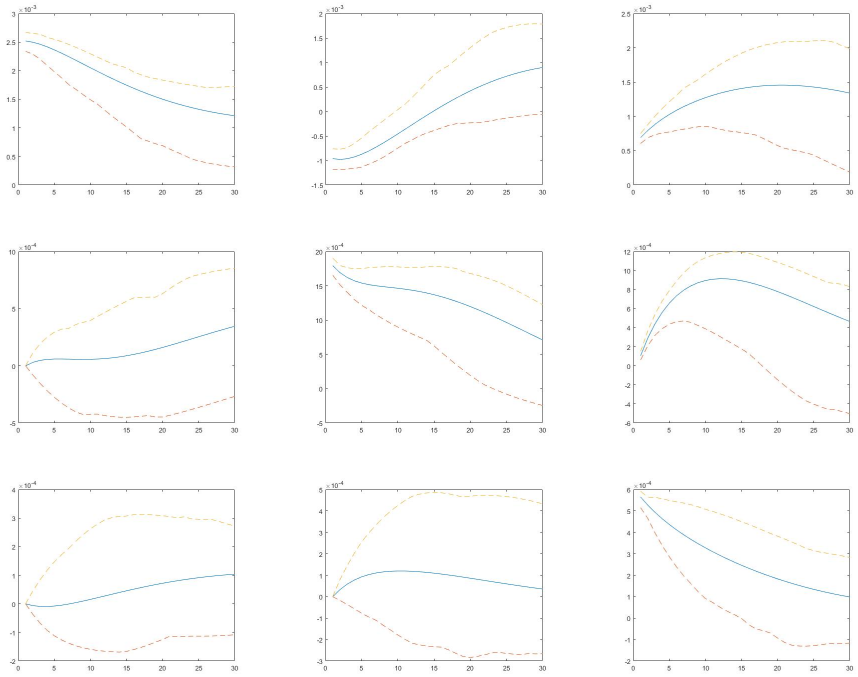

Figure 9: Impulse response functions of the independent variances (IV) macro-finance shadow-rate model estimated on the full sample (Jan 1985 until Dec 2018). From top to bottom, the row represents the effect of one unit of shock to the level, slope, and curvature factor. From left to right, the column represents the effect on the level, slope, and curvature factor. The vertical axis measures the effect of one unit of shock to the factor after k periods, where $k = 1, ..., 30$ months on the horizontal axis. 95% confidence bounds are estimated using Monte Carlo simulation.

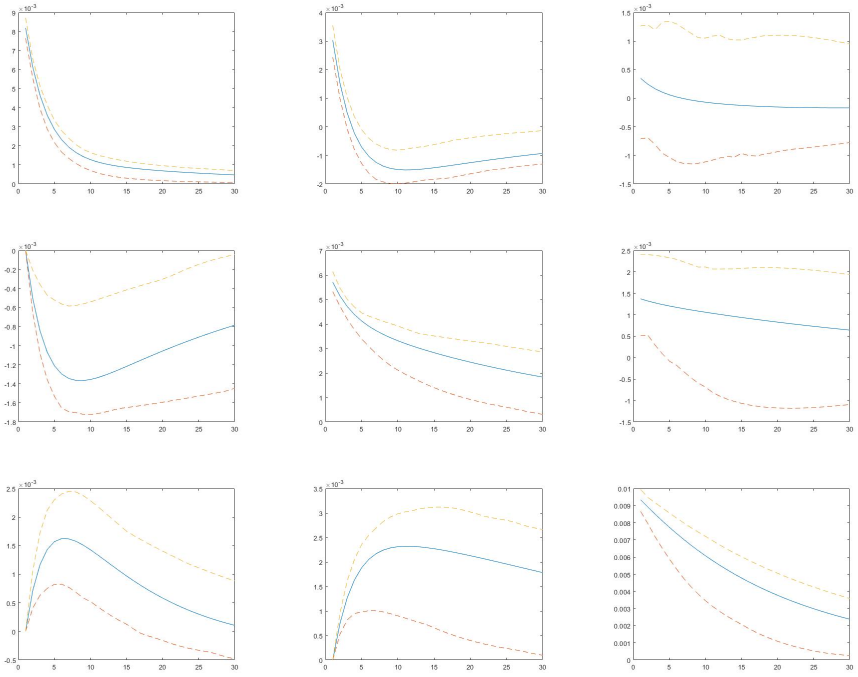

Figure 10: Impulse response functions of the independent variances (IV) yields-only shadow-rate model estimated on the full sample (Jan 1985 until Dec 2018). From top to bottom, the row represents the effect of one unit of shock to the level, slope, and curvature factor. From left to right, the column represents the effect on the level, slope, and curvature factor. The vertical axis measures the effect of one unit of shock to the factor after k periods, where $k = 1, ..., 30$ months on the horizontal axis. 95% confidence bounds are estimated using Monte Carlo simulation.

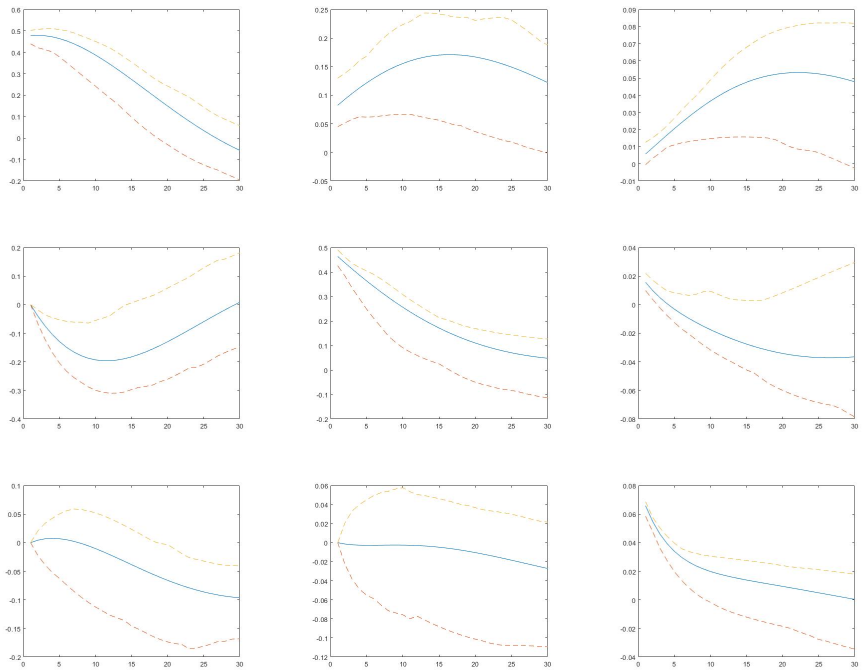

Figure 11: Impulse response functions of the independent variances (IV) macro-finance shadow-rate model estimated on the full sample (Jan 1985 until Dec 2018). From top to bottom, the row represents the effect of one unit of shock to economic activity, inflation, and policy rate. From left to right, the column represents the effect on economic activity, inflation, and policy rate. The vertical axis measures the effect of one unit of shock to the factor after k periods, where $k = 1, ..., 30$ months on the horizontal axis. 95% confidence bounds are estimated using Monte Carlo simulation.

model, a shock to the level factor is much more persistent and causes an initial decrease in the slope, which reverts to zero or becomes positive over time. The decrease in the slope can be explained by the loosening (tightening) of monetary policy, which lowers (increases) short-term interest rates, thus making the curve more (less) steep (Diebold et al., 2006). Instead, in Fig. 10, it causes an initial increase, which quickly becomes negative and slowly reverts to zero.

Considering the macro factors' own-dynamics, as shown in Fig. 11, a positive shock to the economic activity factor yields small increases in the inflation factor and policy rate. The first effect can be attributed to economic growth and the latter as a monetary policy response to macroeconomic conditions given certain inflation and output targets, among others. An inflation shock causes a small initial jump in the policy rate, which quickly reverts to zero. This suggests that a monetary policy response to an inflation shock in the form of tightening, i.e. a policy rate increase, is temporary. Perhaps the anti-inflationary effects of such a policy rate adjustment are realised rather quickly.

Concluding, I find several impulse responses to be substantial, persistent, and significant. Moreover, most dynamics between yield and macro factors reflect important macro-finance linkages in line with economic theory. I thus argue that these linkages should be incorporated in the shadow-rate model. My findings also suggest that the ZLB constraint affects how the slope and curvature are linked to macro factors. In addition, the yields-only model produces own-dynamics that are not consistent with existing literature, especially considering the level and slope factor's responses to shocks of other yield factors.

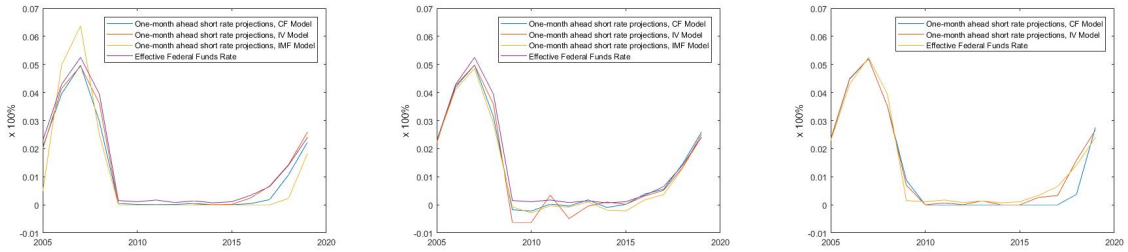

Figure 12: One-month ahead short rate predictions using rolling window re-estimations of the correlated factors (CF), independent variances (IV), and independent macro-finance factors (IMF) models. From left to right, the columns represent the macro-finance shadow-rate (ZLB-MF), macro-finance affine (AFNS-MF), and yields-only shadow-rate (ZLB) models, respectively. The in-sample period is 20 years, the first starting from Jan 1985 until Dec 2004, predicting Jan 2005. The final prediction is for Jan 2019.

5.4 Stylised Facts

The ZLB-MF, AFNS-MF, and ZLB models differ in terms of how well they can reproduce two key stylised facts of yield curves in a ZLB environment. Fig. 12 depicts the one-step ahead short rate projections, for which the computations are presented in Section 3.2[12], and the effective policy rate. Appendix H provides graphical illustrations of the underlying yield factor predictions. The expected short rate is never negative for the ZLB-MF and ZLB model, unlike the AFNS-MF model, which thus cannot replicate the nonnegativity of interest rates.

In terms of forecast accuracy, the IV model outperforms the CF and IMF models, and the ZLB-MF models outperform the ZLB models. The projections in Fig. 12 are in line with Fig. 1, as interest rates remain near the ZLB until the interest rate hike at the end of 2015. Among the ZLB-MF models, the IMF model has a considerably higher peak. The IMF and CF models both show a delayed lift-off from the ZLB. Among the AFNS-MF models, the IV model produces the most negative interest rate predictions. Similar to the macro-finance setting, the ZLB model under the CF restrictions shows a delayed lift-off. Unlike the ZLB-MF and AFNS-MF model, the expected short rate of the ZLB model does not immediately reach its the target rate in 2009, when the Fed's Zero Interest Rate Policy commenced. All in all, the ZLB-MF models seem to forecast the most accurately. Table 10 provides the RMSE values of these forecasts and confirms this, as the ZLB-MF model has lower RMSE values than the ZLB models. Overall, the ZLB-MF IV model yields the highest forecast accuracy (0.46).

Consistent with the literature, I find that the AFNS-MF models are unable to capture yield volatility dynamics between ZLB and pre- or post-ZLB periods, unlike the ZLB-MF and ZLB models. The predicted conditional yield volatilities of ZLB-MF models are the most consistent with realised volatilities. Fig. 13 depicts the predicted conditional yield volatility and realised volatility for the three-month, six-month, one-year, and two-year maturities. Among the ZLB-MF models, the IV model seems to replicate the realised volatility at short maturities best, while it is much less accurate for intermediate maturities, albeit all model variations underestimate volatility for the two-year maturity in the pre- and post-ZLB periods. Concerning the AFNS-MF models, all model variations fail to replicate the up- and downward movements of the realised volatilities. The ZLB models are better able to capture these dynamics relative to the

[12]For the first in-sample period, I use uninformed initialisation. For each next period, I use the parameter estimates of the previous period to initialise the algorithm.

	ZLB	AFNS-MF	ZLB-MF
CF	2.48	1.07	1.72
IV	0.79	1.80	0.46
IMF	-	1.85	9.53

Table 10: Root mean squared error (RMSE) values for one-month ahead short rate predictions using rolling window re-estimations of the correlated factors (CF), independent variances (IV), and independent macro-finance factors (IMF) models. From left to right, the columns represent the yields-only shadow-rate (ZLB), macro-finance shadow-rate (ZLB-MF), and macro-finance affine (AFNS-MF) models, respectively. The errors are computed based on the monthly effective federal funds rate (in %). The in-sample period is 20 years, the first starting from Jan 1985 until Dec 2004, predicting Jan 2005. The final prediction is for Jan 2019.

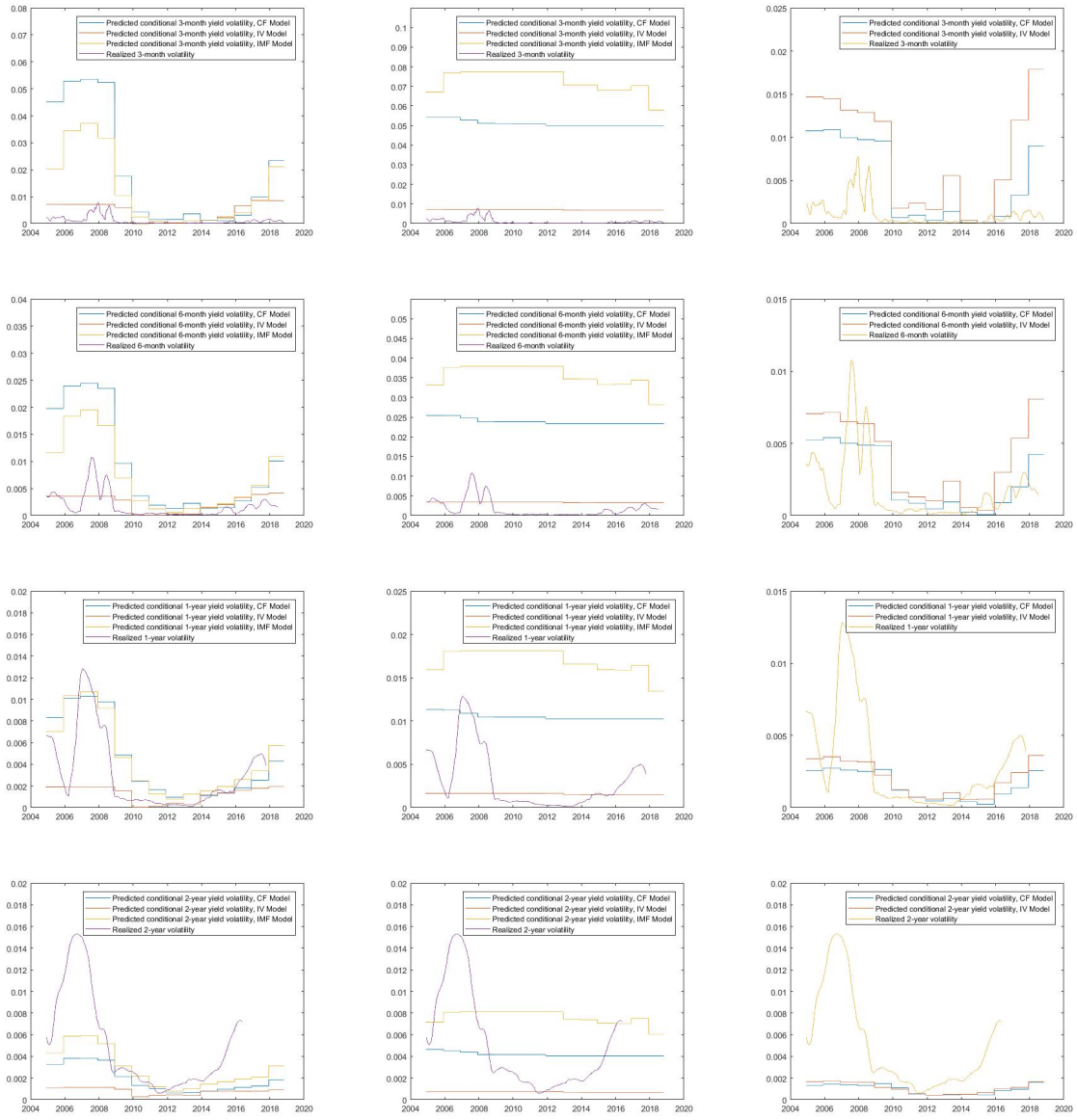

Figure 13: Predicted conditional yield volatilities and realised volatilities for 3-month (first row), 6-month (second row), 1-year (third row), and 2-year (fourth row) maturities using rolling window re-estimations of the correlated factors (CF), independent variances (IV), and independent macro-finance factors (IMF) models. From left to right, the columns represent the macro-finance shadow-rate (ZLB-MF), macro-finance affine (AFNS-MF), and yields-only shadow-rate (ZLB) models, respectively. The in-sample period is 20 years, the first starting from Jan 1985 until Dec 2004, predicting Jan 2005. The final prediction is for Jan 2019. Realised volatility is calculated using daily changes in interest rates for the 91-, 182-, 365-, and 730-day ahead period.

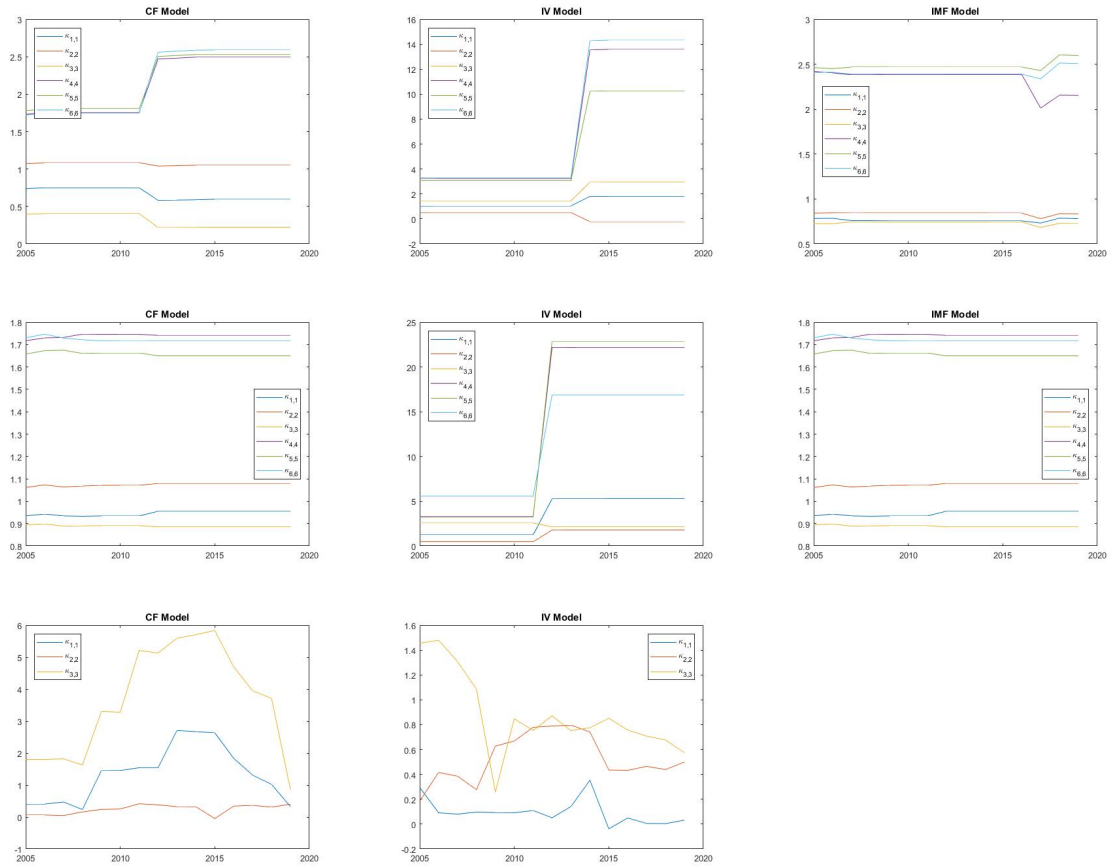

Figure 14: Rolling window re-estimations of κ^P for the correlated factors (CF), independent variances (IV), and independent macro-finance factors (IMF) models. From top to bottom, the rows present the macro-finance shadow-rate (ZLB-MF), macro-finance affine (AFNS-MF), and yields-only shadow-rate (ZLB) models, respectively. The in-sample period is 20 years, the first starting from Jan 1985 until Dec 2004. The full sampling period is from Jan 1985 until Dec 2018. The final prediction is for Jan 2019.

AFNS-MF models, yet still do so rather inaccurately relative to the ZLB-MF models. For the three-month maturity, the realised volatility pre- and post-ZLB is much lower than predicted, while it is much higher for the one-year and two-year maturities.

However, the rolling window re-estimations show that parameter estimates of the ZLB-MF and AFNS-MF models are too stable, indicating that the algorithm converges to an optimum near the initialisation point, which may not be a global optimum. Meanwhile, the estimates for the ZLB model show more variation. Hence, the algorithm diverges from the initialisation point to find the new true optimum. This translates into higher computation time, as the algorithm requires approximately 57.5 hours to run the rolling window re-estimations for the ZLB model, versus 40.1 hours for the ZLB-MF model. Hence, the method is more robust for a yields-only model, of which the optimisation problem is much less complex. To illustrate, Fig. 14 shows the estimates of the diagonal elements of κ^P. Appendix I presents the remaining parameters.

The graphs also show that for the AFNS-MF model under the CF and IMF restrictions, many parameter estimates do not change much at all. For the ZLB-MF model under the IMF restrictions, the shift in parameter values shows a considerable delay relative to the start of the ZLB period. Given the long in-sample period of 20 years, some delay is expected, as only a small part of the in-sample encompasses the ZLB period initially. However, given that this is

	Subset of Variables Full Sample (1985-2018)					All Variables Subsample (1995-2018)				
	ZLB		ZLB-MF			ZLB		ZLB-MF		
	LL	RMSE	JLL	LL	RMSE	LL	RMSE	JLL	LL	RMSE
CF	18218.8	0.28	23161.5	13548.0	0.25	12450.0	0.22	15302.5	10714.7	0.12
IV	17736.4	0.76	27130.6	15049.4	0.18	12303.8	0.22	17376.5	10567.9	0.13
IMF	-	-	23799.8	11612.5	0.49	-	-	22043.1	10580.6	0.13
IF	17894.0	0.25	37372.7	14887.9	0.18	12274.5	0.20	26212.5	10028.9	0.16
B-CR	15605.8	0.72	27590.4	8557.9	1.26	9056.5	0.83	21665.7	4531.1	1.08
KL	-	-	25927.4	6344.5	1.42	-	-	20036.8	4663.9	1.05

Table 11: Joint ($f(y, X_m)$; JLL) and individual ($f(y)$; LL) log likelihood values and root mean squared errors (RMSE) for the yields-only (ZLB) and macro-finance (ZLB-MF) shadow-rate models using uninformed initialisation ($\kappa^P = I, \theta^P = 0.1, \lambda = 0.5, \sigma^2_{i,i} = 0.1, \sigma_{i,j} = 0$, and $h_{j,j} = 0.01$) for a subset of the macroeconomic variables or a subsample of the time period. In the IV, IF, KL, and B-CR models, Σ is diagonal. In the IMF model, the upper-right and lower-left corner of κ^P and Σ are blocks of zero. The IF model has a diagonal κ^P matrix. In the B-CR and KL models, the level factor is a unit-root process, meaning $\kappa^P_{1,1} = 10^{-7}$ and $\theta^P_1 = 0$. In the B-CR model, $\kappa^P_{1,2} = \kappa^P_{1,3} = \kappa^P_{3,1} = \kappa^P_{3,2} = 0$. In the KL model, $\kappa^P_{1,6} = \kappa^P_{2,6} = \kappa^P_{3,6} = \kappa^P_{4,6} = \kappa^P_{5,6} = 0$ and $\kappa^P_{4,3} = \kappa^P_{5,3} = \kappa^P_{6,3} = 0$.

an extreme period, the parameter estimates should still shift within the first few years, as in the ZLB-MF model under the CF and IV restrictions and the AFNS-MF model under the IV restrictions. Thus, these models are better able to reflect new information in the ZLB period.

In summary, including macroeconomic information is valuable for estimating a term structure that can replicate key stylised facts in a ZLB environment. The macro-finance shadow-rate model can replicate the nonnegativity of interest rates and compression of short- and medium-term yield volatility. The yields-only version performs more poorly on this aspect. However, there is a trade-off, as incorporating macro factors causes the algorithm to be more sensitive to initialisation and increases the probability that it does not converge to the global optimum.

5.5 Robustness

The results could be affected by the choice of variables and the proportion of pre-ZLB period to ZLB period in the sampling period. As a robustness check, I first re-estimate the models on a subset of the macro variables, by excluding the least correlated variables with yield rates. By excluding PPI-related variables (PPI All, PPI-F, Core PPI-F), the first PC explains 84.4% of the variation in the inflation group. By excluding CU-related variables (CU-N, CU-S) and EMP, the first PC explains 88.2% of the variation in the economic activity group. Second, I re-estimate the models on a subsample between January 1995 and December 2018, i.e. excluding the first ten years. Hence, the sample covers a substantially smaller pre-ZLB period. Specifically, during the first ten years, yield rates were still very high. Table 11 presents both results.

A subset of the macroeconomic variables yields similar in-sample fit as the complete set, except that the fit considerably worsens under the IMF restrictions in terms of (joint) log likelihood. The assumption that yield factors are independent of macro factors thus receives less support. This is as expected, given the higher correlation of yield and macro factors due to the variable selection. Overall, the IV and IF models yield the highest fit. The B-CR and KL restrictions yield low log likelihood and RMSE values, yet high joint log likelihood.

Excluding the first ten years of data, the CF, IV, IMF, and IF models have almost equal fit in terms of log likelihood and RMSE. In terms of joint log likelihood, the least restricted case has the worst fit, while the IF and IMF restrictions yield the highest fit. Concluding, modelling

with a subset of variables or a subsample yield good fit, yet different restrictions could do well in different settings, rendering it important to test various restrictions on a given data set.

6 Conclusion and Discussion

The growing literature about shadow-rate term structure models shows that they yield higher in-sample fit and are better able to capture the yield curve's stylised facts in a ZLB environment compared to standard affine models. However, due to the ZLB constraint, the yield curve may not be able to incorporate all relevant information (Bauer and Rudebusch, 2016). In this paper, I extend the shadow-rate model presented by Christensen and Rudebusch (2016) to a macro-finance model by including three macro factors: economic activity, inflation, and the policy rate. I elaborate on the estimation method, which I also apply to the macro-finance affine model and yields-only shadow-rate model. By comparing the results relating to the reproduced factor persistence and dynamics, the model's link to economic theory, and the replication of stylised facts, I assess the advantages of a macro extension of the shadow-rate model.

I find that parameter restrictions play an important role in ensuring that the model reproduces the factors' persistence and dynamics. This is key for real applications of term structure models. Generally, the independent factors model, Christensen and Rudebusch (2016)'s macro-extended model, and Krippner and Lewis (2018)'s model perform rather poorly. For application, I suggest testing the remaining three models on a given sample to determine which receives the most support from the data: the correlated factors model, the independent variances model, or the independent macro-finance factors model. Variable selection will also affect model preferences, specifically with respect to restrictions on macro-finance interactions. Hence, combining the methods in this paper with variable selection methods, which is also a growing research topic, could improve model performance. For a simplistic application, I suggest using several macro variables containing different information and having high correlation with yield rates.

Convergence to the global optimum is sensitive to the parameters' initialisation values. Without good initialisation, optimisation from multiple starting points is inevitable. Nevertheless, this does not guarantee finding the global optimum and is time-consuming, especially when re-estimating based on a rolling or expanding window to make conditional predictions. Krippner (2015) suggests using the iterated EKF (IEKF). Alternatively, I recommend extending the methodology with the Expectation Maximisation-based extended Kalman filter (EM-EKF) in future research. This sensitivity points to a potential issue of model identification. In future applications, a simulation study could help to determine whether the model is identified. Additionally, it would be useful to address the topic of identification in the context of a shadow-rate model with macro factors in future research. The derivation of an identification scheme could build upon existing work about identification of GATSMs, such as by Hamilton and Wu (2012).

In general, incorporating macroeconomic information in the shadow-rate model is valuable. I follow Diebold et al. (2006) in incorporating macro factors in the state equation. An alternative model would include macro variables directly in the measurement equation, thereby affecting the yield-adjustment terms and volatility effect. Moreover, in a ZLB environment, the macro-finance shadow-rate models consistently yield nonnegative expected short rates and

are better able to reproduce the compression of yield volatilities for short and, to a lesser extent, intermediate maturities than the yields-only and affine models. As this analysis is based on approximate predicted conditional volatilities, approximation could yield inaccuracies that accumulate for longer maturities, explaining the weaker performance in replicating intermediate-maturity volatilities. I suggest using Monte Carlo simulations if higher accuracy is desired. In sum, by adhering to the lower bound and incorporating additional macroeconomic information, the macro-finance shadow-rate term structure model replicates important macro-finance linkages and stylised facts of the yield curve.

Bibliography

Ang, A. and Piazzesi, M. (2003). A no-arbitrage vector autoregression of term structure dynamics with macroeconomic and latent variables. *Journal of Monetary Economics*, 50(4):745–787.

Bauer, M. D. and Rudebusch, G. D. (2016). Monetary policy expectations at the zero lower bound. *Journal of Money, Credit and Banking*, 48(7):1439–1465.

Black, F. (1995). Interest rates as options. *Journal of Finance*, 50(5):1371–1376.

Carriero, A., Mouabbi, S., and Vangelista, E. (2018). UK term structure decompositions at the zero lower bound. *Journal of Applied Econometrics*, 33(5):643–661.

Centre for Economic Policy Research (2015). Codes & slides. Retrieved from https://cepr.org/event/1854/Codes_slides. Accessed: 14 April 2019.

Christensen, J. H. (2015). How efficient is the extended Kalman filter at estimating shadow-rate models? *Centre for Economic Policy Research*. Draft.

Christensen, J. H., Diebold, F. X., and Rudebusch, G. D. (2011). The affine arbitrage-free class of Nelson-Siegel term structure models. *Journal of Econometrics*, 164:4–20.

Christensen, J. H. and Rudebusch, G. D. (2015). Estimating shadow-rate term structure models with near-zero yields. *Journal of Financial Econometrics*, 13:226–259.

Christensen, J. H. and Rudebusch, G. D. (2016). Modeling yields at the zero lower bound: are shadow rates the solution? *Advances in Econometrics*, 35:75–125.

Dai, Q. and Singleton, K. J. (2000). Specification analysis of affine term structure models. *The Journal of Finance*, 55(5):1943–1978.

Dewachter, H. and Lyrio, M. (2006). Macro factors and the term structure of interest rates. *Journal of Money, Credit, and Banking*, 38(1):119–140.

Diebold, F. X. and Li, C. (2006). Forecasting the term structure of government bond yields. *Journal of Econometrics*, 130(2):337–364.

Diebold, F. X., Rudebusch, G. D., and Aruoba, S. B. (2006). The macroeconomy and the yield curve: a dynamic latent factor approach. *Journal of Econometrics*, 131(1-2):309–338.

Federal Reserve Bank of San Francisco (2006). What steps has the Federal Reserve taken to improve transparency? Retrieved from https://www.frbsf.org/education/publications/doctor-econ/2006/september/transparency/. Accessed: 30 April 2019.

Fisher, M. and Gilles, C. (1996). Estimating exponential-affine models of the term structure. *Board of Governors of the Federal Reserve System*. Manuscript.

Gürkaynak, R. S., Sack, B., and Wright, J. H. (2007). The US Treasury yield curve: 1961 to the present. *Journal of Monetary Economics*, 54(8):2291–2304.

Hamilton, J. D. and Wu, J. C. (2012). Identification and estimation of Gaussian affine term structure models. *Journal of Econometrics*, 168(2):315–331.

Holmes, E. E. (2018). Derivation of an EM algorithm for constrained and unconstrained multivariate autoregressive state-space (MARSS) models. Retrieved from https://cran.r-project.org/web/packages/MARSS/. Accessed: 2 May 2019.

Joslin, S., Singleton, K. J., and Zhu, H. (2011). A new perspective on Gaussian dynamic term structure models. *The Review of Financial Studies*, 24(3):926–970.

Krippner, L. (2012). Modifying Gaussian term structure models when interest rates are near the zero lower bound. *Discussion Paper Series DP2012/02*.

Krippner, L. (2013). A tractable framework for zero lower bound Gaussian term structure models. *Discussion Paper Series DP2013/02*.

Krippner, L. (2015). *Zero lower bound term structure modeling: A practitioner's guide*. Springer.

Krippner, L. and Lewis, M. (2018). Real-time forecasting with macro-finance models in the presence of a zero lower bound. *Discussion Paper Series DP2018/04*.

Lange, R.-J. (2018). Advanced time series econometrics. *Erasmus University Rotterdam*. Lecture slides retrieved from Canvas.

Wu, T. (2003). What makes the yield curve move? *FRBSF Economic Letter*, 15.

Xi, Y., Peng, H., and Mo, H. (2017). Parameter estimation of RBF-AR model based on the EM-EKF algorithm. *Acta Automatica Sinica*, 43(9):1636–1643.

Variables

FFR	Effective Federal Funds Rate

Inflation	
Core CPI	Consumer Price Index for All Urban Consumers: All Items Less Food and Energy
Core PCE	Personal Consumption Expenditure Excluding Food and Energy: Chain-type Price Index
Core PPI-F	Producer Price Index by Commodity for Final Demand: Finished Goods Less Food and Energy
CPI	Consumer Price Index for All Urban Consumers: All Items
PCE	Personal Consumption Expenditure: Chain-type Price Index
PPI All	Producer Price Index for All Commodities
PPI-F	Producer Price Index by Commodity for Final Demand: Finished Goods

Economic Activity	
CU-N	Capacity Utilisation: Manufacturing (NAICS)
CU-S	Capacity Utilisation: Manufacturing (SIC)
EMP	Civilian Employment Level
IP	Industrial Production Index
IP-N	Industrial Production: Manufacturing (NAICS)
IP-S	Industrial Production: Manufacturing (SIC)
UNEMP	Civilian Unemployment Rate

Appendix A

I follow the steps of Christensen et al. (2011) and Krippner (2013), respectively, to derive the forward rate yield-adjustment term and the volatility effect in the macro-finance model. Both terms are functions of state variable innovation variance and covariance terms and scalar exponential functions of τ. As a result, the ZLB forward rate curve is a closed-form analytical expression, such that yields are evaluated using an elementary univariate numerical integration of this expression with respect to τ (Krippner, 2013). I derive the equations for a model with one macro factor, $M_{1,t}$, as the solution extends readily to multiple macro factors.

The instantaneous risk-free rate r_t is an affine function of state variables $X_t = (L_t, S_t, C_t, M_{1,t})$,

$$r_t = \rho_0(t) + \rho_1(t)' X_t = L_t + S_t, \tag{42}$$

and zero-coupon bond prices $P(t,T)$ are exponential affine functions of the state variables,

$$P(t,T) = E_t^Q \left[\exp\left(- \int_t^T r_u du \right) \right] = \exp(B(t,T)' X_t + A(t,T)). \tag{43}$$

The pricing functions imply that zero-coupon yields are

$$y(t,T) = -\frac{1}{T-t} \log P(t,T) = -\frac{B(t,T)'}{T-t} X_t - \frac{A(t,T)}{T-t}. \tag{44}$$

Using $\tau = T - t$, I can rewrite the yield rate representation in Eq. (4) as

$$\begin{pmatrix} y_t(\tau_1) \\ \vdots \\ y_t(\tau_N) \end{pmatrix} = \begin{pmatrix} 1 & \frac{1-e^{-\lambda\tau_1}}{\lambda\tau_1} & \frac{1-e^{-\lambda\tau_1}}{\lambda\tau_1} - e^{-\lambda\tau_1} & 0 \\ \vdots & \vdots & \vdots & \vdots \\ 1 & \frac{1-e^{-\lambda\tau_N}}{\lambda\tau_N} & \frac{1-e^{-\lambda\tau_N}}{\lambda\tau_1} - e^{-\lambda\tau_N} & 0 \end{pmatrix} \begin{pmatrix} L_t \\ S_t \\ C_t \\ M_{1,t} \end{pmatrix} - \begin{pmatrix} A(\tau_1)/\tau_1 \\ \vdots \\ A(\tau_N)/\tau_N \end{pmatrix}, \tag{45}$$

which implies the following solutions for $B(t,T)$

$$\begin{aligned} B^1(t,T) &= -(T-t), \\ B^2(t,T) &= -\frac{1-e^{-\lambda(T-t)}}{\lambda}, \\ B^3(t,T) &= (T-t)e^{-\lambda(T-t)} - \frac{1-e^{\lambda(T-t)}}{\lambda}, \\ B^4(t,T) &= 0. \end{aligned} \tag{46}$$

Using the formula for the yield-adjustment term by Christensen et al. (2011), I derive

$$\begin{aligned}\frac{A(t,T)}{T-t} &= \frac{1}{2}\frac{1}{T-t}\int_t^T \sum_{j=1}^{4}(\Sigma' B(s,T)B(s,T)'\Sigma)_{j,j}ds \\ &= \frac{1}{2}\frac{1}{T-t}\int_t^T \sum_{j=1}^{4}\left[\begin{pmatrix}\sigma_{11} & \sigma_{21} & \sigma_{31} & \sigma_{41}\\ \sigma_{12} & \sigma_{22} & \sigma_{32} & \sigma_{42}\\ \sigma_{13} & \sigma_{23} & \sigma_{33} & \sigma_{43}\\ \sigma_{14} & \sigma_{24} & \sigma_{34} & \sigma_{44}\end{pmatrix}\begin{pmatrix}B^1(s,T)\\ B^2(s,T)\\ B^3(s,T)\\ B^4(s,T)\end{pmatrix}\right. \\ &\quad \left.\times \begin{pmatrix}B^1(s,T) & B^2(s,T) & B^3(s,T) & B^4(s,T)\end{pmatrix}\begin{pmatrix}\sigma_{11} & \sigma_{12} & \sigma_{13} & \sigma_{14}\\ \sigma_{21} & \sigma_{22} & \sigma_{23} & \sigma_{24}\\ \sigma_{31} & \sigma_{32} & \sigma_{33} & \sigma_{34}\\ \sigma_{41} & \sigma_{42} & \sigma_{43} & \sigma_{44}\end{pmatrix}\right]_{j,j} ds,\end{aligned} \tag{47}$$

which can be simplified to

$$\begin{aligned}\frac{A(t,T)}{T-t} = \frac{1}{2}\frac{1}{T-t}\int_t^T &\left([\sigma_{11}B^1(s,T)+\sigma_{21}B^2(s,T)+\sigma_{31}B^3(s,T)+\sigma_{41}B^4(s,T)]^2\right. \\ &+[\sigma_{12}B^1(s,T)+\sigma_{22}B^2(s,T)+\sigma_{32}B^3(s,T)+\sigma_{42}B^4(s,T)]^2 \\ &+[\sigma_{13}B^1(s,T)+\sigma_{23}B^2(s,T)+\sigma_{33}B^3(s,T)+\sigma_{43}B^4(s,T)]^2 \\ &\left.+[\sigma_{14}B^1(s,T)+\sigma_{24}B^2(s,T)+\sigma_{34}B^3(s,T)+\sigma_{44}B^4(s,T)]^2\right) ds.\end{aligned} \tag{48}$$

Given $B^4(t,T)=0$, the expression becomes

$$\begin{aligned}\frac{A(t,T)}{T-t} &= \frac{\overline{A}}{2}\int_t^T [B^1(s,T)]^2 ds + \frac{\overline{B}}{2}\int_t^T [B^2(s,T)]^2 ds + \frac{\overline{C}}{2}\int_t^T [B^3(s,T)]^2 ds \\ &\quad + \frac{\overline{D}}{2}\int_t^T B^1(s,T)B^2(s,T)ds + \frac{\overline{E}}{2}\int_t^T B^1(s,T)B^3(s,T)ds + \frac{\overline{F}}{2}\int_t^T B^2(s,T)B^3(s,T)ds,\end{aligned} \tag{49}$$

for which the integral terms are given by Christensen et al. (2011). Moreover, in

$$\begin{aligned}\overline{A} &= \sigma_{11}^2+\sigma_{12}^2+\sigma_{13}^2+\sigma_{14}^2,\\ \overline{B} &= \sigma_{21}^2+\sigma_{22}^2+\sigma_{23}^2+\sigma_{24}^2,\\ \overline{C} &= \sigma_{31}^2+\sigma_{32}^2+\sigma_{33}^2+\sigma_{34}^2,\\ \overline{D} &= \sigma_{11}\sigma_{21}+\sigma_{12}\sigma_{22}+\sigma_{13}\sigma_{23}+\sigma_{14}\sigma_{24},\\ \overline{E} &= \sigma_{11}\sigma_{31}+\sigma_{12}\sigma_{32}+\sigma_{13}\sigma_{33}+\sigma_{14}\sigma_{34},\\ \overline{F} &= \sigma_{21}\sigma_{31}+\sigma_{22}\sigma_{32}+\sigma_{23}\sigma_{33}+\sigma_{24}\sigma_{34},\end{aligned} \tag{50}$$

many of the state variable innovation covariance terms equal zero, given the lower triangular form of Σ in a maximally flexible model. Hence, the expressions in Eq. (49) and (50) reduce to those used by Christensen et al. (2011) and Christensen and Rudebusch (2016). Consequently,

I use the same yield-adjustment expression for the forward rate equation,

$$\begin{aligned}
A^f(\tau) =& -\frac{\delta A(\tau)}{\delta \tau} \\
=& -\frac{1}{2}\sigma_{11}^2\tau^2 - \frac{1}{2}(\sigma_{21}^2+\sigma_{22}^2)\left(\frac{1-e^{-\lambda\tau}}{\lambda}\right)^2 \\
& -\frac{1}{2}(\sigma_{31}^2+\sigma_{32}^2+\sigma_{33}^2)\left[\frac{1}{\lambda^2}-\frac{2}{\lambda^2}e^{-\lambda\tau}-\frac{2}{\lambda}\tau e^{-\lambda\tau}+\frac{1}{\lambda^2}e^{-2\lambda\tau}+\frac{2}{\lambda}\tau e^{-2\lambda\tau}+\tau^2 e^{-2\lambda\tau}\right] \\
& -\sigma_{11}\sigma_{21}\tau\left(\frac{1-e^{-\lambda\tau}}{\lambda}\right)-\sigma_{11}\sigma_{31}\left[\frac{1}{\lambda}\tau-\frac{1}{\lambda}\tau e^{-\lambda\tau}-\tau^2 e^{-\lambda\tau}\right] \\
& -(\sigma_{21}\sigma_{31}+\sigma_{22}\sigma_{32})\left[\frac{1}{\lambda^2}-\frac{2}{\lambda^2}e^{-\lambda\tau}-\frac{1}{\lambda}\tau e^{-\lambda\tau}+\frac{1}{\lambda^2}e^{-2\lambda\tau}+\frac{1}{\lambda}\tau e^{-2\lambda\tau}\right].
\end{aligned} \tag{51}$$

By the same line of reasoning and using solutions for integral terms from Krippner (2013), I can derive the volatility effect equation of Christensen and Rudebusch (2016), namely

$$\begin{aligned}
\omega(\tau) =& \int_0^\tau \left[\begin{pmatrix}1 & e^{-\lambda u} & \lambda u e^{-\lambda u} & 0\end{pmatrix}\begin{pmatrix}\sigma_{11} & 0 & 0 & 0\\ \sigma_{21} & \sigma_{22} & 0 & 0\\ \sigma_{31} & \sigma_{32} & \sigma_{33} & 0\\ \sigma_{41} & \sigma_{42} & \sigma_{43} & \sigma_{44}\end{pmatrix}\begin{pmatrix}\sigma_{11} & \sigma_{21} & \sigma_{31} & \sigma_{41}\\ 0 & \sigma_{22} & \sigma_{32} & \sigma_{42}\\ 0 & 0 & \sigma_{33} & \sigma_{43}\\ 0 & 0 & 0 & \sigma_{44}\end{pmatrix}\begin{pmatrix}1\\ e^{-\lambda u}\\ \lambda u e^{-\lambda u}\\ 0\end{pmatrix}\right] du \\
=& \sigma_{11}^2\int_0^\tau 1du + (\sigma_{21}^2+\sigma_{22}^2)\int_0^\tau (e^{-2\lambda u})du \\
& +(\sigma_{31}^2+\sigma_{32}^2+\sigma_{33}^2)\int_0^\tau(\lambda^2u^2e^{-2\lambda u})du \\
& +2\sigma_{11}\sigma_{21}\int_0^\tau(e^{-\lambda u})du + 2\sigma_{11}\sigma_{31}\int_0^\tau(\lambda u e^{-\lambda u})du \\
& +2(\sigma_{21}\sigma_{31}+\sigma_{22}\sigma_{32})\int_0^\tau(\lambda u e^{-2\lambda u})du \\
=& \sigma_{11}^2\tau + (\sigma_{21}^2+\sigma_{22}^2)\frac{1-e^{-2\lambda\tau}}{2\lambda} \\
& +(\sigma_{31}^2+\sigma_{32}^2+\sigma_{33}^2)\left[\frac{1-e^{-2\lambda\tau}}{4\lambda}-\frac{1}{2}\tau e^{-2\lambda\tau}-\frac{1}{2}\lambda\tau^2e^{-2\lambda\tau}\right] \\
& +2\sigma_{11}\sigma_{21}\left(\frac{1-e^{-\lambda\tau}}{\lambda}\right)+2\sigma_{11}\sigma_{31}\left[-\tau e^{-\lambda\tau}+\frac{1-e^{-\lambda\tau}}{\lambda}\right] \\
& +(\sigma_{21}\sigma_{31}+\sigma_{22}\sigma_{32})\left[-\tau e^{-2\lambda\tau}+\frac{1-e^{-2\lambda\tau}}{2\lambda}\right].
\end{aligned} \tag{52}$$

Appendix B

In describing the extended Kalman filter, I closely follow the exposition of Christensen and Rudebusch (2016) and Christensen (2015). Furthermore, I follow the steps of Ang and Piazzesi (2003) and Hamilton and Wu (2012) in deriving the joint log likelihood function. However, they assume that some yields are measured without error. Instead, I assume non-zero variance for all maturities. By linear approximation,

$$\begin{aligned} \underline{y}_t &= z(X_t;\theta) + u_t \\ &\approx z(X_{t|t-1};\theta) + \frac{\delta z(X_t;\theta)}{\delta X_t}|_{X_t=X_{t|t-1}}(X_t - X_{t|t-1}) + u_t, \end{aligned} \tag{53}$$

where θ represents the set of parameters and u_t has diagonal covariance matrix

$$H(\theta) = diag(\sigma_\varepsilon^2(\tau_1), ..., \sigma_\varepsilon^2(\tau_N)). \tag{54}$$

By defining

$$A_t(\theta) = z(X_{t|t-1};\theta) - \frac{\delta z(X_t;\theta)}{\delta X_t}|_{X_t=X_{t|t-1}}X_{t|t-1}, \tag{55}$$

$$B_t(\theta) = \frac{\delta z(X_t;\theta)}{\delta X_t}|_{X_t=X_{t|t-1}}X_{t|t-1}, \tag{56}$$

where the derivatives are calculated numerically, the measurement equation given by Eq. (53) can be presented in an affine form as

$$\begin{aligned} \underline{y}_t &= A_t(\theta) + B_t(\theta)X_t + u_t \\ &= A_t(\theta) + \begin{pmatrix} B_t^l(\theta) & B_t^m(\theta) \end{pmatrix} \begin{pmatrix} X_t^l \\ X_t^m \end{pmatrix} + u_t. \end{aligned} \tag{57}$$

The state equation is

$$\begin{pmatrix} X_t^l \\ X_t^m \end{pmatrix} = \Phi^0 + \Phi^1 \begin{pmatrix} X_{t-1}^l \\ X_{t-1}^m \end{pmatrix} + \varepsilon_t. \tag{58}$$

Extended Kalman Filter: Prediction

The prediction step of the extended Kalman filter is

$$\begin{aligned} X_{t|t-1} &= \Phi_t^0(\theta) + \Phi_t^1(\theta)X_{t-1}, \\ \Sigma_{t|t-1} &= \Phi_t^1(\theta)\Sigma_{t-1}\Phi_t^1(\theta)' + Q(\theta), \end{aligned} \tag{59}$$

where

$$\begin{aligned} \Phi_t^0(\theta) &= (I - \exp(-\kappa^P\Delta t))\theta^P, \\ \Phi_t^1(\theta) &= \exp(-\kappa^P\Delta t), \\ Q(\theta) &= \int_0^{\Delta t} \exp(-\kappa^P s)\Sigma\Sigma'\exp(-\kappa^P s)'ds. \end{aligned} \tag{60}$$

Extended Kalman Filter: Update

The update step of the extended Kalman filter is

$$\begin{aligned} X_t &= X_{t|t-1} + \Sigma_{t|t-1} B_t(\theta)' F_t^{-1} \nu_t, \\ \Sigma_t &= \Sigma_{t|t-1} - \Sigma_{t|t-1} B_t(\theta)' F_t^{-1} B_t(\theta) \Sigma_{t|t-1}, \end{aligned} \tag{61}$$

where

$$\nu_t = \underline{y}_t - y_t^{implied}. \tag{62}$$

Computing $y_t^{implied}$ requires numerical integration. I first create a grid of maturities from 0.01 to 10 years, $[0.01, 10]$, using step sizes of 0.01. For each grid point i, $\omega(i)$, $B^f(i)$, and $A^f(i)$ are computed and subsequently substituted into Eq. (5). The model-implied yield rates are

$$y_t^{implied}(\tau) = \frac{0.01}{\tau} \sum_{i=1}^{\tau \cdot 100} \underline{f}_t(i), \tag{63}$$

where $\underline{f}_t(i)$ is computed as in Eq. (9) and $\tau = 0.25, 0.5, 1, 2, 3, 5, 7, 10$ in years. Meanwhile, the covariance matrix of the error term, F_t, is calculated using $B_t(\theta)$ from Eq. (56), such that

$$F_t = cov(\nu_t) = B_t(\theta) \Sigma_{t|t-1} B_t(\theta)' + H(\theta). \tag{64}$$

Unlike the AFNS model, the state vector is also updated with real observations, namely the macro variables. Specifically, X_t^m is updated using the macro observations (z_t, π_t, r_t).

Extended Kalman Filter: Maximum Likelihood

The log likelihood function of the yield observations is

$$LL(\theta) = \sum_{t=1}^{T} \left(-\frac{N}{2} \log(2\pi) - \frac{1}{2} \log|F_t| - \frac{1}{2} \nu_t' F_t^{-1} \nu_t \right). \tag{65}$$

For a yields-only model, one would maximise this log likelihood (Christensen et al., 2011). For the macro-finance model, I follow Ang and Piazzesi (2003) and Hamilton and Wu (2012) in maximising the joint log likelihood of the yield observations and macro factors,

$$\begin{aligned} LL(\theta) &= \sum_{t=1}^{T} f(y_t, X_t^m | y_{t-1}, X_{t-1}^m) \\ &= \sum_{t=1}^{T} -\log|det(J_t)| + \log f_x(X_t^m, X_t^l | X_{t-1}^m, X_{t-1}^l) + \log f_u(u) \\ &= \sum_{t=1}^{T} -\log|det(J_t)| - \frac{k}{2} \log - \frac{N}{2} \log(2\pi) \\ &\quad - \frac{1}{2} \log(det(\Sigma_t)) - \frac{1}{2} (X_t - \Phi^0 - \Phi^1 X_{t-1})' (\Sigma_t)^{-1} (X_t - \Phi^0 - \Phi^1 X_{t-1}) \\ &\quad - \frac{1}{2} \log \sum_{i=1}^{N} H_{i,i} - \frac{1}{2} \sum_{i=1}^{N} \frac{(u_{t,i})^2}{H_{i,i}}, \end{aligned} \tag{66}$$

where k is the number of states. The Jacobian matrix is

$$J_t = \begin{pmatrix} \frac{X_t^m}{\delta X_t^m} & \frac{\delta X_t^m}{\delta X_t^l} & \frac{\delta X_t^m}{\delta u_t} \\ \frac{\delta y_t}{\delta X_t^m} & \frac{\delta y_t}{\delta X_t^l} & \frac{\delta y_t}{\delta u_t} \end{pmatrix} = \begin{pmatrix} I & 0 & 0 \\ B_t^m & B_t^l & I \end{pmatrix}, \tag{67}$$

where I use the approximation of B at time t as in Eq. (56), given the nonlinear structure.

Extended Kalman Filter: Initialisation

Initialisation usually requires the unconditional distribution, where $X_0 = \theta^P$ and

$$\Sigma_0 = \int_0^\infty \exp(-\kappa^P s)\Sigma\Sigma' \exp(-\kappa^P s)' ds. \tag{68}$$

Analytical solutions are provided in Fisher and Gilles (1996). However, for the case of a unit-root level factor, Christensen and Rudebusch (2016) use the first observation and a least squares approach to derive an initial distribution,

$$\begin{aligned} X_0 &= (B(\theta)'B(\theta))^{-1}B(\theta)'(y_0 - A(\theta)), \\ \Sigma_0 &= (B(\theta)'B(\theta))^{-1}B(\theta)'H(\theta)B(\theta)(B(\theta)'B(\theta))^{-1}. \end{aligned} \tag{69}$$

This assumes a linear term structure, which is accurate as the shadow-rate model collapses to its equivalent affine model if yields are far away from the ZLB, i.e. in the beginning of the sample. However, for the macrofinance model, there is no solution for $(B'B)^{-1}$, since $B^m = 0$. Hence, I initialise the state vector using $X_0^m = \theta^{m,P}$ and

$$X_0^l = (B^l(\theta)'B^l(\theta))^{-1}B^l(\theta)'(Y_0 - A(\theta)). \tag{70}$$

I initialise the covariance matrix using

$$\Sigma_0 = \int_0^\infty \exp(-\kappa^P s)\Sigma\Sigma' \exp(-\kappa^P s)' ds, \tag{71}$$

and substitute the top left 3-by-3 block, i.e. the covariance matrix for the yield factors, with

$$\Sigma_0 = (B^l(\theta)'B^l(\theta))^{-1}B^l(\theta)'H(\theta)B^l(\theta)(B^l(\theta)'B^l(\theta))^{-1}. \tag{72}$$

Additionally, I substitute the initial state and variance term of the level factor with a diffuse initialisation ($X_0^L = 0, \Sigma_0^{L,L} = 10$). This setting only applies to the B-CR and KL models. For the remainder, I use the unconditional distribution.

Appendix C

The expression for the ZLB zero-coupon bond yields can be elaborated as

$$\begin{aligned}\underline{y}_t(\tau) &= \frac{1}{\tau}\int_t^{t+\tau}\left[f_t(s)\Phi\left(\frac{f_t(s)}{\omega(s)}\right)+\omega(s)\frac{1}{\sqrt{2\pi}}\exp\left(-\frac{1}{2}\left[\frac{f_t(s)}{\omega(s)}\right]^2\right)\right]ds \\ &= \frac{1}{\tau}\int_t^{t+\tau}\left[\frac{f_t(s)}{\sqrt{2\pi}}\int_0^s \exp\left(-\frac{1}{2}\frac{[f_t(u)]^2}{[\omega(u)]^2}\right)du+\frac{\omega(s)}{\sqrt{2\pi}}\exp\left(-\frac{1}{2}\frac{[f_t(s)]^2}{[\omega(s)]^2}\right)\right]ds.\end{aligned} \tag{73}$$

I thus require an expression for the squared forward rate curve

$$[f_t(\tau)]^2 = [L_t + e^{-\lambda\tau}S_t + \lambda\tau e^{-\lambda\tau}C_t + A^f(\tau)]^2, \tag{74}$$

which, along with the integrals, shows that the measurement equation, given by Eq. (73), is a nonlinear function of the state variables $X_t = (L_t, S_t, C_t, z_t, \pi_t, r_t)$. This suggests using a nonlinear technique for estimating the state space.

Appendix D

Unconstrained Optimisation

Optimisation using the Nelder-Mead simplex method is sensitive to the initialisation values. Hence, the algorithm is not guaranteed to converge to the global optimum. I suggest employing the Expectation Maximisation (EM) method for the first 10-20 iterations. Xi et al. (2017) derive the EM steps for the extended Kalman filter. I repeat their steps for my model. First, I require the Kalman smoothing steps, equivalent to those provided by Lange (2018)[13],

$$\begin{aligned}X_{t|T} &= X_{t|t} + \Sigma_{t|t}\Phi_1'\Sigma_{t+1|t}^{-1}(X_{t+1|T} - X_{t+1|t}), \\ \Sigma_{t|T} &= \Sigma_{t|t} - \Sigma_{t|t}\Phi_1'\Sigma_{t+1|t}^{-1}(\Sigma_{t+1|t} - \Sigma_{t+1|T})\Sigma_{t+1|t}^{-1}\Phi_1\Sigma_{t|t}, \\ \Sigma_{t+1,t|T} &= \Sigma_{t+1|T}\Sigma_{t+1|t}^{-1}\Phi_1\Sigma_{t|t}.\end{aligned} \tag{75}$$

The complete data log likelihood, including latent factors, is

$$\begin{aligned}LL(\theta) =& \ln p(X_{0:T}, y_{1:T}|\theta) \\ =& -\frac{T(k+N)+k}{2}\ln 2\pi + \frac{1}{2}\ln|\Sigma_0^{-1}| - \frac{1}{2}[X_0-\mu_0]'\Sigma_0^{-1}[X_0-\mu_0] \\ &+ \frac{T}{2}\ln|Q^{-1}| - \sum_{t=1}^{T}\frac{1}{2}[X_t - \Phi_0 - \Phi_1 X_{t-1}]'Q^{-1}[X_t - \Phi_0 - \Phi_1 X_{t-1}] \\ &+ \frac{T}{2}\ln|H^{-1}| - \sum_{t=1}^{T}\frac{1}{2}[y_t - z(X_t;\theta)]'H^{-1}[y_t - z(X_t;\theta)].\end{aligned} \tag{76}$$

Xi et al. (2017) derive the expected log likelihood and subsequently maximises it. Instead, I follow Lange (2018)'s method in maximising the log likelihood and correcting the solutions for

[13] Lange (2018)'s state equation does not include Φ_0. However, this does not affect the smoothing steps as it is a constant and cancels out when deriving the joint distribution $(X_t, X_{t+1}|I_T)$.

the expectations afterwards.

First, it is clear that optimising for the prior parameters, I can derive $\mu_0 = X_{0|T}$ and $\Sigma_0 = \Sigma_{0|T}$. Next, I optimise for state parameters Φ_0 and Φ_1, such that

$$\begin{aligned}
0 =& -\frac{1}{2}\frac{\delta}{\delta\Phi_0} tr\left(Q^{-1}\sum_{t=1}^{T}(X_t - \Phi_0 - \Phi_1 X_{t-1})(X_t - \Phi_0 - \Phi_1 X_{t-1})'\right) \\
=& -\frac{1}{2}\frac{\delta}{\delta\Phi_0} tr\Bigg(\sum_{t=1}^{T} -X_t'Q^{-1}\Phi_0 - Q^{-1}X_t\Phi_0' + Q^{-1}\Phi_0\Phi_0' \\
&+ Q^{-1}\Phi_1 X_{t-1}\Phi_0' + X_{t-1}'\Phi_1'Q^{-1}\Phi_0\Bigg) \\
=& -Q^{-1}\sum_{t=1}^{T}(-X_t + \Phi_0 + \Phi_1 X_{t-1}) \\
\Phi_0 =& \frac{1}{T}\sum_{t=1}^{T}(X_t - \Phi_1 X_{t-1}),
\end{aligned} \tag{77}$$

$$\begin{aligned}
0 =& -\frac{1}{2}\frac{\delta}{\delta\Phi_1} tr\left(Q^{-1}\sum_{t=1}^{T}(X_t - \Phi_0 - \Phi_1 X_{t-1})(X_t - \Phi_0 - \Phi_1 X_{t-1})'\right) \\
=& -\frac{1}{2}\frac{\delta}{\delta\Phi_1} tr\Bigg(\sum_{t=1}^{T}(-X_{t-1}X_t'Q^{-1}\Phi_1 + X_{t-1}\Phi_0'Q^{-1}\Phi_1 - Q^{-1}X_tX_{t-1}'\Phi_1' \\
&+ Q^{-1}\Phi_0 X_{t-1}'\Phi_1' + Q^{-1}\Phi_1 X_{t-1}X_{t-1}'\Phi_1')\Bigg) \\
=& -Q^{-1}\sum_{t=1}^{T}(X_tX_{t-1}' - \Phi_0 X_{t-1}' - \Phi_1 X_{t-1}X_{t-1}') \\
\Phi_1 =& \sum_{t=1}^{T}((X_t - \Phi_0)X_{t-1}')(\sum_{t=1}^{T} X_{t-1}X_{t-1}')^{-1}.
\end{aligned} \tag{78}$$

The parameters Φ_0 and Φ_1 are needed for updating the measurement parameters

$$\begin{aligned}
H &= \frac{1}{T}\sum_{t=1}^{T}(y_t - z(X_t;\theta))(y_t - z(X_t;\theta))', \\
Q &= \frac{1}{T}\sum_{t=1}^{T}(X_t - \Phi_0 - \Phi_1 X_{t-1})(X_t - \Phi_0 - \Phi_1 X_{t-1})'.
\end{aligned} \tag{79}$$

To correct for the expectation terms, I use that $E[X_t|I_T] = X_{t|T}$, $E[X_tX_t'|I_T] = X_{t|T}X_{t|T}' + \Sigma_{t|T}$, and $E[X_tX_{t-1}'|I_T] = X_{t|T}X_{t-1|T}' + \Sigma_{t,t-1|T}$. Hence, the update equations are

$$\begin{aligned}
\Phi_0 &= \frac{1}{T}\sum_{t=1}^{T}(X_{t|T} - \Phi_1 X_{t-1|T}), \\
\Phi_1 &= \sum_{t=1}^{T}(X_{t|T}X_{t-1|T}' + \Sigma_{t,t-1|T} - \Phi_0 X_{t-1|T}')(\sum_{t=1}^{T} X_{t-1|T}X_{t-1|T}' + \Sigma_{t-1|T})^{-1},
\end{aligned} \tag{80}$$

$$
\begin{aligned}
Q = \frac{1}{T}\sum_{t=1}^{T} \big(& X_{t|T}X'_{t|T} + \Sigma_{t|T} - \Phi_0 X'_{t|T} - \Phi_1 (X_{t|T}X'_{t-t|T} + \Sigma_{t,t-1|T})' \\
& - X_{t|T}\Phi'_0 + \Phi_0\Phi'_0 + \Phi_1 X_{t-1|T}\Phi'_0 - (X_{t|T}X'_{t-1|T} + \Sigma_{t,t-1|T})\Phi'_1 \\
& + \Phi_0 X'_{t-1|T}\Phi'_1 + \Phi_1 (X_{t-1|T}X'_{t-1|T} + \Sigma_{t-1|T})\Phi'_1 \big).
\end{aligned} \tag{81}
$$

Finally, Xi et al. (2017) show that

$$
H \approx \frac{1}{T}\sum_{t=1}^{T} \big(y_t - z(X_{t|T};\theta)\big)(y_t - z(X_{t|T};\theta)\big)' + B_t(\theta)\Sigma_{t|T}B_t(\theta)', \tag{82}
$$

where $z(X_{t|T};\theta)$ is calculated numerically. Generally, Φ_0 and Φ_1 are updated first, so they can be used to update Q and H (Lange, 2018). After 10-20 EM iterations, the parameter estimates serve as input for the Maximum Likelihood procedure. Instead of maximising the (joint) log likelihood by optimising κ^P and θ^P, the algorithm can directly optimise for Φ_0 and Φ_1.

Constrained Optimisation

Eq. (80), (81), and (82) apply to a fully flexible model. However, for the model variations described in Section 2.4, the solutions should account for parameter restrictions. Next, I present the solutions derived by Holmes (2018), which apply to a general form of multivariate autoregressive state-space models. I simplify them and account for nonlinearity in the measurement equation so they directly apply to the macro-finance shadow-rate model. For consistency, I use the same notation as for the fully flexible model.

First, I rewrite the model in terms of constrained parameters, as in

$$
\begin{aligned}
X_t &= \Phi_0 + (X'_{t-1} \otimes I_k)vec(\Phi_1) + \varepsilon_t, \\
y_t &= z(X_t;\theta) + u_t, \\
X_0 &= \mu_0 + \nu_t,
\end{aligned} \tag{83}
$$

where $k = 6$ is the number of states. The parameters are defined as follows

$$
\begin{aligned}
\Phi_0 &= D_0\phi_0, \\
vec(\Phi_1) &= D_1\phi_1, \\
vec(Q) &= D_q q, \\
vec(H) &= D_h h, \\
\mu_0 &= D_m m, \\
vec(\Sigma_0) &= D_s s,
\end{aligned} \tag{84}
$$

where ϕ_0, ϕ_1, q, h, m, and s are hyperparameters, i.e. the unconstrained parameters. The design matrices D_0, D_1, D_q, D_h, D_m, and D_s consist of 0s and 1s. For example, under the B-CR and

KL restrictions, the unit-root restriction on the level factor implies that

$$D_0 = \begin{pmatrix} 0 & 0 & 0 & 0 & 0 \\ 1 & 0 & 0 & 0 & 0 \\ 0 & 1 & 0 & 0 & 0 \\ 0 & 0 & 1 & 0 & 0 \\ 0 & 0 & 0 & 1 & 0 \\ 0 & 0 & 0 & 0 & 1 \end{pmatrix}. \tag{85}$$

Closely following the exposition of Holmes (2018), the log likelihood function is given by

$$\begin{aligned} LL(\theta) = &-\frac{1}{2}\ln|\Sigma_0| - \frac{1}{2}[X_0 - \mu_0]'\Sigma_0^{-1}[X_0 - \mu_0] \\ &- \frac{1}{2}\sum_{t=1}^{T}\ln|Q| - \frac{1}{2}\sum_{t=1}^{T}[X_t - \Phi_0 - (X'_{t-1}\otimes I_k)vec(\Phi_1)]'Q^{-1}[X_t - \Phi_0 - (X'_{t-1}\otimes I_k)vec(\Phi_1)] \\ &- \frac{1}{2}\sum_{t=1}^{T}\ln|H| - \frac{1}{2}\sum_{t=1}^{T}[y_t - z(X_t;\theta)]'H^{-1}[y_t - z(X_t;\theta)], \end{aligned} \tag{86}$$

ignoring the constant term. By setting the derivatives of the expected log likelihood with respect to ϕ_0, ϕ_1, q, h, and m equal to zero and substituting the expectation terms by the smoothed estimates, the update equations of Holmes (2018) for the $(j+1)$-th iteration are

$$\begin{aligned} m^{j+1} &= \left(D'_m\Sigma_0 D_m\right)^{-1} D'_m\Sigma_0 X_{0|T}, \\ \phi_0^{j+1} &= \left(\sum_{t=1}^{T} D'_0 Q^{-1} D_0\right)^{-1} \sum_{t=1}^{T} D'_0 Q^{-1}\left(X_{t|T} - (X'_{t-1|T}\otimes I_k)vec(\Phi_1)\right), \\ \phi_1^{j+1} &= \left(\sum_{t=1}^{T} D'_1\left[(X_{t-1|T}X'_{t-1|T} + \Sigma_{t-1|T})\otimes Q^{-1}\right]D_1\right)^{-1} \\ &\quad \times \sum_{t=1}^{T} D'_1\left[vec(Q^{-1}(X_{t|T}X'_{t-1|T} + \Sigma_{t,t-1|T})) - vec(Q^{-1}\Phi_0 X'_{t-1|T})\right], \\ q^{j+1} &= \left(\sum_{t=1}^{T}(D'_q D_q)\right)^{-1} D'_q \sum_{t=1}^{T} vec(S_t), \\ h^{j+1} &= \left(\sum_{t=1}^{T}(D'_h D_h)\right)^{-1} D'_h \sum_{t=1}^{T} vec(T_t^{j+1}), \end{aligned} \tag{87}$$

where

$$\begin{aligned} S_t = &X_{t|T}X'_{t|T} + \Sigma_{t|T} - (X_{t|T}X'_{t-1|T} + \Sigma_{t,t-1|T})\Phi'_1 - \Phi_1(X_{t-1|T}X'_{t|T} + \Sigma_{t-1,t|T}) \\ &- X_{t|T}\Phi'_0 - \Phi_0 X'_{t|T} + \Phi_1(X_{t-1|T}X'_{t-1|T} + \Sigma_{t-1|T})\Phi'_1 \\ &+ \Phi_1 X_{t-1|T}\Phi'_0 + \Phi_0 X'_{t-1|T}\Phi'_1 + \Phi_0\Phi'_0, \end{aligned} \tag{88}$$

$$T_t^{j+1} \approx \frac{1}{T}\sum_{t=1}^{T}(y_t - z(X_{t|T};\theta))(y_t - z(X_{t|T};\theta))' + B_t(\theta)\Sigma_{t|T}B_t(\theta)'. \tag{89}$$

I base the approximation in Eq. (89) on Xi et al. (2017)'s derivation of Eq. (82). If Q is constrained to be diagonal, then it is updated as

$$q^{j+1} = \frac{1}{T}(D_q' D_q)^{-1} D_q' \sum_{t=1}^{T} vec(S_t). \tag{90}$$

For the complete derivation, I refer to the paper by Holmes (2018).

Replicating the steps of Holmes (2018) for solving q^{j+1}, I differentiate Eq. (86) with respect to s^*, which is a vector containing $1/s_i$ for each row i, such that

$$vec(\Sigma_0^{-1}) = D_s s^*. \tag{91}$$

I arrive at the following update equation for s

$$\begin{aligned} 0 &= -\frac{1}{2}\frac{\delta\left(\ln|\Sigma_0| + E[(X_0-\mu_0)'\Sigma_0^{-1}(X_0-\mu_0)]\right)}{\delta s^*} \\ &= -\frac{1}{2}\left(\frac{\delta(-\ln|\Sigma_0^{-1}|)}{\delta s^*} + E[(X_0-\mu_0)'\otimes(X_0-\mu_0)]\frac{\delta\left(vec(\Sigma_0^{-1})\right)}{\delta s^*}\right) \\ &= \frac{1}{2}D_s' D_s s - \frac{1}{2}D_s' vec(V^{j+1}) \\ s &= (D_s' D_s)^{-1} D_s' vec(V^{j+1}), \end{aligned} \tag{92}$$

where

$$V^{j+1} = X_{0|T}X_{0|T}' + \Sigma_{0|T} + \mu_0\mu_0' - \mu_0 X_{0|T}' - X_{0|T}\mu_0'. \tag{93}$$

Appendix E

AFNS-MF Initialisation

	CF Model	IV Model	IMF Model	IF Model	B-CR Model	KL Model
Mean-reversion						
$\kappa^P_{1,1}$	1.1923	-0.7193	1.4264	0.0096	10^{-7}*	10^{-7}*
$\kappa^P_{2,2}$	1.1696	2.2374	0.9342	0.0042	1.2531	1.2452
$\kappa^P_{3,3}$	1.1664	6.2163	0.9341	0.0898	1.2519	1.2444
$\kappa^P_{4,4}$	1.2994	5.4441	1.8717	9.9981	1.2518	1.2500
$\kappa^P_{5,5}$	1.3271	8.0474	2.6629	9.6925	1.2507	1.2531
$\kappa^P_{6,6}$	1.3075	6.1480	2.1339	9.6925	1.2502	1.2520
Long-term average						
θ_1	0.0806	0.1254	0.1547	0.1287	0*	0*
θ_2	-0.0224	-0.0400	-0.0831	-0.0356	0.1175	0.0830
θ_3	-0.0229	0.0058	-0.0579	-0.0336	0.1272	0.1401
θ_4	0.1538	2.7508	-0.1819	0.0986	0.1264	0.1303
θ_5	0.1049	1.0297	-0.1787	0.0986	0.1264	0.1277
θ_6	0.1630	0.7530	-0.1852	0.0986	0.1248	0.1250
State innovation						
$\sigma^2_{1,1}$	0.0326	0.0046	0.0056	0.0066	$2.2 \cdot 10^{-5}$	0.0002
$\sigma^2_{2,2}$	0.0429	0.0074	0.00001	0.0093	$4.9 \cdot 10^{-5}$	$3.8 \cdot 10^{-5}$
$\sigma^2_{3,3}$	0.0404	0.0004	0.0172	0	$7.7 \cdot 10^{-5}$	$8.4 \cdot 10^{-5}$
$\sigma^2_{4,4}$	0.0417	0.0679	$-5.5 \cdot 10^{-9}$	0	0.0004	0.0003
$\sigma^2_{5,5}$	0.0068	0.00001	0.0056	0	$7.6 \cdot 10^{-5}$	$1.1 \cdot 10^{-5}$
$\sigma^2_{6,6}$	0.4471	0.0016	$-3.5 \cdot 10^{-7}$	0	$4.1 \cdot 10^{-5}$	0.0018
Loading parameter						
λ	0.4999	0.4163	0.4761	0.4109	0.4999	0.4994

Table 12: Parameter estimates for the macro-finance shadow-rate models when initialising at the macro-finance affine models' parameter estimates. * denotes a restriction. In the IV, IF, B-CR, and KL models, Σ is diagonal. In the B-CR and KL models, the level factor is a unit-root process, meaning $\kappa^P_{1,1} = 10^{-7}$ and $\theta^P_1 = 0$. In the B-CR model, $\kappa^P_{1,2} = \kappa^P_{1,3} = \kappa^P_{3,1} = \kappa^P_{3,2} = 0$. In the KL model, $\kappa^P_{1,6} = \kappa^P_{2,6} = \kappa^P_{3,6} = \kappa^P_{4,6} = \kappa^P_{5,6} = 0$ and $\kappa^P_{4,3} = \kappa^P_{5,3} = \kappa^P_{6,3} = 0$. In the IMF model, the upper-right and lower-left corner of κ^P and Σ are blocks of zero. The IF model has a diagonal κ^P matrix. The sampling period is from Jan 1985 until Dec 2018.

OLS-VAR Initialisation

	CF Model	IV Model	IMF Model	IF Model
Mean-reversion				
$\kappa^P_{1,1}$	2.1948	2.1948	2.1473	39.4891
$\kappa^P_{2,2}$	1.7275	1.7274	1.7541	27.1372
$\kappa^P_{3,3}$	1.2701	1.2701	1.2280	69.7389
$\kappa^P_{4,4}$	0.1759	0.1759	0.2083	68.7564
$\kappa^P_{5,5}$	0.6180	0.6179	0.6319	68.6925
$\kappa^P_{6,6}$	1.0867	1.0867	1.0916	68.9861
Long-term average				
θ_1	0.0510	0.0510	0.0175	-9.9996
θ_2	-0.0268	-0.0268	-0.0591	-9.9995
θ_3	-0.0185	-0.0185	-0.0344	-9.9977
θ_4	-0.0898	-0.0897	-0.0898	2.0664
θ_5	-0.6631	-0.6631	-0.6631	2.2294
θ_6	-0.3804	-0.3804	-0.3804	1.9350
State innovation				
$\sigma^2_{1,1}$	0.4500	0.4500	0.4477	$1.0 \cdot 10^{-5}$
$\sigma^2_{2,2}$	0.4500	0.4500	0.4485	$1.0 \cdot 10^{-5}$
$\sigma^2_{3,3}$	0.4500	0.4500	0.4505	$1.0 \cdot 10^{-5}$
$\sigma^2_{4,4}$	0.2458	0.2458	0.2443	$1.0 \cdot 10^{-5}$
$\sigma^2_{5,5}$	0.2158	0.2158	0.2138	$1.0 \cdot 10^{-5}$
$\sigma^2_{6,6}$	0.0037	0.0037	$6.8 \cdot 10^{-5}$	$1.0 \cdot 10^{-5}$
Loading parameter				
λ	0.4900	0.4900	0.4917	0.9897

Table 13: Parameter estimates for the macro-finance shadow-rate models initialised by a two-step OLS-VAR estimation. In the IV and IF models, Σ is diagonal. In the IMF model, the upper-right and lower-left corner of κ^P and Σ are blocks of zero. The IF model has a diagonal κ^P matrix. The sampling period is from Jan 1985 until Dec 2018.

Appendix F

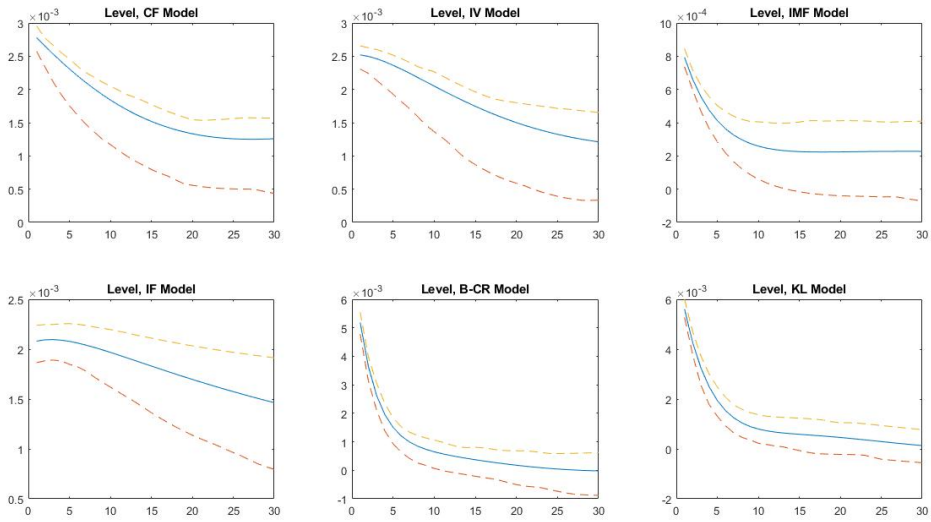

Figure 15: Impulse response functions of the level factor of the six shadow-rate models: correlated factors (CF), independent variances (IV), independent macro-finance factors (IMF), independent factors (IF), Christensen and Rudebusch (2016)'s macro-extended model (B-CR), and Krippner and Lewis (2018)'s model (KL). The vertical axis measures the effect of one unit of shock to the factor after k periods, where $k = 1, ..., 30$ months on the horizontal axis. 95% confidence bounds are estimated using Monte Carlo simulation. The sampling period is from Jan 1985 until Dec 2018.

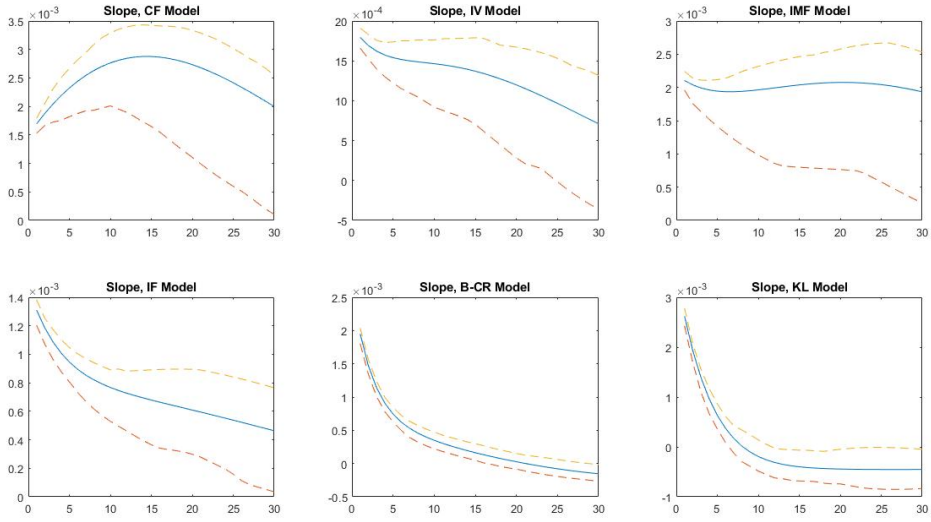

Figure 16: Impulse response functions of the slope factor of the six shadow-rate models: correlated factors (CF), independent variances (IV), independent macro-finance factors (IMF), independent factors (IF), Christensen and Rudebusch (2016)'s macro-extended model (B-CR), and Krippner and Lewis (2018)'s model (KL). The vertical axis measures the effect of one unit of shock to the factor after k periods, where $k = 1, ..., 30$ months on the horizontal axis. 95% confidence bounds are estimated using Monte Carlo simulation. The sampling period is from Jan 1985 until Dec 2018.

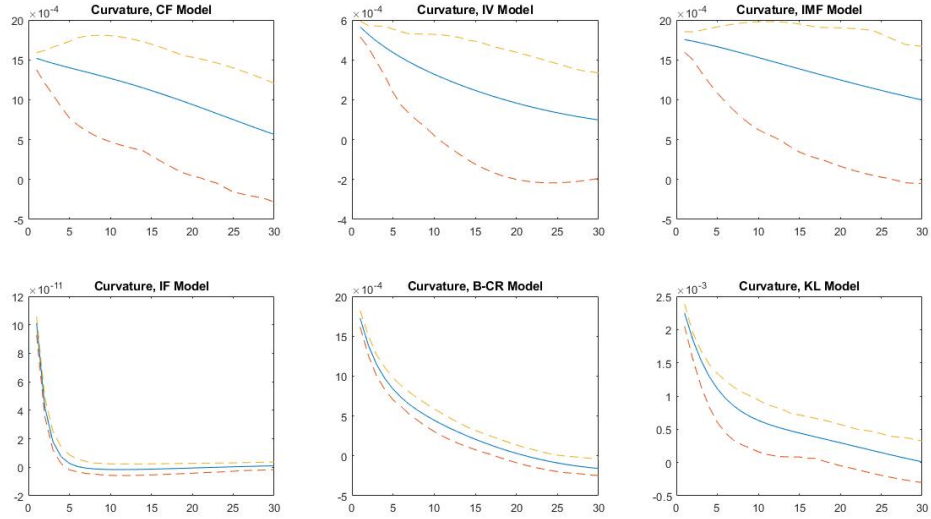

Figure 17: Impulse response functions of the curvature factor of the six shadow-rate models: correlated factors (CF), independent variances (IV), independent macro-finance factors (IMF), independent factors (IF), Christensen and Rudebusch (2016)'s macro-extended model (B-CR), and Krippner and Lewis (2018)'s model (KL). The vertical axis measures the effect of one unit of shock to the factor after k periods, where $k = 1, ..., 30$ months on the horizontal axis. 95% confidence bounds are estimated using Monte Carlo simulation. The sampling period is from Jan 1985 until Dec 2018.

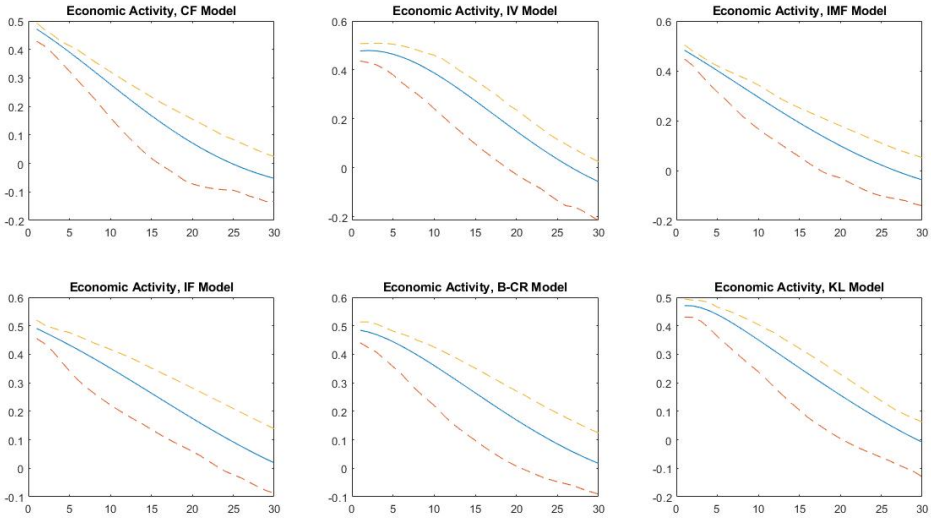

Figure 18: Impulse response functions of the economic activity factor of the six shadow-rate models: correlated factors (CF), independent variances (IV), independent macro-finance factors (IMF), independent factors (IF), Christensen and Rudebusch (2016)'s macro-extended model (B-CR), and Krippner and Lewis (2018)'s model (KL). The vertical axis measures the effect of one unit of shock to the factor after k periods, where $k = 1, ..., 30$ months on the horizontal axis. 95% confidence bounds are estimated using Monte Carlo simulation. The sampling period is from Jan 1985 until Dec 2018.

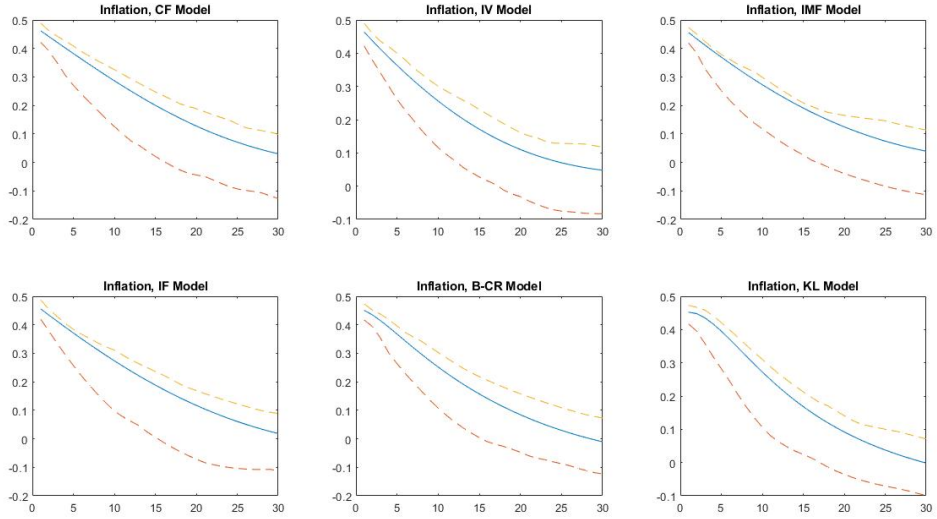

Figure 19: Impulse response functions of the inflation factor of the six shadow-rate models: correlated factors (CF), independent variances (IV), independent macro-finance factors (IMF), independent factors (IF), Christensen and Rudebusch (2016)'s macro-extended model (B-CR), and Krippner and Lewis (2018)'s model (KL). The vertical axis measures the effect of one unit of shock to the factor after k periods, where $k = 1, ..., 30$ months on the horizontal axis. 95% confidence bounds are estimated using Monte Carlo simulation. The sampling period is from Jan 1985 until Dec 2018.

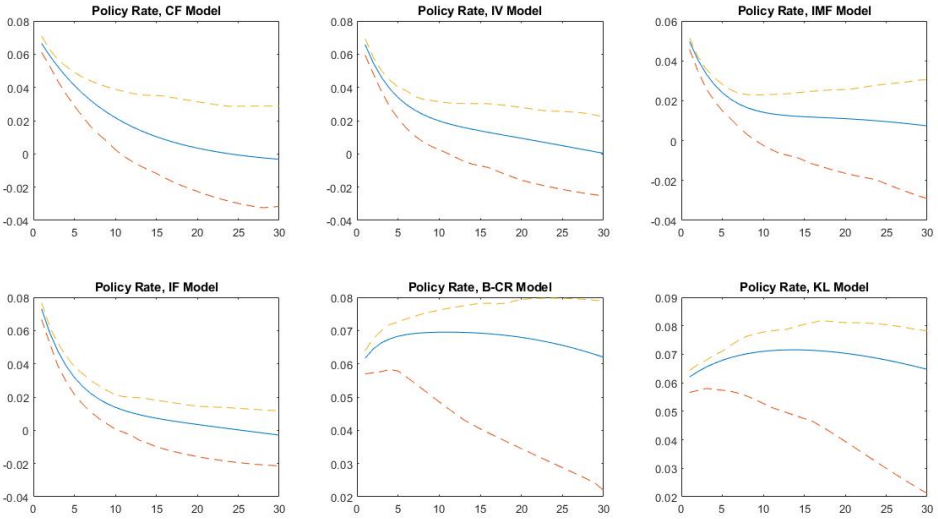

Figure 20: Impulse response functions of the policy rate of the six shadow-rate models: correlated factors (CF), independent variances (IV), independent macro-finance factors (IMF), independent factors (IF), Christensen and Rudebusch (2016)'s macro-extended model (B-CR), and Krippner and Lewis (2018)'s model (KL). The vertical axis measures the effect of one unit of shock to the factor after k periods, where $k = 1, ..., 30$ months on the horizontal axis. 95% confidence bounds are estimated using Monte Carlo simulation. The sampling period is from Jan 1985 until Dec 2018.

Appendix G

Correlated Factors

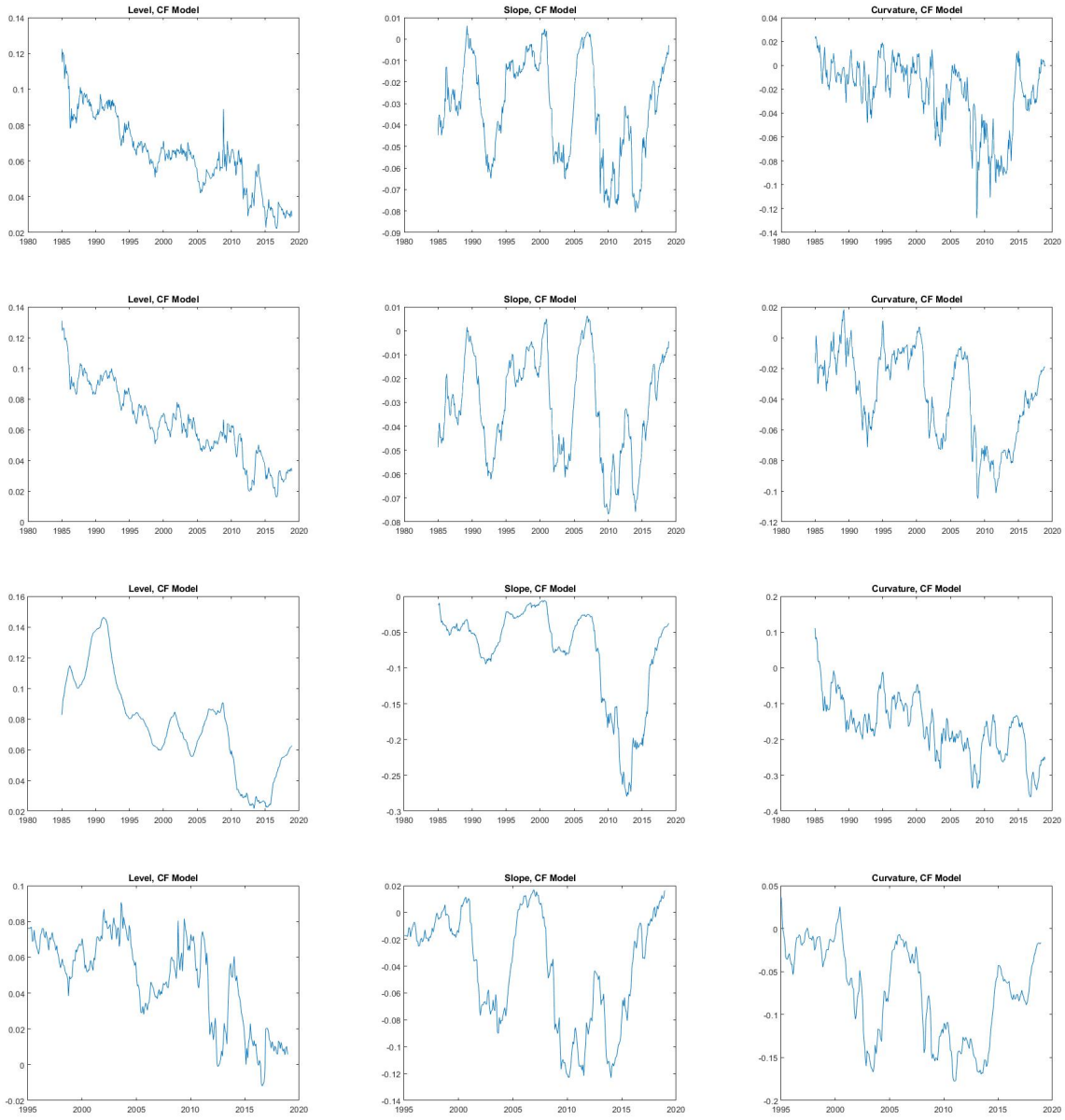

Figure 21: Evolution of three state variables (level, slope, curvature) by applying the extended Kalman filter on the correlated factors shadow-rate model. The first, second, third, and fourth rows respectively depict the yields-only model, the macro-finance model, the macro-finance model with a subset of variables, and the macro-finance model with a subsample (excluding the first ten years). The full sampling period is from Jan 1985 until Dec 2018.

Independent Variances

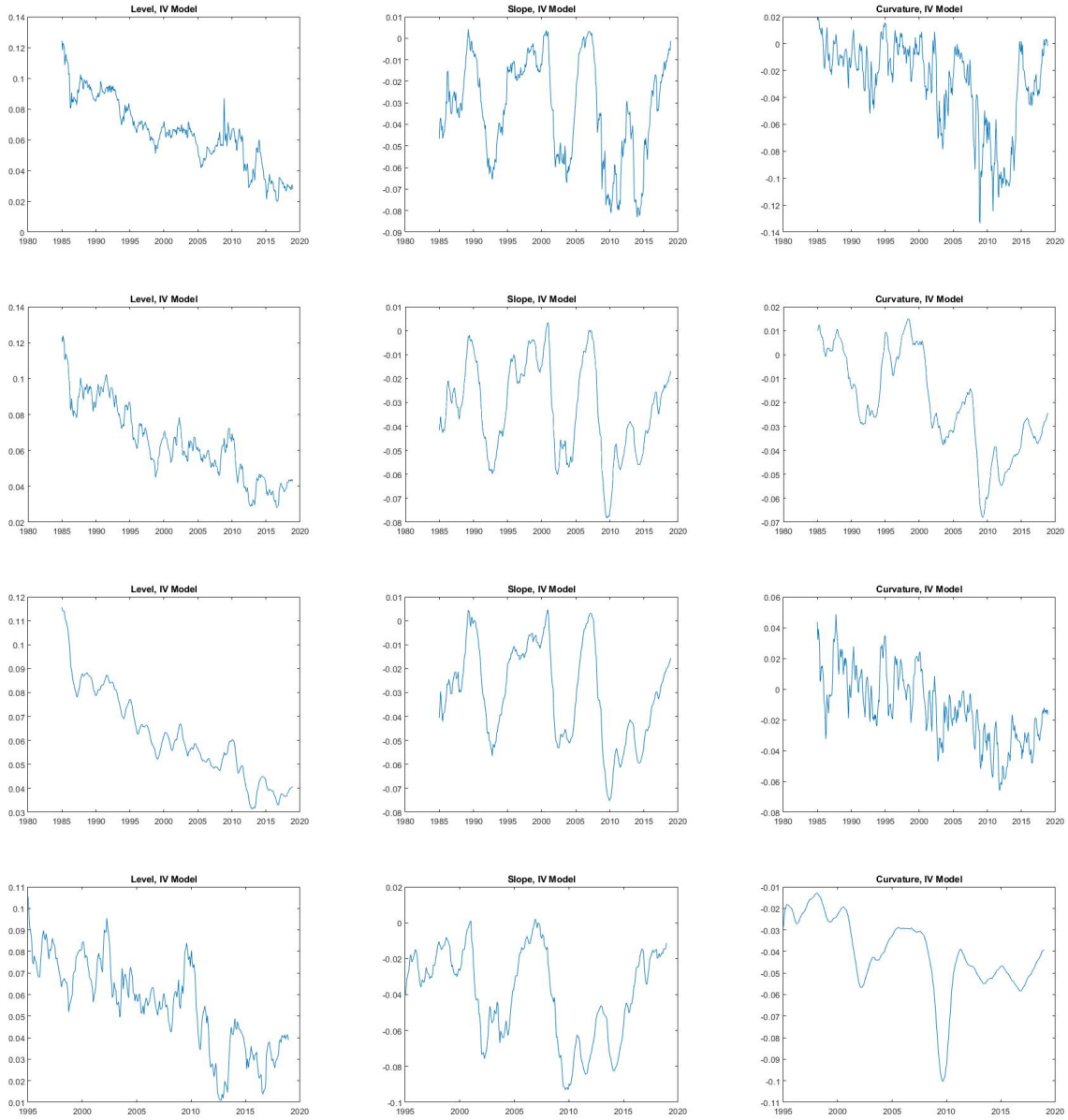

Figure 22: Evolution of three state variables (level, slope, curvature) by applying the extended Kalman filter on the independent variances shadow-rate model. The first, second, third, and fourth rows respectively depict the yields-only model, the macro-finance model, the macro-finance model with a subset of variables, and the macro-finance model with a subsample (excluding the first ten years). The full sampling period is from Jan 1985 until Dec 2018.

Independent Macro-Finance Factors

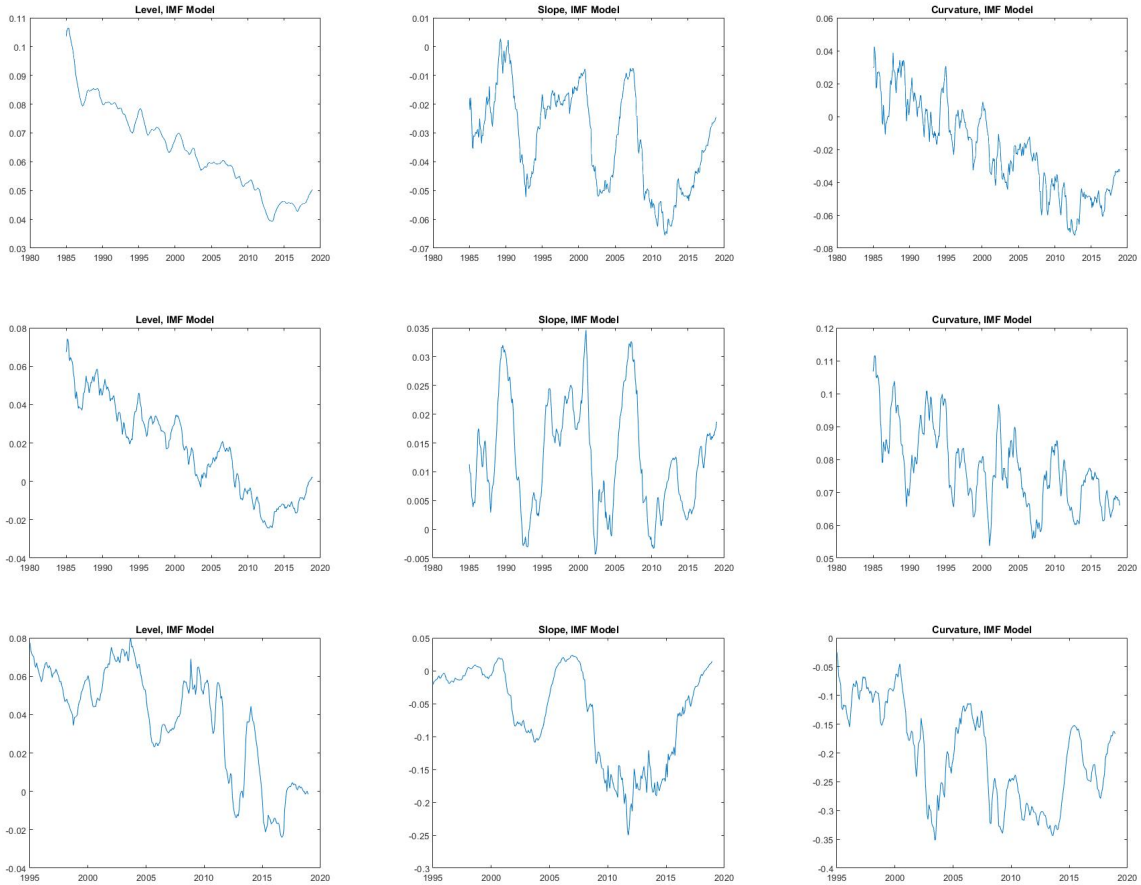

Figure 23: Evolution of three state variables (level, slope, curvature) by applying the extended Kalman filter on the independent macro-finance factors shadow-rate model. The first, second, and third rows respectively depict the macro-finance model, the macro-finance model with a subset of variables, and the macro-finance model with a subsample (excluding the first ten years). The full sampling period is from Jan 1985 until Dec 2018.

Independent Factors

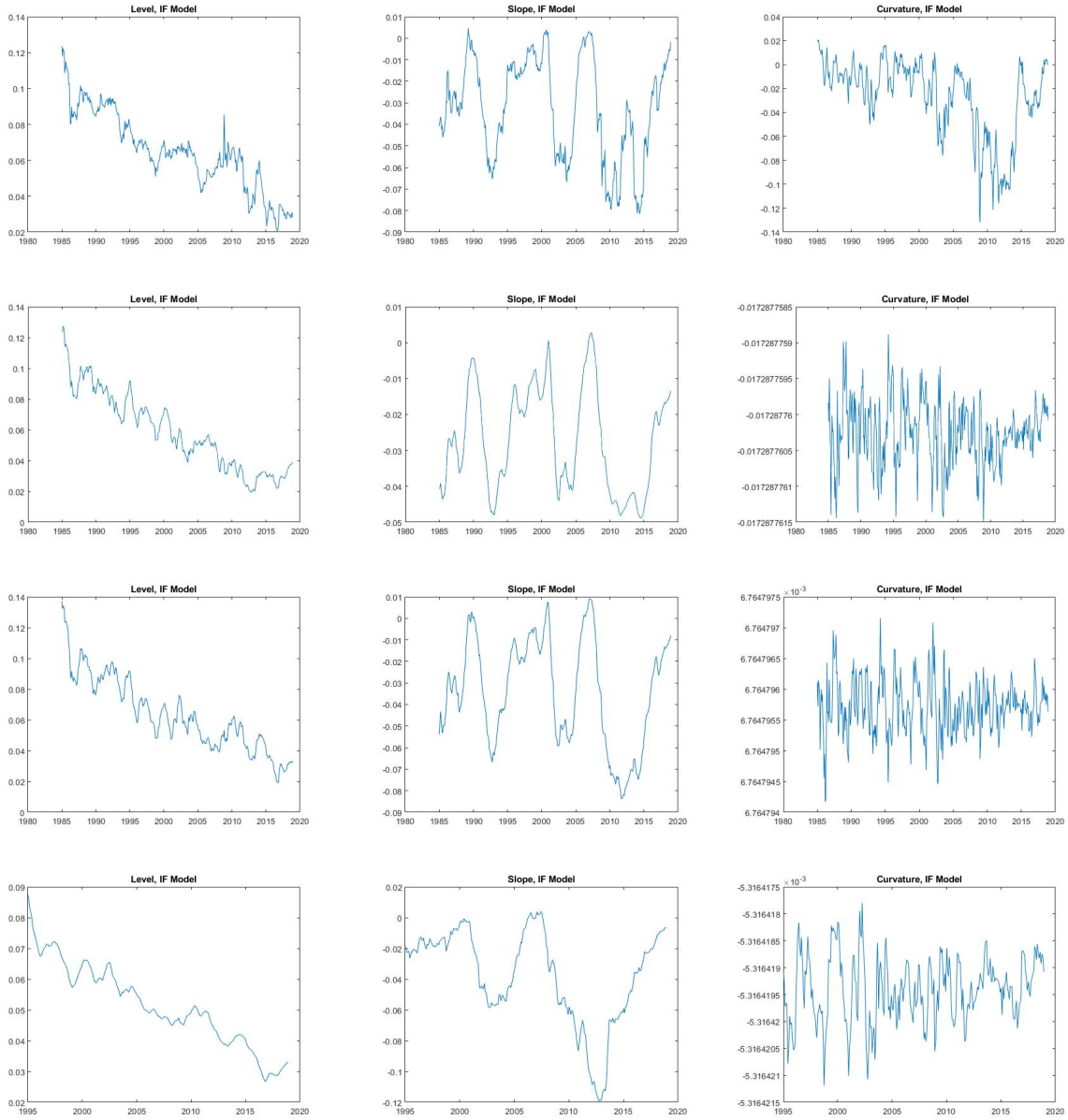

Figure 24: Evolution of three state variables (level, slope, curvature) by applying the extended Kalman filter on the independent factors shadow-rate model. The first, second, third, and fourth rows respectively depict the yields-only model, the macro-finance model, the macro-finance model with a subset of variables, and the macro-finance model with a subsample (excluding the first ten years). The full sampling period is from Jan 1985 until Dec 2018.

Christensen and Rudebusch (2016)'s Restrictions

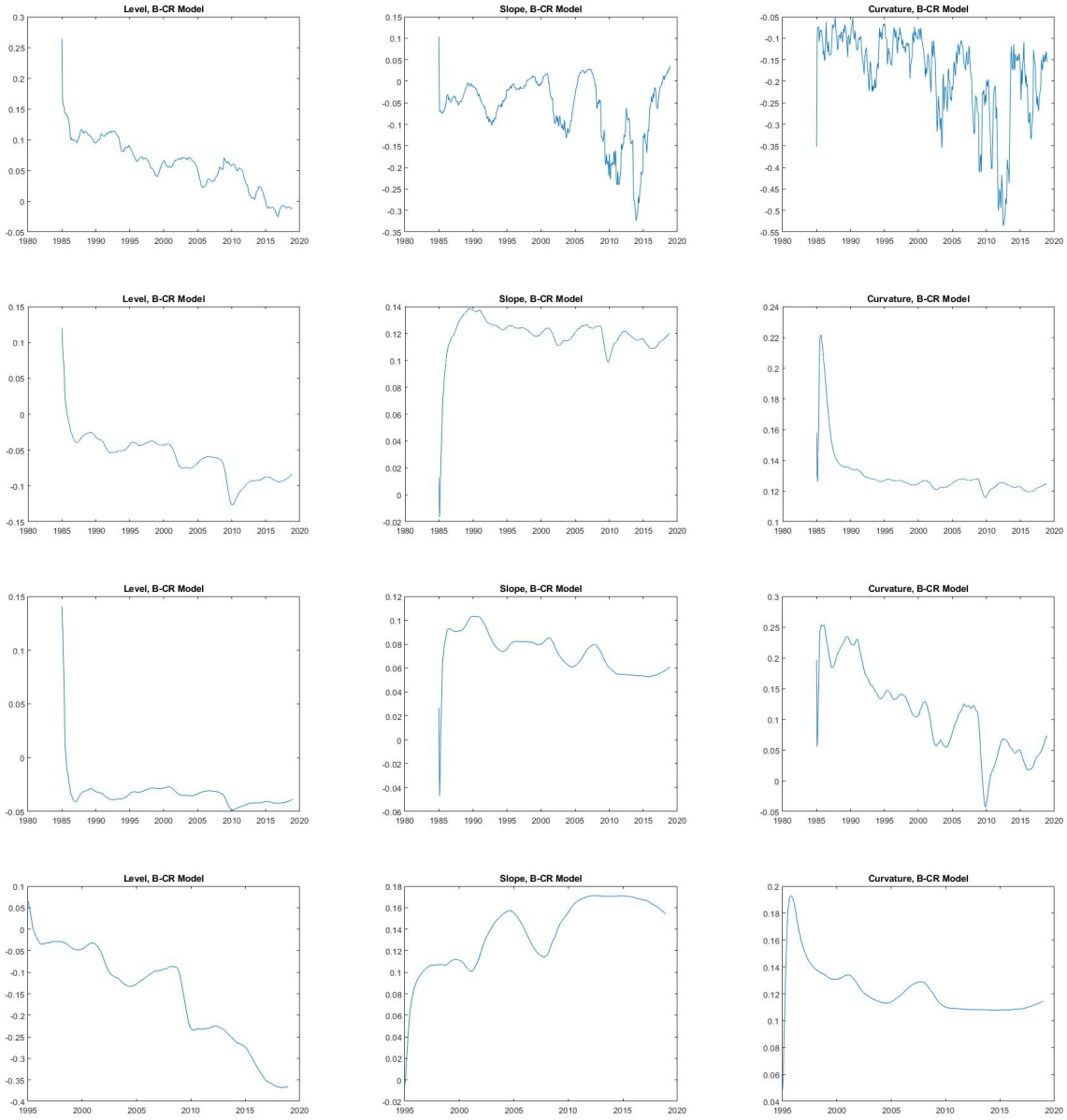

Figure 25: Evolution of three state variables (level, slope, curvature) by applying the extended Kalman filter on the shadow-rate model under the restrictions proposed by Christensen and Rudebusch (2016). The first, second, third, and fourth rows respectively depict the yields-only model, the macro-finance model, the macro-finance model with a subset of variables, and the macro-finance model with a subsample (excluding the first ten years). The full sampling period is from Jan 1985 until Dec 2018.

Krippner and Lewis (2018)'s Restrictions

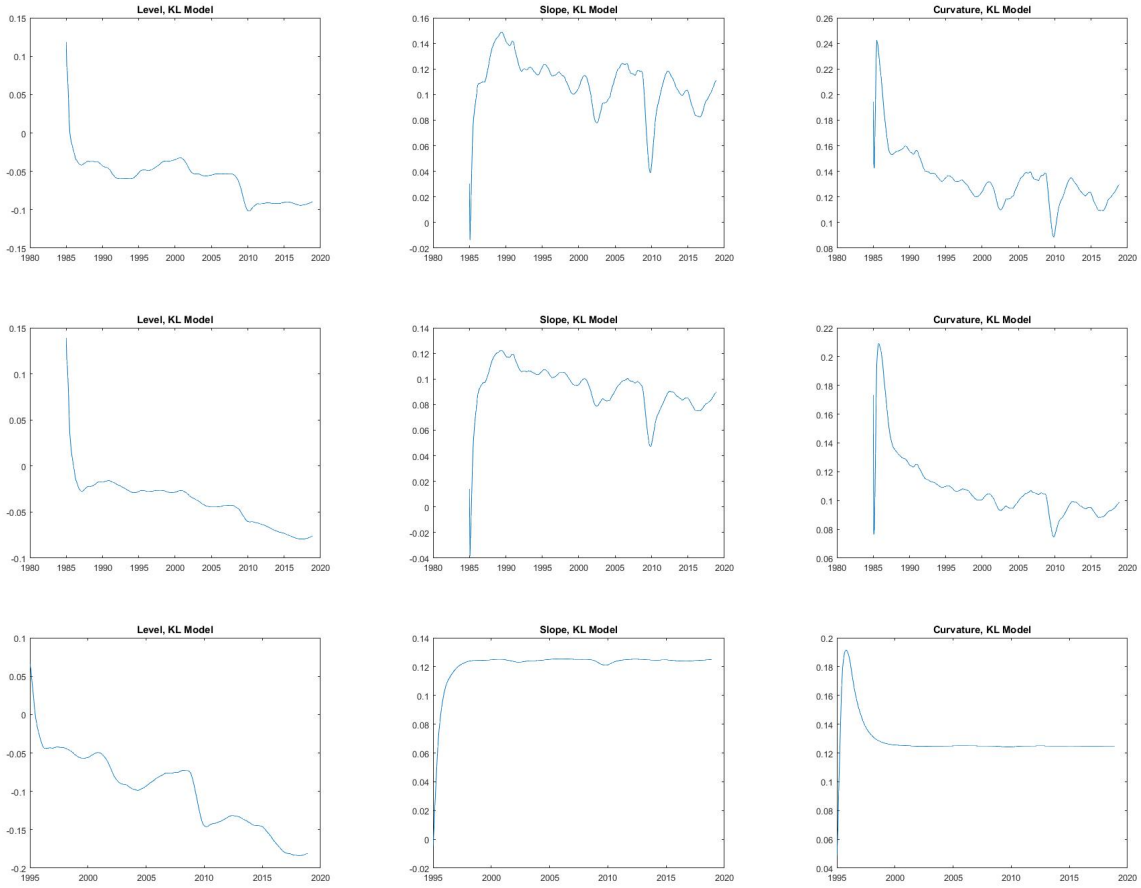

Figure 26: Evolution of three state variables (level, slope, curvature) by applying the extended Kalman filter on the shadow-rate model under the restrictions proposed by Krippner and Lewis (2018). The first, second, and third rows respectively depict the macro-finance model, the macro-finance model with a subset of variables, and the macro-finance model with a subsample (excluding the first ten years). The full sampling period is from Jan 1985 until Dec 2018.

Appendix H

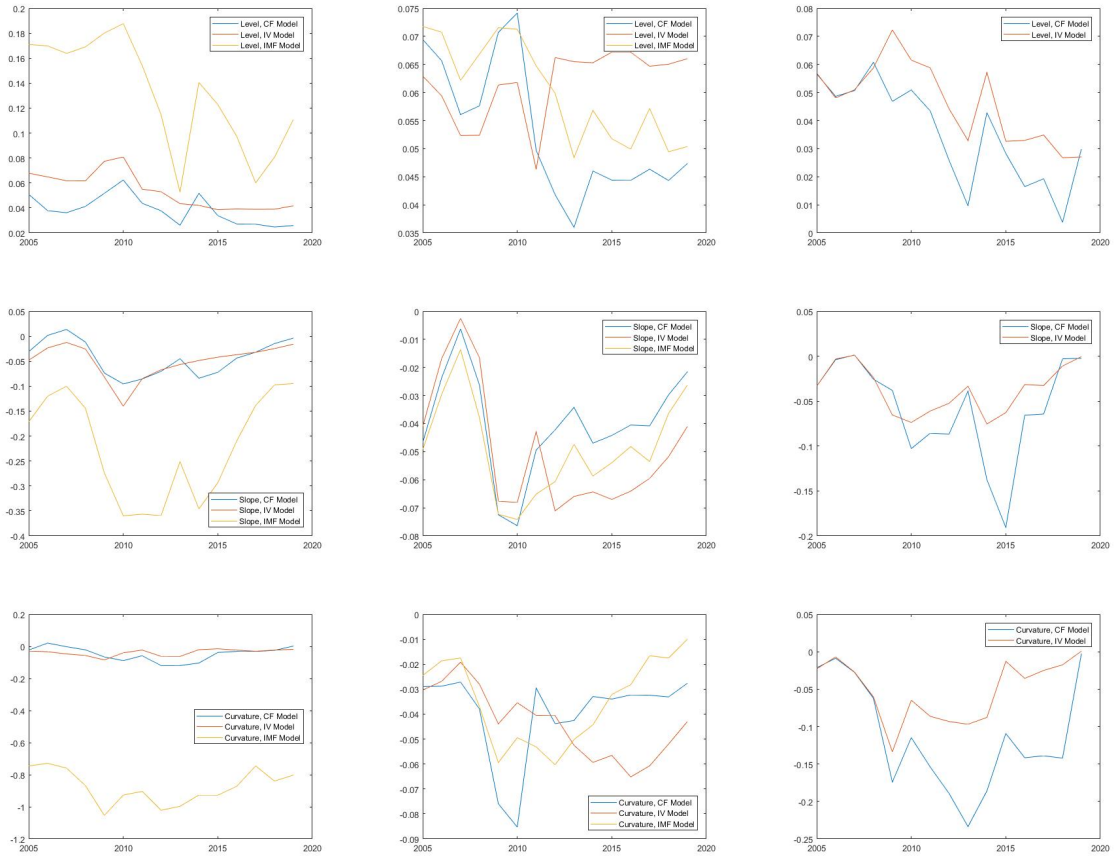

Figure 27: Yield factor predictions using rolling window re-estimations of the correlated factors (CF), independent variances (IV), and independent macro-finance factors (IMF) models. From left to right, the graphs represent the macro-finance shadow-rate, macro-finance affine, and yields-only shadow-rate models. From top to bottom, the graphs depict the level, slope, and cuvature factors. The in-sample period is 20 years, the first starting from Jan 1985 until Dec 2004, predicting Jan 2005. The final prediction is for Jan 2019.

Appendix I

Macro-Finance Shadow-Rate Model

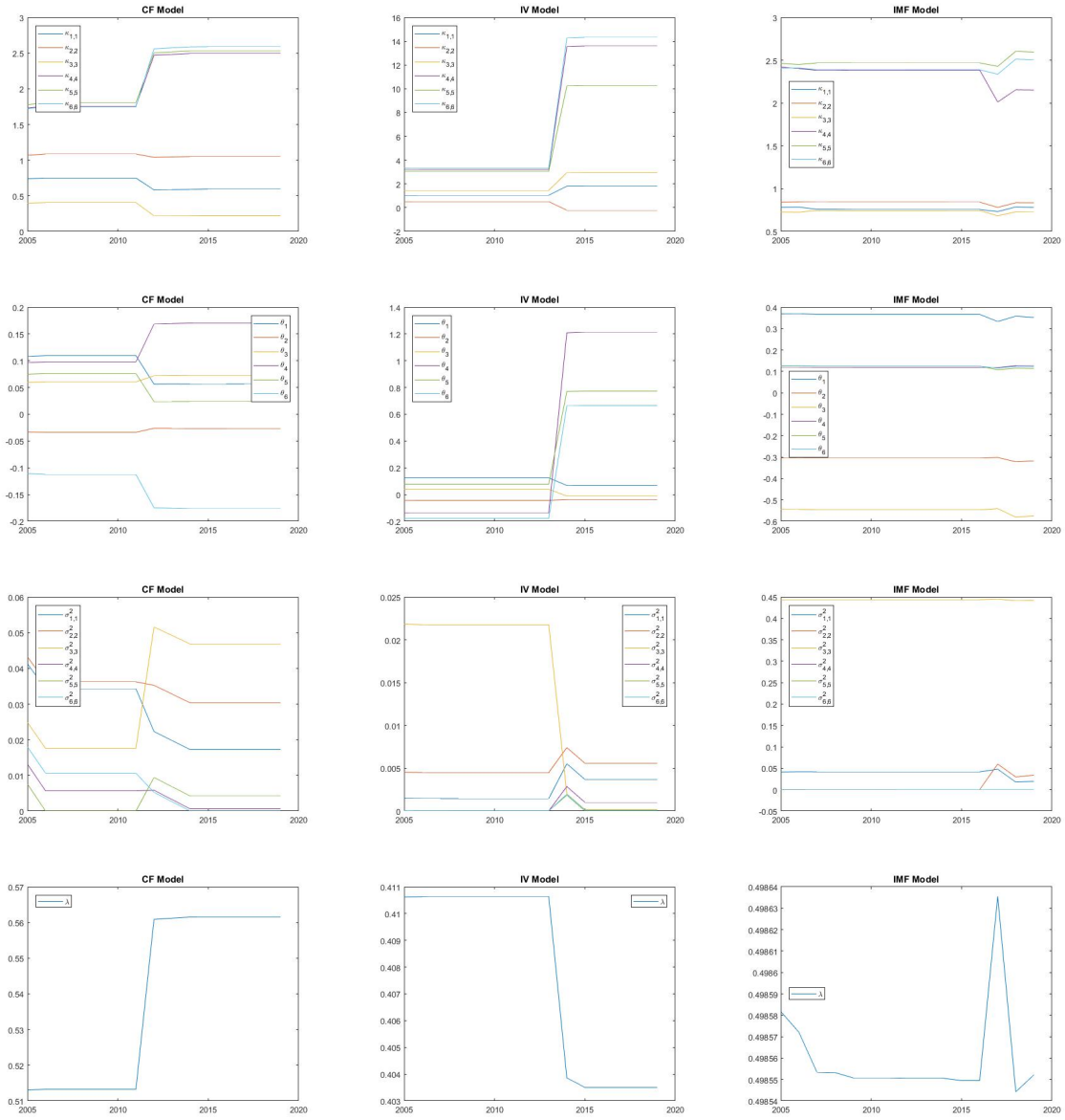

Figure 28: Rolling window re-estimations of κ^P, θ^P, σ^2, and λ (top to bottom) for the correlated factors (CF), independent variances (IV), and independent macro-finance factors (IMF) macro-finance shadow-rate models (left to right). The in-sample period is 20 years, the first starting from Jan 1985 until Dec 2004. The full sampling period is from Jan 1985 until Dec 2018.

Macro-Finance Affine Model

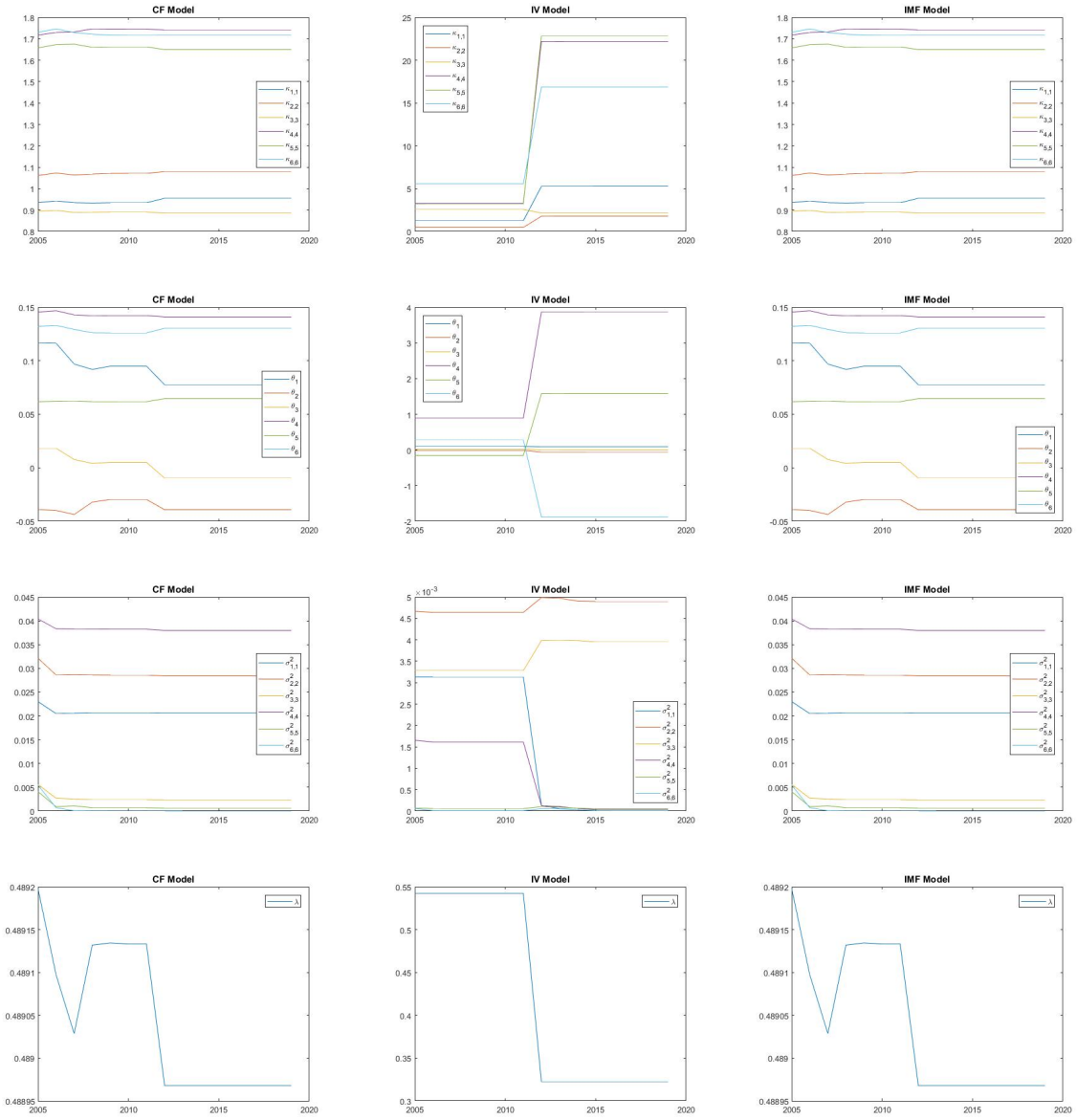

Figure 29: Rolling window re-estimations of κ^P, θ^P, σ^2, and λ (top to bottom) for the correlated factors (CF), independent variances (IV), and independent macro-finance factors (IMF) macro-finance affine models (left to right). The in-sample period is 20 years, the first starting from Jan 1985 until Dec 2004. The full sampling period is from Jan 1985 until Dec 2018.

Yields-Only Shadow-Rate Model

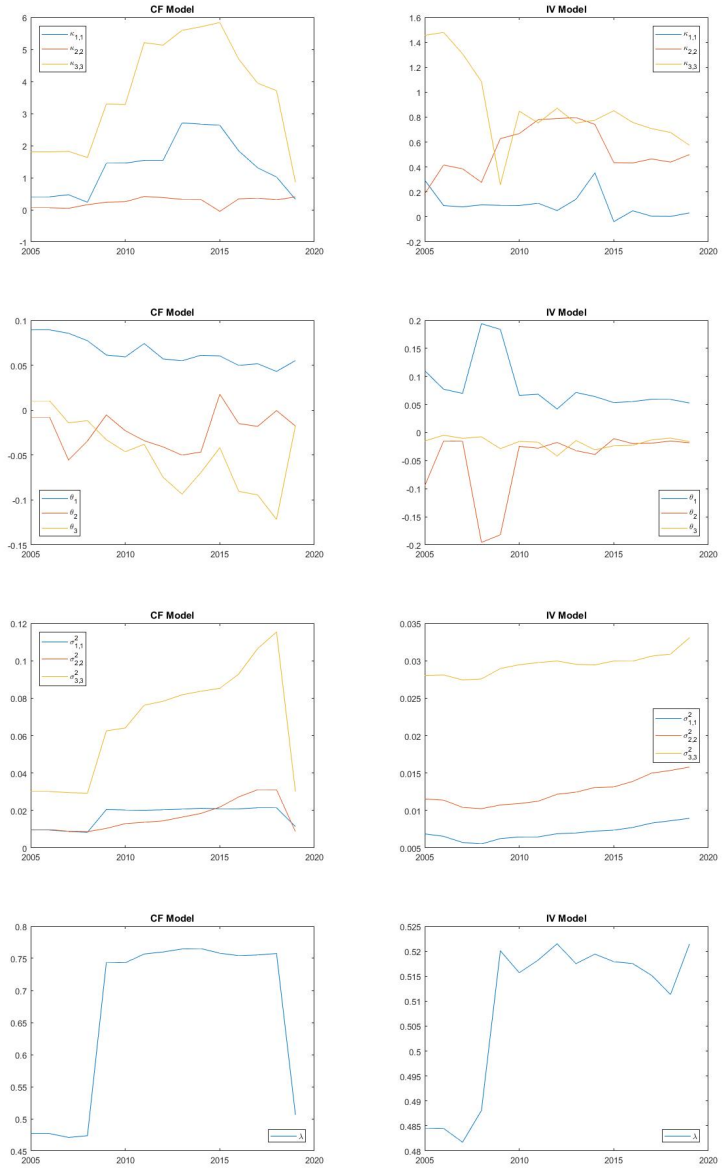

Figure 30: Rolling window re-estimations of κ^P, θ^P, σ^2, and λ (top to bottom) for the correlated factors (CF) and independent variances (IV) yields-only shadow-rate models (left to right). The in-sample period is 20 years, the first starting from Jan 1985 until Dec 2004. The full sampling period is from Jan 1985 until Dec 2018.